2011

The Effect of Oxidation and Support on TiO2(110)-Supported Pdn (n=1-7) Clusters

S. Vincent Ong
Virginia Commonwealth University

The Effect of Oxidation and Support on TiO_2(110)-Supported Pd_n (n=1-7) Clusters

A dissertation submitted in partial fulfillment of the requirements for the degree of Doctor of Philosophy in Chemistry at Virginia Commonwealth University

by

S. Vincent Ong

B.S. in Physics

Virginia Commonwealth University, 2006

M.S. in Physics

Virginia Commonwealth University, 2008

Director: Shiv N. Khanna

Commonwealth Professor, Department of Physics

Virginia Commonwealth University

Richmond, Virginia

December, 2011

Acknowledgements

The completion of this dissertation and the years of work that have been put into it would not be possible without the support of many caring people. I would like to thank Professor Khanna for his warm welcome into his research group about 5 years ago. My development as a research scientist stems from the many hours, weeks, and years of discussion that he has invested in me and the projects that I have worked on. I am very grateful for that. The members of my PhD committee, Prof. Alison Baski, Prof. Everett Carpenter, and Prof. Maryanne Collinson, have graciously spent their time to advise me and have brought their skills and expertise into discussion that has further refined my development as a researcher. I would like to thank all of the members of the Khanna research group, with a special thank you to Dr. Art Reber, Dr. Roberto Robles, and Dr. Victor Manuel. The constant support by the entire Department of Physics at VCU is what makes this department one of the greatest, and Janice Guyer and Evelyn Perham are two wonderful ladies who make this place feel like home. I would like to thank my family, especially my parents Stephen and Sharon Ong for their support and prayers throughout these years. Finally, I thank Meghann Broderick for the utmost love and support.

Contents

List of Figures

ABSTRACT

THE EFFECT OF OXIDATION AND SUPPORT ON TIO_2(110)-SUPPORTED PD_N (N=1-7) CLUSTERS

By S. Vincent Ong, Ph.D.

A dissertation submitted in partial fulfillment of the requirements for the degree of Doctor of Philosophy in Chemistry at Virginia Commonwealth University.

Virginia Commonwealth University, 2011.

Director: Shiv N. Khanna, Commonwealth Professor, Department of Physics

First principles theoretical studies based on a gradient-corrected density functional approach have been carried out on the atomic and electronic properties and oxidation of Pd_n (n=1-7) clusters supported on the TiO_2(110) surface. The studies are aimed to address some of the fundamental issues related to the properties of supported Pd_n clusters used as catalysts in oxidation reactions. Of those issues are the following: What are the atomic structures of Pd_n clusters on the TiO_2 surface? Upon oxidation, do O atoms from a dissociated O_2 molecule spill over onto the underlying TiO_2 support? How strongly does spillover oxygen bind? What is the microscopic mechanism for the experimentally observed strong metal support interaction (SMSI) state where the Pd catalyst becomes encapsulated by the surface? Is this related to spillover

oxygen? How do the properties of the Pd_n clusters change when the TiO_2 surface is marked with oxygen vacancies?

As will be shown, the ground state geometries of supported Pd_n clusters are driven by competing effects including intra-cluster interactions favoring compact structures and cluster support interactions favoring geometries that flatten out in the TiO_2(110) surface channel. When exposed to O_2, a single Pd atom only activates the O-O bond while all other clusters energetically favor a broken O-O bond. For Pd_nO_2 (n=2-7), while one O is adsorbed on the Pd_n cluster, the second O spills over to a lattice Ti site binding at the Pd-Ti interface. The binding strength of these spillover atoms is calculated to be surprisingly high, which is identified to be a result of long-range ionic interactions between Pd and spilled over oxygen. When oxygen spills onto lattice Ti sites, composite TiO motifs are formed that can exchange sites with Pd atoms with a minimal energy, opening the pathway for Ti migration and strong metal support interactions. For the TiO_2 surface with oxygen vacancies, clusters bound at the vacancy site possess atomic and electronic properties that resemble bulk palladium. The theoretical findings are compared with recent experiments and are believed to provide insight toward developing a fundamental understanding of supported Pd_n clusters as oxidation catalysts.

1. Introduction

1.1 Size Matters

The foundations of nanoscience are rooted in the idea that "size matters". Many physical and chemical properties of materials have a dependence on size, which can roughly be grouped into three regimes. Towards one extreme, the bulk limit is approached and constitutes the most traditionally studied size regime. A decrease in size leads to a scaling regime where some properties scale in proportion to a materials dimensions (e.g., melting temperature of gold nanoparticle).[1] Finally, the smallest regime is approached as the dimensions are confined to within a few nanometers. These "materials" can be considered "particles" as their dimensionality is reduced to zero. The dimensionality is considered zero because the typical length scales that are critically associated to certain physical properties (e.g., mean free path of an electron) exceed all three dimensions of the particle, giving rise to unexpected phenomenon. In the gas phase, these particles are referred to as clusters, consisting of anywhere between 2-100 atoms. In this cluster regime, the physical and chemical properties have a fascinating behavior and change erratically with size, shape, charge state, and composition.[2–5] Their properties can no longer be described within the classical laws of physics as their nature is dominated by quantum effects. To this end, classical physics can be said to lose its power of predictability, inviting new rules and models to be established.

Such models are aimed at explaining the unusual properties of clusters, whether it pertains to a cluster's stability, reactivity, electronic, optical, or magnetic properties. Perhaps the most prominent model that holds the power of predicting stability of clusters is the jellium model. This model shows that the electronic states in small, symmetric metal clusters bunch into electronic shells much in the same way as atoms, and that clusters with filled shells exhibit enhanced energetic and chemical stability. The jellium model explains why the compact Al_{13}^- cluster, for example, shows enhanced stability and a resiliency to react with oxygen, while the removal of just a single atom leads to an Al_{12}^- cluster that is highly reactive with oxygen.[6,7] The unique behavior is even more exemplified when considering bulk aluminum's extremely high exothermicity toward oxide formation.[8] Another example is the unusual magnetic properties that clusters have been shown to possess. Elements known to be non-magnetic in the bulk phase (e.g., bulk rhodium), possess strong magnetic moments that vary considerably with size.[9]

The implications of research in cluster science extend far beyond establishing a set of rules that predict the stability or magnetic moments of small gas phase particles. Clusters can also be used as model systems to elucidate the details of otherwise complex phenomenon, for example catalytic reactions. In regards to reactivity, the size, charge state, stoichiometry, and active sites of a catalyst are among the factors shown to have a critical effect on its activity.[10–12] These factors all depend on the atomic, electronic, and magnetic structure of the catalyst. Because clusters consist of a countable number of atoms, identifying the critical factors that control reactivity is a manageable task. The understanding gained by identifying these factors can then be related back to the realistic catalytic systems for further optimization and design.[13] Traditionally, clusters have been studied in the gas phase.[14–17] However, advances in phosphate and thiolate chemistry have led to ligand-stabilized clusters, which can

be immersed in solutions.[18–21] Even solid phase materials have been synthesized by exploiting the superatomic-like nature of stable clusters and assembling them as the building blocks in so-called "cluster assembled materials".[22,23] Lastly, with the advent of modern surface science techniques such as ultra high vacuum (UHV) technology, clusters can now be supported and stabilized on solid surfaces in highly controlled environments where their properties can be probed.[24,25]

1.2 Supported Clusters

Transitioning from gas phase to supported clusters introduces an entirely new realm of important factors. For instance, where do the clusters bind and in what atomic arrangement? How do the clusters interact with the support and does this modify their electronic properties? For supported metal clusters, these questions pertain to understanding metal growth on a surface, which has fundamental implications in a variety of industrial applications. In the semiconductor industry, the challenge to epitaxially grow thin metal films on oxide supports requires a rigorous understanding of the physical and chemical interactions that take place between metal and support. In heterogeneous catalysis, efforts are aimed at reducing the size of supported metal clusters in an attempt to maximize the surface-to-volume ratio of the catalyst and identify the most reactive species. Yet, an ever-prominent obstacle to these efforts is that clusters are thermodynamically driven to aggregate at elevated temperatures, and upon aggregation the catalytic activity decreases as the exposed active surface of the metal catalyst is also decreased. A first step towards maximizing catalytic activity is to understand how clusters configure on the support. For example, understanding whether a vapor-deposited metal prefers to form a second layer of atoms or contribute to a monolayer instead yields insight on cluster nucleation and growth. In a supported

cluster study, this translates to determining the cluster size at which the transition to three-dimensionality occurs. Supported metal clusters, starting as small as two atoms, represents the ideal template to study this since the transition from 2D to 3D may likely occur at small sizes. Many supported cluster studies employ metal oxide surfaces as the support because they are typically non-reactive with the clusters. This means the clusters are in fact *on* the surface and typically with a high dispersion. In most cases, details of the interfacial reactions between cluster and oxide support lack a fundamental understanding. This includes charge transfer either to or from the supported cluster and the effect of the support on the cluster's atomic configuration. Out of all oxide surfaces, rutile $TiO_2(110)$ is the most studied;[26] and the properties of a wide range of sizes of Pt, Au, and Ag clusters on TiO_2 have previously been investigated.[27–31] However, the scientific literature for Pd_n clusters on TiO_2 is mainly limited to single atoms and dimers.[32–34] It should be noted that theoretical studies on supported Pd_6 and Pd_{13} have been reported, but fail to provide a comprehensive view as only the gas phase cluster geometries were considered.[35]

In addition to bare cluster binding at a support, the chemical and physical factors that control the oxidation of supported clusters are not fully understood. Knowledge of these factors is required for the development of catalysts that can act in oxidation reactions (e.g., oxidation of CO), especially when considering that most oxidation reactions proceed via the initial oxidation by O_2. Characterizing the oxidation properties is of key importance because of the critical relationship known to exist between the catalytic efficiency of oxidation reactions and the strength to which atomic oxygen binds to the metal surface. This relationship, an example of Sabatier's principle, states that a certain range of metal-oxygen binding energies optimizes the catalytic activity. For CO_2 oxidation, this range of binding energies is roughly around 3.3 to 4.0 eV, as can be seen in Figure 1.1.[36] At energies above that range, a stable oxide

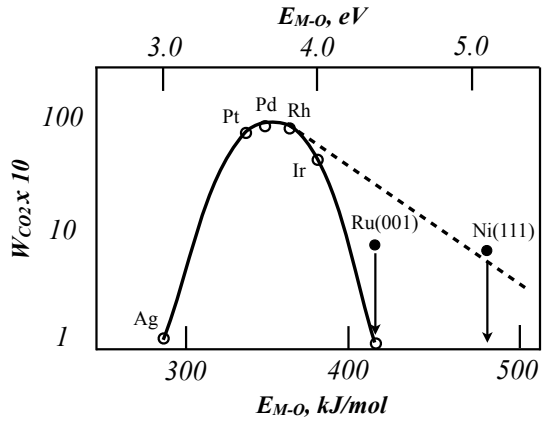

Figure 1.1: Relationship between rate of CO oxidation W_{CO_2} and metal oxygen bond energy E_{M-O}. Figure based on data from Santra et al. where T = 793 K, $P_{O2} = P_{CO} = 10^{-7}$ Torr.[36]

phase is thermodynamically preferred (e.g., Ru and Ni). At binding energies below that range, binding between the metal and oxygen is not strong enough to break the O-O bond, leaving oxygen in its molecular form (e.g., Ag and Au). Several platinum group metals (e.g., Pt, Pd, Rh, and Ir) bind to oxygen in this optimal range, making them suitable catalysts for CO oxidation.[36]

Depositing clusters on a support in sub-monolayer concentrations introduces additional factors. Gaseous O_2 and CO can now adsorb not only at the cluster site, but also directly on the support or even at the cluster support interface. Further, the TiO_2 surface is known to be reactive toward O_2 when surface defects are present, further increasing the complexity of the situation.[37,38] An O_2 molecule dissociated at a TiO_2 surface defect site can now leave single oxygen adatoms on the surface, which may be mobile on the surface provided sufficient temperatures to overcome diffusion barriers, an observation supported by experiments.[38,39] On the other hand, even if adsorbent molecules initially bind directly at the cluster site, mobility on the cluster surface may lead to so-called "spillover" mode binding. Such effects have

been observed for palladium nanoparticles supported on rutile TiO_2 that undergo an oxidation at high temperatures, where O_2 dissociatively adsorbs at the palladium surface and either one or both of the dissociated O atoms "spills over" to the titania support.[40] This highlights one of the unique features of supported cluster catalysis, especially in comparison to catalysis by a bulk metal surface. Figure 1.1 indicates that a metal with too low of a metal-oxygen binding energy cannot oxidize CO because it does not dissociate O_2 in the first place. If oxidation by a supported Pd_n cluster results in spillover oxygen atoms, this may provide opportunities to have lower binding energies than possible with bulk surfaces. Thus, efforts to design a supported cluster catalyst can be directed at decreasing the binding strength of the spillover oxygen.

Another issue arises when considering the strong interactions that can take place between cluster and support. Such interactions have been reported to modify the chemisorption properties of certain metal particles on oxide supports after they undergo a high temperature reduction.[41,42] These strong interactions lead to what is referred to as "strong metal support interaction" (SMSI) state, and have been reported for a variety of metal-support systems including Pd/TiO_2.[43,44] The effect, initially reported in 1978 by Tauster, is known to reduce the supported metal's capacity to sorb (adsorb and absorb) gaseous molecules such as H_2 and O_2.[41] This was originally reported with regards to the implications in H_2 chemisorption saturation experiments, which were commonly performed for supported metal systems to provide a quantitative measurement of exposed metal surface.[45] However, modern research efforts are aimed toward providing insight to the nature of these interactions, specifically in determining why the sorption properties are reduced. Current models suggest the supported particle is either encapsulated by or forms an inter-metallic alloy with atoms of the underlying titania support.[44,46,47] It has been proposed that the oxy-

gen spillover phenomenon and SMSI effect are somehow related, yet a molecular-level depiction is lacking in the literature to draw conclusive evidence connecting the two.[48]

Major advancements in experimental and theoretical techniques now permit accurate studies on supported cluster systems with an unprecedented level of control. Combined with UHV technology, mass-selected cluster deposition techniques can be employed to achieve narrow particle size distributions of supported metal clusters. Such experiments truly characterize the size dependent nature of supported clusters and can be performed in parallel with a variety of experimental techniques such as: X-ray Photoelectron Spectroscopy (XPS), Scanning Tunneling Microscopy (STM), and Ion Scattering Spectroscopy (ISS) among many others.[24,25,49–53] This functionality is complemented by advances in computational techniques that allow for accurate simulation of surfaces with supercells containing hundreds to thousands of atoms. And with the accurate representation of surfaces, the atomic, electronic, and magnetic properties of clusters bound to those surfaces can be accurately probed by theoretical techniques. Together, the advances in experiments and theory provide the means for developing a microscopic understanding of the underlying processes.

Within this PhD, state-of-the-art electronic structure calculations have been performed to study these interactions of palladium clusters on a titanium dioxide surface. The goal is to identify the nature of cluster-support interactions on both the perfect, single crystal surface as well as the surface marked with oxygen vacancy defects. The primary motivation behind the latter is to provide an accurate representation of the experimental surface, where 7-12% of the surface unit cells are known to contain bridging oxygen vacancies.[38,54] The specific issues of interest in the present studies are the following:

- What are the atomic structures of the deposited clusters and how do the structures evolve with size?
- How strongly do the clusters bind to the surfaces and how is the support perturbed by the deposited cluster?
- What is the electronic and magnetic structure of the deposited cluster and how are they controlled by the support?
- How mobile are single Pd atoms on oxide surfaces, and does this mobility promote the nucleation and growth of larger clusters?
- Considering that the TiO_2 surfaces are often marked by oxygen vacancies, how do the clusters bind to these vacancies and how do the vacancies control their electronic character?
- For oxidation reactions, how does the addition of oxygen modify the cluster behavior and how strongly are the oxygen atoms bound to the cluster?
- The oxidation reactions are governed by the binding energy of oxygen to the surface. One way to accomplish this is to enhance coverage. How does the binding energy evolve with oxygen coverage?
- Many catalytic reactions involve charging of clusters during the oxidation/reduction process. How does the support change the charged state of the cluster?
- The Pd_n clusters lead to a splitting of an O_2 molecule into two O atoms. Do the O atoms stay on the Pd_n cluster or are some of them "spilled over" to the TiO_2 substrate?
- What are the microscopic mechanisms leading to strong metal support interactions and what motifs are likely to initiate such effects?

The present work is a part of the Multi University Research Initiative (MURI) effort supported by the Air Force Office of Scientific Research (AFOSR) for the development of novel palladium catalysts in fuels, propulsion, and other applications. The MURI effort combines the theoretical work performed within this PhD at Virginia Commonwealth University with experimental efforts at Pennsylvania State University, Princeton University, University of Utah, and University of Southern California. The specific interest in palladium as a catalyst is due to its short fuel ignition delay times and the possibility of reducing the ignition temperature during the catalytic combustion of methane.[55] The fundamental studies of this PhD on the size-dependent properties of Pd_n clusters on rutile TiO_2 are in direct correspondence to the UHV, soft-landing cluster deposition experiments by the group of Anderson.[56,57] Similar studies of Pd_n clusters supported on alumina/NiAl(110) have previously been reported within the collaboration,[58,59] and the results are referred to throughout the chapters in this thesis.

1.3 Organization of this Thesis

The overall objective of this thesis is to provide the reader with an understanding of how Pd_n clusters interact with the support and the oxidation properties of the supported Pd_n clusters. Since this is a theoretical study based on Density Functional Theory, the numerical methods used to calculate the properties of supported clusters is overviewed. This is followed by a description of the computational methodology, which was written with the intent for an incoming graduate student familiar with DFT to be able to reproduce this work and extend the project further. The results chapters begin with an introduction to the TiO_2 surface, with an emphasis on the surface properties as calculated within DFT. Additionally, the calculated properties

for free (gas phase) Pd_n clusters are presented. The remaining chapters (Chapters 4 thru 7) are purposely ordered to build certain concepts that are referred back to in the chapters that follow. Each of these chapters has been written up as an article that has either been accepted for publication or is in the process of publication. Chapter 4 uses the Pd_4 cluster as a template to introduce the nature of adsorbate-induced reconstructions on the TiO_2 surface, as well as oxygen induced reconstructions that the Pd_n clusters undergo upon oxidation. The study reported in Chapter 5 uses a single PdO molecule on the TiO_2 surface as a model system to introduce the long range interactions that are shown to take place between Pd and O as they are separated to long distances. This chapter directly addresses the oxygen spillover binding modes and the implications that they may have in the SMSI effect. The remaining two chapters refer back to the results from the previous ones to present the stability and oxidation properties of Pd_n clusters on the perfect (Chapter 6) and reduced (Chapter 7) TiO_2 surface. Supplemental calculations were performed for the results of select chapters, and for the sake of clarity and flow, are reported in the Appendices.

2. Numerical Methods

2.1 Introduction

This chapter is intended to provide a brief overview of the theoretical methods used within this PhD, namely those based on Density Functional Theory (DFT). The following sections begin with quantum mechanics and statistical mechanics to introduce the two theorems proposed by Hohenberg and Kohn, and the methods by Kohn and Sham that led to the formulation of DFT.

2.2 Background

2.2.1 Quantum Mechanics

The ultimate goal of most electronic structure calculations, such as those performed within this PhD, is to solve the time-independent Schrödinger equation,

$$\hat{H}\Psi = E\Psi, \tag{2.1}$$

a second order partial differential equation, which can be solved to obtain the wavefunctions Ψ_i and allowed energy levels E_i associated with the i^{th} state of a particular system. When applied to the motion of interacting nuclei and electrons, the Hamil-

tonian operator $\hat{H}$ adopts the form,

$$\hat{H} = -\frac{\hbar^2}{2m_e}\sum_i \nabla_i^2 - \sum_{i,I}\frac{Z_I e^2}{|\mathbf{r}_i - \mathbf{R}_I|} + \frac{1}{2}\sum_{i\neq j}\frac{e^2}{|\mathbf{r}_i - \mathbf{r}_j|} - \sum_I \frac{\hbar^2}{2M_I}\nabla_I^2 + \frac{1}{2}\sum_{I\neq J}\frac{Z_I Z_J e^2}{|\mathbf{R}_I - \mathbf{R}_J|}, \tag{2.2}$$

where the lower and upper case subscripts denote electron and nuclei indices, respectively. The terms of this general Hamiltonian operator as they appear in Equation 2.2 represent the following: electron kinetic energy, electron-nuclei Coulomb potential, electron-electron Coulomb potential, nuclei kinetic energy, and nuclei-nuclei Coulomb potential. Additional terms, related to magnetic or electric fields for example, may also be added to the Hamiltonian. It is useful to know that "zero energy" refers to all particles infinitely away from each other (all Coulomb terms go to zero) and not moving (all kinetic terms go to zero). For this reason, total energy calculations of chemically bound systems should always result in negative energies.

The wavefunction Ψ of the system depends on 3N spatial coordinates of the electrons, N spin coordinates of the electrons, and 3M spatial coordinates of the nuclei; N and M are the total number of electrons and nuclei in the system, respectively. This makes Schrödinger's equation a partial differential equation in 4N+3M coordinates and impossible to solve, analytically, for systems containing more than one electron. Several approximations can be applied to simplify solving of the equation. The first accounts for the significant difference between the masses of electrons and nuclei (the mass of the lightest nuclei being about 1800 times larger than the mass of an electron), and considers the electrons moving in a field of fixed, or clamped, nuclei. This is referred to as the Born-Oppenheimer approximation,[60] and the fourth term of Equation 2.2 is removed as the movement of nuclei. For fixed nuclei the fifth term simply becomes a constant. Equation 2.2 can now be reduced to the electronic

Hamiltonian operator,

$$\hat{H}_{elec} = -\frac{\hbar^2}{2m_e}\sum_i \nabla_i^2 - \sum_{i,I}\frac{Z_I e^2}{|\mathbf{r}_i - \mathbf{R}_I|} + \frac{1}{2}\sum_{i\neq j}\frac{e^2}{|\mathbf{r}_i - \mathbf{r}_j|} = \hat{T} + \hat{V}_{Ne} + \hat{V}_{ee}, \tag{2.3}$$

which operates on only the electronic wave function Ψ_{elec} to get the electronic energies E_{elec}. The total energy of the system is simply the sum of the electronic energy and that constant nuclear repulsion energy term

$$E_{nuc} = \frac{1}{2}\sum_{I\neq J}\frac{Z_I Z_J e^2}{|\mathbf{R}_I - \mathbf{R}_J|}. \tag{2.4}$$

The electronic wavefunction,

$$\Psi_{elec} = \Psi_{elec}(\vec{x}_1, \vec{x}_2, ..., \vec{x}_N), \tag{2.5}$$

is a function of spatial ($\vec{r}_i$) and spin (s_i) coordinates, collectively grouped as ($\vec{x}_i$), and the square of the wavefunction gives the probability density of finding the electrons in state $\vec{x} = \vec{x}_1, \vec{x}_2, ...\vec{x}_N$. The property that electrons are indistinguishable from each other requires that a probability density must not change if the position of two electrons (i and j) are switched. That is,

$$|\Psi(\vec{x}_1, \vec{x}_2, ..., \vec{x}_i, \vec{x}_j, ..., \vec{x}_N)|^2 = |\Psi(\vec{x}_1, \vec{x}_2, ..., \vec{x}_j, \vec{x}_i, ..., \vec{x}_N)|^2. \tag{2.6}$$

The mathematical constraint required for this to be true is that these two wavefunctions can differ at most by a complex number $e^{i\phi}$. Electrons, being *fermions* (particles with spin 1/2), have anti-symmetric wavefunctions, meaning that a change

in the state of two electrons requires a sign change in the wavefunction. That is,

$$\Psi(\vec{x}_1, \vec{x}_2, ..., \vec{x}_i, \vec{x}_j, ..., \vec{x}_n) = -\Psi(\vec{x}_1, \vec{x}_2, ..., \vec{x}_j, \vec{x}_i, ..., \vec{x}_n). \tag{2.7}$$

This antisymmetry principle is what enforces the Pauli exclusion principle, which states that no two electrons can occupy the same state.

2.2.2 Variational Principle

The first step towards finding a solution to Schrödinger's equation is to set up the Hamiltonian for the system. By close inspection of the electronic Hamiltonian in Equation 2.3, this requires the knowledge of only the number of electrons in the system and the position and charge of the nuclei. The other terms, such as the kinetic energy of the electrons ($\hat{T}$) and electron-electron Coulomb potential ($\hat{V}_{ee}$), are independent of the particular molecule of interest. The second step is to obtain the wavefunctions Ψ_i, and subsequently the corresponding allowed energies E_i for the Hamiltonian. Of course, it is this step which poses the most prominent challenge of quantum mechanics since no analytic method of solving Schrödinger's equation exists, at least for systems containing more than one electron. However, several methods to determine the wavefunctions have been proposed, the most prominent of which invokes the variational principle. From quantum mechanics, we know that the expectation value of any observable $\hat{O}$ requires the integration over all coordinates,

$$\langle \hat{O} \rangle = \int ... \int \Psi^*_{trial} \, \hat{O} \, \Psi_{trial} d\vec{x}_1 d\vec{x}_2 ... d\vec{x}_N = \langle \Psi_{trial} | \hat{O} | \Psi_{trial} \rangle, \tag{2.8}$$

where Ψ is normalized, $d\vec{x}_1 d\vec{x}_2 ... d\vec{x}_N$ are volume elements, and the rightmost equality is the integral in Dirac notation. Thus, the total energy of a system is given by

the expectation value of the Hamiltonian. The variational principle states that the energy, as determined by the expectation value of the Hamiltonian operator $\hat{H}$ from a trail wavefunction Ψ_{trial}, will always be an upper bound to the ground state energy, and that equality will only hold when the trail wavefunction is identical to the ground state wavefunction. That is,

$$\langle \Psi_{trial} | \hat{H} | \Psi_{trial} \rangle = E_{trial} \geq E_0 = \langle \Psi_0 | \hat{H} | \Psi_0 \rangle. \tag{2.9}$$

Thus, the ground state wavefunction of the system Ψ_0 is approached as the total energy is lowered, and the energy given by the ground state wavefunction is the ground state energy E_0. In summary, the ground state total energy is obtained by a minimization of the total energy, a functional of the wavefunction, which is the expectation of the Hamiltonian operator integrated over all coordinates in the wavefunction. The word *functional* is used in regards to the energy $E[\Psi]$ being a function of another function $\Psi(\vec{x})$. Conceptually, the variational principle appears as

$$E_0 = \min E[\Psi] = \min \langle \Psi | \hat{H} | \Psi \rangle = \min \langle \Psi | \hat{T} + \hat{V}_{Ne} + \hat{V}_{ee} | \Psi \rangle. \tag{2.10}$$

2.2.3 Hartree Fock Approximation

The variational principles provides a mathematical construct that can be used to obtain the ground state wavefunction and ground state energy of the system. However, in practice, searching over all possible wavefunctions is impossible. The methods by Hartree and Fock, provide an approximation to the exact wavefunction of a many electron system that allows for practical utilization of the solving the Schrödinger equation. In this method, the N electron wavefunction is approximated by a Slater determinant, an antisymmetrized product of N single electron wavefunctions. The

Slater determinant, Φ_{SD}, is written as a matrix of the form:

$$\Psi_0 \approx \Phi_{SD} = \frac{1}{\sqrt{N!}} \begin{vmatrix} \chi_1(\vec{x}_1) & \chi_2(\vec{x}_1) & ... & \chi_N(\vec{x}_1) \\ \chi_1(\vec{x}_2) & \chi_2(\vec{x}_2) & ... & \chi_N(\vec{x}_2) \\ \vdots & \vdots & \ddots & \vdots \\ \chi_1(\vec{x}_N) & \chi_2(\vec{x}_N) & ... & \chi_N(\vec{x}_N). \end{vmatrix} \tag{2.11}$$

The functions $\chi_i(\vec{x}_i)$ are single electron wavefunctions and contain both a spatial function $\phi_i(\vec{r})$ and one of two spin functions $\alpha(s)$ or $\beta(s)$. The spin functions must hold the property of orthonormality, meaning $\langle\alpha|\alpha\rangle = \langle\beta|\beta\rangle = 1$, and $\langle\alpha|\beta\rangle = \langle\beta|\alpha\rangle = 0$. The antisymmetrized nature of the Slater determinant comes from the property that upon exchanging two rows or two columns, the determinant undergoes a change in sign. The variational principle within the Hartree-Fock approximation now appears similar to the leftmost equality of Equation 2.10, except the energy E_0 is now the Hartree-Fock energy, E_{HF}. The Hartree-Fock energy is obtained by computing the expectation value of the Hamiltonian given by the Slater determinant of a system, not the total wavefunction. The Hamiltonian operator, with use of the Slater determinant, is written as:

$$E_{HF} = \langle\Phi_{SD}|\hat{H}|\Phi_{SD}\rangle = \sum_i^N (i|\hat{h}|i) + \frac{1}{2}\sum_i^N \sum_j^N (ii|jj) - (ij|ji), \tag{2.12}$$

where

$$(i|\hat{h}|i) = \int \chi_i^*(\vec{x}_1) \left\{ -\frac{1}{2}\nabla^2 - \sum_A^M \frac{Z_A}{r_{1A}} \right\} \chi_i(\vec{x}_1) d\vec{x}_1, \tag{2.13}$$

$$(ii|jj) = \int\int |\chi_i(\vec{x}_1)|^2 \frac{1}{r_{12}} |\chi_j(\vec{x}_2)|^2 d\vec{x}_1 d\vec{x}_2, \tag{2.14}$$

and

$$(ij|ji) = \int\int \chi_i(\vec{x}_1)\chi_j^*(\vec{x}_1)\frac{1}{r_{12}}\chi_j(\vec{x}_2)\chi_i^*(\vec{x}_2)d\vec{x}_1 d\vec{x}_2. \tag{2.15}$$

Equation 2.13 is the sum of the electron kinetic energy term and the electron-nuclear attraction term. Equations 2.14 and 2.15 are the Coulomb and exchange integrals, respectively, and together form the Hartree-Fock potential, V_{HF}, felt by single electron. The Coulomb term represents the potential experienced by an electron in spin orbital χ_i and at position $\vec{x}_1$ due to another electron in spin orbital χ_j and at position $\vec{x}_2$, and the term is integrated over all space. The exchange term arises from the possibility of an exchange between an electron in spin orbital χ_i and at position $\vec{x}_1$ and an electron in spin orbital χ_j and at position $\vec{x}_2$. It is important to note that the property of orthonormality for spin orbitals causes the exchange term to go to zero for electrons with different spins, meaning that electron exchange only exists for electrons of the same spin. Lastly, within the Hartree-Fock equations, an electron can interact with itself when $i = j$ in Equation 2.14. However, this unphysical *self-interaction* term is cleverly removed, because when $i = j$ the Coulomb and exchange integrals exactly cancel out. Thus in the Hartree-Fock method, this artificial electron self-interaction is removed by a mathematical "trick"; but, as will be shown later, self-interaction is not entirely removed in DFT, and can lead to errors in certain types of calculations.

In summary, the Hartree-Fock approximation provides a practical approach to solving the Schrödinger equation by using a simplified, yet reasonable, representation of a given system's wavefunction. With the implementation of the Slater determinant and the HF operator, the N electron interaction problem is reduced to N single electrons interacting in a potential V_{HF}. Lastly, the HF approach introduces the nature of the *self-consistent field* (SCF) approximation as a method for solving the

HF equations. The overall concept of this technique is to initially guess a set of orbitals that are used to construct the HF potential, V_{HF}. The potential is then used to solve the HF equations to gain a new set of orbitals, which again construct a new HF potential. This iterative approach is continued until a point where the output orbitals match (at least to within a certain precision) the input orbitals, and thus self-consistency is achieved. The SCF method is at the core of Density Functional Theory, which is introduced in the following sections.

2.3 Density Functional Theory

2.3.1 Introduction

The methods introduced so far provide the mathematical framework to construct a Hamiltonian from which the ground state wavefunction of a chemical system can be determined. With the ground state wavefunction one can obtain all the ground state properties of the system. In practice, using the N electron wavefunction, consisting of $3N$ spatial plus N spin coordinates, to solve the Schrödinger equation is highly complex task and even the simplified techniques of Hartree and Fock are limited to small molecules. This has led to rethinking of the necessity of the wavefunction Ψ as the principle variable in solving these equations, and the the following sections introduce the use of the electron density $\rho(\vec{r})$ as an alternative to the N electron wavefunction. As will be shown, the electron density can be used to uniquely construct an external potential which, as discussed in the previous section, can be used to self-consistently solve the Hartree-Fock equations; and this external potential will correspond to a unique ground state energy. That is, each electron density yields its own ground state energy. However, it will also be shown that there is no universal

functional to compute the total energy from the electron density. The purpose of DFT is to approximate a method that does.

The electron density is similar to the probability density first shown in Equation 2.7, and is defined by

$$\rho(\vec{r}) = N \int ... \int |\Psi(\vec{x}_1, \vec{x}_2, ..., \vec{x}_N)|^2 d\vec{r}, \tag{2.16}$$

which is the probability of finding the i^{th} electron out of a system of N electrons at any point in volume $d\vec{r}$, where $d\vec{r}$ contains all the volume elements $d\vec{x}_1 d\vec{x}_2 ... d\vec{x}_N$. The electron density holds the property

$$\int \rho(\vec{r}) d\vec{r} = N, \tag{2.17}$$

that states upon integration over all the volume elements will result in the total number of electrons N.

The most famous early example of using the electron density as a principle variable in determining properties of a species dates back to Thomas and Fermi in 1927.[61] The Thomas-Fermi model used solely the electron density to determine the total energy of an atom by the equation

$$E_{TF}[\rho(\vec{r})] = \frac{3}{10}(3\pi^2)^{\frac{2}{3}} \int \rho^{\frac{5}{3}}(\vec{r}) d\vec{r} - Z \int \frac{\rho(\vec{r})}{r} d\vec{r} + \frac{1}{2} \int \int \frac{\rho(\vec{r}_1)\rho(\vec{r}_2)}{r_{12}} d\vec{r}_1 d\vec{r}_2 \tag{2.18}$$

The first term represents the kinetic energy and is derived from a quantum statistical treatment of electrons interacting in a uniform, delocalized electron gas. The second and third terms are the nuclear-electron attraction and electron-electron repulsion terms, respectively, and are treated by a classical description of interacting charged particles. Clearly, this third term includes only Coulombic electron-electron repulsion

and not electron exchange. Further improvements to the method by Dirac includes an exchange term,

$$K_D[\rho] = -\frac{3}{4}\left(\frac{3}{\pi}\right)^{1/3} \int \rho^{4/3}(\vec{r})d\vec{r}, \tag{2.19}$$

and its inclusion leads to what is referred to as the Thomas-Fermi-Dirac model.[62] The importance of Equation 2.18 is not in its accuracy in defining the total energy, which it is not accurate at all.[63] The importance is that it uses only the electron density to do so. One of the major flaws arises from representing the kinetic energy by electrons interacting in a uniform electron gas.

2.3.2 Hohenberg-Kohn Theorems

The next major cornerstone that used the electron density as the principle variable to determine the properties of a system came almost 40 years after Thomas-Fermi model when Hohenberg and Kohn published their two infamous theorems in 1964.[64] These two theorems are central to density functional theory and established the theoretical framework of modern day efforts that use the electron density to determine properties of a system. Their first theorem justifies the use of the electron density to uniquely construct the Hamiltonian operator. As it is stated in their original paper:

> The external potential $V_{ext}(\vec{r})$ is (to within a constant) a unique functional of $\rho(\vec{r})$; since, in turn $V_{ext}(\vec{r})$ fixes $\hat{H}$ we see that the full many particle ground state is a unique functional of $\rho(\vec{r})$.

Their proof showed that two different potentials $V_{ext}(\vec{r})$ and $V'_{ext}(\vec{r})$ cannot produce the same electron density $\rho(\vec{r})$, which means that the true ground state density $\rho(\vec{r})$ uniquely defines the external potential $V_{ext}(\vec{r})$ (to within a constant). The key here is that the electron density is now justified as a physically sound parameter in determining the external potential, which in a Hamiltonian operator for a chemical system,

would be the electron-Nuclear potential. However, the Hamiltonian contains other terms (electron kinetic energy and electron-electron repulsion), which Hohenberg and Kohn proposed are, like V_{ext}, also functionals of the electron density. That is,

$$F_{HK}[\rho] = T[\rho] + V_{ee}[\rho] = \langle \Psi | \hat{T} + \hat{V}_{ee} | \Psi \rangle, \tag{2.20}$$

where F_{HK} is a functional that when operates on the electron density, produces the expectation value of the kinetic $\hat{T}$ and electron-electron repulsion $\hat{V}_{ee}$ operators in the ground state wavefunction. This is followed by a second theorem, which essentially is the variational principle applied to the Hohenberg-Kohn functional $F_{HK}[\rho]$, and as it is written in their original paper, states:

> A universal functional for the energy $E[\rho]$ in terms of the density $\rho(\vec{r})$ can be defined, valid for any external potential $V_{ext}(\vec{r})$. For any particular potential, the exact ground state energy of the system is the global minimum value of this functional, and the density that minimizes the functional is the exact ground state density $\rho_0(\vec{r})$.

The theorems by Hohenberg and Kohn states that the electron density is a physically sound parameter that *can* be used in place of the wavefunction to initially construct the Hamiltonian and arrive at the ground state total energy through the variational principle. It is important to note however, that the theorems does not explain *how* this can be done and *how* to construct the functional F_{HK}. How to apply the theorems by Hohenberg and Kohn was not known until a year later in 1965, when Kohn and Sham suggested a method to construct a universal functional,[65] which can be used to determine the ground state properties of a system.

2.3.3 The Kohn-Sham Approach

Density functional theory, as it is known today, holds its practical origins in the *ansatz* by Kohn and Sham that the exact calculation of many-body properties can, in principle, be determined by independent particle methods.[65] The approach takes the many-body, interacting-particle system, which is difficult to solve, and replaces it with an auxiliary system of non-interacting particles. The auxiliary system is made of single electron orbitals used to construct a Slater determinant, similar to how single electron wavefunctions were used to construct a Slater determinant in the Hartree-Fock approach.

As stated earlier, one of the major problems with the Thomas-Fermi approach was that it poorly represented the kinetic energy. This is particularly because the electron density is represented by nothing more than a uniform electron gas, and the kinetic contributions to the electron correlation are neglected. The Kohn-Sham approach splits the kinetic energy into two terms: one where the exact kinetic energy of non-interacting electrons is computed (the main contribution to the kinetic energy), and another where the electron correlation contribution to the kinetic energy is approximated (a relatively small contribution to the kinetic energy). This non-interacting, auxiliary system is fictitious, but as it turns out provides a reasonably accurate method to calculate the kinetic energy.

To actually represent this auxiliary system, a set of single electron orbitals, or Kohn-Sham orbitals as they are commonly referred to, are used. These single electron orbitals are used to construct the auxiliary electron density,

$$\rho = \sum_{i=1}^{N_{elec}} |\phi_i|^2 , \tag{2.21}$$

which is operated on by the kinetic energy operator

$$T[\rho] = \sum_{i=1}^{N_{elec}} \langle \phi_i \left| -\frac{1}{2}\nabla^2 \right| \phi_i \rangle \tag{2.22}$$

to give the exact kinetic energy of a system of non-interacting electrons. This is the same kinetic energy operator used in the Hartree-Fock method, except here the Laplace operator ∇^2 operates on single electron Kohn-Sham orbitals $\phi(\vec{r})$ rather than single electron wavefunctions $\chi_i(\vec{x}_i)$.

The total energy within the Kohn-Sham approach becomes a functional of the electron density ρ and is written as

$$E_{KS} = T[\rho] + J[\rho] + E_{Ne}[\rho] + E_{XC}[\rho], \tag{2.23}$$

where T$[\rho]$ is the exact kinetic energy of the non-interacting system, and Coulomb repulsion J$[\rho]$ is

$$J[\rho] = \frac{1}{2}\sum_{i}^{N}\sum_{j}^{N} \int\int |\phi_i(\vec{r}_1)|^2 \frac{1}{r_{12}} |\phi_j(\vec{r}_2)|^2 \, d\vec{r}_1 d\vec{r}_2, \tag{2.24}$$

and Coulomb Nuclear-electron attraction E$_{Ne}[\rho]$ is

$$E_{Ne}[\rho] = \sum_{i}^{N} \int \sum_{A}^{M} \frac{Z_A}{r_{1A}} |\phi_i(\vec{r}_1)|^2 \, d\vec{r}_1. \tag{2.25}$$

The importance here is that, with the exception E$_{XC}[\rho]$, each of these terms has an explicit functional form. And that the functional form is dependent on only the electron density, which is the sum of the single electron orbitals (Equation 2.21). The three terms $J[\rho]$, $E_{Ne}[\rho]$, and $E_{XC}[\rho]$ of the Kohn-Sham energy now make up a V$_{eff}$ potential felt by the single electrons, which with the kinetic energy operator, operates

on the single electron orbitals as an eigenvalue problem:

$$\left(-\frac{1}{2}\nabla^2 + V_{eff}(\vec{r}_1)\right)\phi_i = \epsilon_i\phi_i. \tag{2.26}$$

Now, solving the Kohn-Sham orbitals is done self-consistently, as in the Hartree-Fock approximation, since solving the Kohn-Sham equations produces a new V_{eff}, which in turn produces a new set of orbitals. The beauty of the Kohn-Sham approach is that it turned a many-body problem into an independent-particle problem. It did this by separating the exact kinetic energy for a system of non-interacting particles, and then putting the remaining contribution to the kinetic energy (as well as contributions to the potential energy) in the E_{XC} term. This stated, the exchange-correlation energy is the only remaining term in the Kohn-Sham energy (Equation 2.23) for which there exists no explicit functional form. Much progress has been made to yield an approximate form, but modern research efforts are still aimed at improving E_{XC}.

2.3.4 Exchange-Correlation Functionals

Within the DFT framework, most major differences in results stem from the treatment of electron exchange and correlation. Each contribute as separate terms to the exchange-correlation energy, and within DFT are calculated as a functional of the electron density at all points in space. A popularly implemented treatment of E_{XC} is called the Local Density Approximation (LDA), which treats the local electron density as a slowly varying function that is essentially a homogeneous electron gas. Recall from the introduction to this section that the Dirac exchange (Equation 2.19) was an extension to the Thomas-Fermi model and thus pertains to a uniform electron gas. The LDA method derives its roots from the Dirac exchange, and is calculated by this same equation. An extension of the LDA method applies for systems open-shell

systems (systems containing unpaired electrons) and is referred to as the Local Spin Density Approximation (LSDA). Similar to the Dirac exchange of Equation 2.19, the LSDA exchange becomes

$$E_X^{LSDA}[\rho_\alpha, \rho_\beta] = -\frac{3}{4}\left(\frac{3}{\pi}\right)^{1/3} \int \left(\rho_\alpha^{4/3}(\vec{r}) + \rho_\beta^{4/3}(\vec{r})\right) d\vec{r}, \tag{2.27}$$

where the subscripts α and β denote the spin-up and spin-down electrons, respectively. Analytic expressions of the correlation contribution ($E_C^{L[S]DA}$) have been proposed by a number of groups, but will quickly become cumbersome if discussed here. The reader is referred to some of the most widely used treatments, such as the one developed by Vosko, Wilk, and Nusair in 1980 and referred to as the VWN potential.[66] Despite any lengthy equations that could be written here, the L[S]DA approach is praised for its simplicity and inexpensive computational cost, especially in comparison to an exact calculation of electron exchange (e.g., Hartree exchange).

Improving the accuracy of the LDA method, the Generalized Gradient Approximation (GGA) formalism is introduced. The GGA method includes not only information of the electron density $\rho(\vec{r})$ at a particular point in space, but also the gradient of the electron density between two points $\nabla\rho(\vec{r})$. The purpose is to account for the realistic nature of the true electron density, which is not the homogeneous electron gas the LDA method approximates it as. Perhaps the most commonly implemented variation of the GGA method is that implemented by Perdew, Burke, and Ernzerhof in 1996,[67] where the electron exchange energy is defined as a multiplicative factor of the LDA exchange as

$$E_X^{PBE} = E_X^{LDA} F(x), \tag{2.28}$$

where

$$F(x) = 1 + a - \frac{a}{1 + bx^2}, \tag{2.29}$$

and

$$x = \frac{|\nabla \rho|}{\rho^{4/3}}. \tag{2.30}$$

Again, for full details of the functional form, the reader is referred to the original work of the developing authors.[67]

One last important aspect of DFT is the manner in which it accounts for electron self-interaction. Recall that in the Hartree-Fock approximation, the Coulomb term (Equation 2.14) allowed for electron self-interaction (i.e., when $i = j$), but that mathematically this was corrected because the exchange term exactly equaled the Coulomb term when $i = j$. In DFT, electron self-interaction is again allowed since the two electron densities $\phi_i(\vec{r}_1)$ and $\phi_j(\vec{r}_2)$ used to compute the Coulomb repulsion (Equation 2.24) can both be equal when $i = j$. However, now the exchange term, which is part in the exchange-correlation functional, is computed entirely separate from the Coulomb repulsion. So, while most exchange-correlation functionals partially account for the self-interaction, they are not 100% self-interaction free. As will be discussed in Section 3.2, this drawback of DFT leads to some intrinsic errors, especially for narrow d-band metal oxides such as TiO_2.[68]

2.4 Computational Methodology

Within this PhD, all geometry optimizations and total energy calculations were performed within the GGA formalism as implemented by Perdew, Burke, and Ernzerhof.[67] The Kohn-Sham equations were solved using the commercial software Vienna Ab-initio Simulation Package (VASP),[69] which uses a plane-wave basis set to expand

the Kohn-Sham orbitals. Because it is unnecessary (and computationally expensive) to explicitly solve the Kohn-Sham equations for core electrons that are chemically inert, core-potentials were employed. While in localized basis sets (e.g., Gaussian type orbitals) the use of core potentials it strictly related to a computational expense advantage; however, it is necessary to use them with plane-wave basis sets, because the high density of nodal features at the atomic core would require an infinitely large basis set. In this PhD, the core potentials are treated by the projector-augmented wave (PAW) method.[70,71] With the core electrons accounted for in the PAW potential, the valence states of Ti, O, and Pd are then described by [Ar] $3p^6 3d^3 4s^1$, [He] $2s^2 2p^4$, and [Kr] $5s^1 4d^9$ electron configurations, respectively. Geometry optimizations were performed using the conjugate-gradient algorithm,[72] and atomic positions were only considered optimized when all cartesian force components were 0.01 eV/Å or less. When the conjugate-gradient failed to reach the optimization threshold, the optimizations were continued using a quasi-Newton algorithm. The actual algorithm is called the residual minimization method and it is combined with a direct inversion of the iterative subspace (RMM-DIIS) as proposed by Pulay.[73] With a good initial guess at the atomic positions, the RMM-DIIS algorithm is said to efficiently relax the atomic positions to their ground state.[74]

Convergence tests must be performed to determine the completeness of the plane-wave basis set in representing the single electron Kohn-Sham orbitals. With plane-wave basis sets, the completeness is determine by the plane wave with the highest kinetic energy (i.e., kinetic energy cut-off), and governs the inherent accuracy of the total energy calculation. The computational expense increases drastically with an increasingly large basis set, hence the goal is to balance the trade-off between computational expense and inherent accuracy. By performing a series of single-point calculations on the 1x1 unit cell of bulk TiO_2, the kinetic energy cut-off of 400 eV

was found to provide convergent results. The reader is referred to a report by Hafner for addtional details on the advantages and uses of a plane-wave basis set.[75]

Similar to basis set completeness, an increase in mesh size used for Brillouin zone sampling, at least in principle, provides more accurate results. To this end, calculations of a mesh consisting of only the Γ point, as well as calculations using a 2x2x1 Monkhorst Pack $\vec{k}$-points mesh, were performed. The two mesh sizes were found to give identical results (to within 0.01 eV). This stated, the Brillouin zone was sampled at only the Γ point for all calculations.

2.4.1 Analyzing Cluster Support Interactions

For pure (un-oxidized) Pd_n clusters, there are several energetic quantities of interest to help quantify the interaction with the surface and any structural changes the cluster undergoes upon adsorption. To analyze the amount of deformation both the cluster and surface undergo upon adsorption, several single point calculations are performed where the coordinates are kept in the positions obtained from the surface optimizations. The energy difference between the ground state free cluster and ground state supported cluster is the cluster deformation energy $E_{def}(cluster)$, and will be calculated by the following equation:

$$E_{def}(cluster) = E'(Pd_n) - E(Pd_n), \tag{2.31}$$

where $E(Pd_n)$ is the energy of the free cluster and $E'(Pd_n)$ is the energy of the cluster in the adsorbed geometry. Likewise, the surface deformation energy $E_{def}(surface)$ will be evaluated by:

$$E_{def}(surface) = E'(TiO_2) - E(TiO_2), \tag{2.32}$$

where $E(TiO_2)$ and $E'(TiO_2)$ are the energies of the pure surface and the surface in cluster-adsorbed geometry, respectively. These deformation energies are associated with any structural change the cluster undergoes during adsorption, and will be reported for all cluster sizes.

While deformation energies provide useful information on the structural changes, the cluster binding energy will provide useful information that will lead directly to catalytically-relevant information. The binding energy of the Pd cluster to the surface, $E_{b,surf}$ is given by:

$$E_{b,surf} = E(Pd_n) + E(surf) - E(Pd_n/surf), \tag{2.33}$$

where $E(Pd_n)$, $E(surf)$, $E(Pd_n/surf)$ are the energies of the isolated Pd cluster, the pure surface, and the lowest energy Pd structure adsorbed on the surface, respectively. Likewise, the oxygen binding energy is given by,

$$E_{b,ads} = E(ads) + E(Pd_n/surf) - E(ads/Pd_n/surf), \tag{2.34}$$

which will be used to calculate the binding energetics of O or O_2. Here, $E_{b,ads}$ is the binding energy of the *adsorbate* molecule (O or O_2).

2.4.2 Bader Charge Analysis

A Bader charge analysis were performed to analyze the charge state of all atomic sites.[76] The analysis is performed on the converged electron density calculated within DFT. The charge state is calculated before and after clusters are adsorbed to have a reference for comparison. The same applies to before and after oxygen is adsorbed on the Pd_n cluster. By determining the surfaces which divide local maximum in the

charge density, atomic sites can be defined. The charge density is then integrated around the atomic site and assigned to the atom nearest to it.

2.4.3 Total and Projected Density of States

Electronic density of states (DOS) calculations will be performed to analyze the electronic structure of the cluster and support. The DOS will be calculated self-consistently as either the total (TDOS) or site-projected (PDOS). The electronic states will be integrated between a given energy range, which will typically be several electron-Volts above and below the calculated Fermi energy. For PDOS, the wave-function character will be calculated at each of the atomic sites and projected onto spherical harmonics within a given radius for that atomic type.

2.4.4 Nudged Elastic Band (NEB) Calculations

When appropriate, NEB calculations will be performed to determine transition states and minimum energy reaction pathways for reactions and diffusion profiles. In this calculation, the atomic positions corresponding to an initial and final state are specified, and a certain number of reaction steps (referred to as images) represent the atomic structure at steps along the reaction pathway. The images are optimized under the constraint that they are attracted to their neighboring images by a predetermined force that can be thought of as a mechanical spring. Each image, then, is optimized to the lowest energy configuration while maintaining a connection between neighboring images. This determines the reaction pathway, or "band", that connects the initial and final states. An odd number of image is used, along with the constraint that the energy of the center image is maximized in the direction of the band, but minimized in other directions. This effectively leads to a saddle point in

the potential energy surface, and the center image then corresponds to the transition state geometry.

3. The Bare TiO_2(110) Surface and Free Pd_n Clusters

3.1 Introduction

Titanium dioxide is the most studied single-crystal oxide surface. This is due to its variety of industrially relevant applications and its common use as a model system to investigate many basic scientific properties.[26] The three most common crystal structures of TiO_2 are rutile, anatase, and brookite. The rutile (110) surface is by far the most commonly studied form of TiO_2 due primarily to its high surface stability, making it a relatively easy surface to experimentally characterize. Further contributing to its popularity, rutile is a wide band-gap semiconductor, an active photo-catalyst, a template commonly used to investigate the surface chemistry of small adsorbant molecules, and a model system ideal for studying metal overlayer growth. Specifically, the growth of metal overlayers has largely contributed to TiO_2 surface science research, and an extensive list of the systems that have been studied has previously been reviewed.[26] The most prominent focus of this list has been on the characteristics of growth morphology, the extent of epitaxy, and interfacial charge transfer (oxidation/reduction) reactions. Additionally, since certain transition metals supported on TiO_2 are found in the strong metal support interaction (SMSI) state upon high temperature reduction, many modern research efforts are aimed at characterizing the

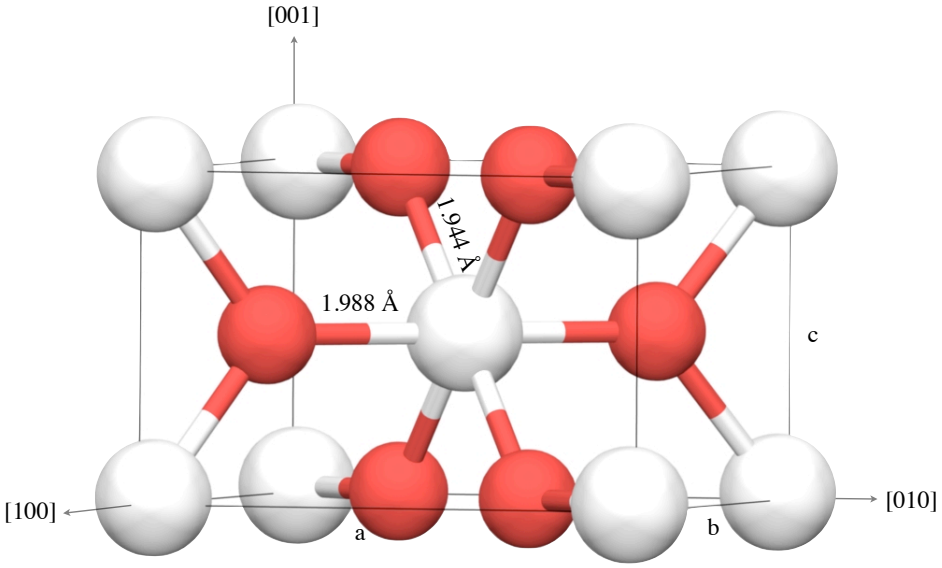

Figure 3.1: The 1x1 unit cell of bulk rutile TiO_2. Red spheres represent oxygen, white spheres represent titanium.

source of this SMSI state and the effect on the supported metal that result from it. This is of particular interest for supported catalysts, as the overall nature of the supported particle surface, including exposed active sites of a supported metal catalyst, are likely affected.

A ball and stick drawing of the 1x1 unit cell of bulk rutile TiO_2 is shown in Figure 3.1. Rutile has a tetragonal unit cell with D_{4h}^{14}-$P4_2/mnm$ symmetry and lattice constants of a = b = 4.584 Å and c = 2.953 Å. The unit cell consists of two Ti and four O atoms, and each Ti atom is surrounded by six oxygen atoms in a distorted octahedral configuration. The sixfold coordination number of Ti arises from four "short" Ti-O bonds and two "long" Ti-O bonds, which have been experimentally determined to be 1.944 and 1.988 Å, respectively.[77] Local charge transfer between Ti and O sites results in formal charge states of +4 and -2, respectively. Charge-charge repulsion between O atoms is said to be the source of elongation in the longer of the two Ti-O bonds and is what gives rise to the distorted nature of the octahedral symmetry.[78]

Like most metal oxides, bonding within TiO_2 is partially ionic and partially covalent.

3.2 Theoretical Description

In this section, a discussion of the strengths and shortcomings in describing the atomic and electronic structure of rutile by DFT is presented. As described in Chapter 2, the Kohn-Sham equations were solved within the generalized gradient approximation (GGA) formalism. Within this formalism, the lattice constants were calculated to be a = 4.64 Å and c = 2.99 Å; and the short and long Ti-O bonds were calculated to be 1.97 and 2.00 Å, respectively. The ground state lattice constant was determined variationally by performing a series of single-point calculations of the 1x1 unit cell across a range of lattice constant values. The value with the lowest total energy corresponds to the ground state lattice constant. With the lattice constant established, the atomic positions are then relaxed within a unit cell of fixed dimensions to determine the optimized Ti-O bond lengths. In comparison to the experimental values reported above, GGA predicts lattice constants and characteristic bond lengths in good agreement with the known experimental values.

While the atomic structure is predicted with good accuracy, one disadvantage of treating the exchange-correlation potentials within the GGA formalism is that it notoriously underestimates the TiO_2 band gap.[79,80] This error is implicit in many density functionals as it pertains to the electron self-interaction that is present in conventional DFT. This self-interaction results is an overestimated Coulomb repulsion between electrons, and thus an increased delocalization. This is particularly problematic for narrow d-band metal oxides, where d-orbital electrons typically form a localized set of states. The delocalization directly translates to DFT predicting a more metallic-like behavior for such systems. For bulk rutile, the result of this

artifact is a GGA-calculated band gap of about 1.9 eV, about 37% less than the experimental value of 3.0 eV.[81] Two approximation methods that attempt to correct this self-interaction have been proposed: hybrid functionals[82–84] and the DFT+U approximation.[85–87] Hybrid functionals correct the error by mixing a pre-determined amount of Hartree-Fock exact-exchange with the DFT exchange.[88] By including some of the exact exchange, a solution resembling the Hartree-Fock approximation is approached, where self-interaction is entirely removed (Section 2.2.3). The improvements in quality come at an extremely high computational cost as the calculation of exact exchange is extremely expensive. Further, the method requires parameterization based on empirical data (e.g., experimental TiO_2 band gap) to determine the amount of mixing between exact and DFT exchange. Thus, the method is no longer *ab initio*, and loses the feature of transferability. Loss of transferability means that the parameters used to exactly reproduce the band gap in a bulk TiO_2 calculation may not be transferrable to a calculation when Pd_n clusters are supported on TiO_2. Clearly, this is an undesirable feature.

The second option to correct for self-interaction is the DFT+U approximation, which can be applied in either the LDA or GGA formalism by adding a Hubbard U term to the Hamiltonian to artificially increase electron correlation. This method prevents artificial delocalization of electrons by energetically penalizing the occupation of a delocalized solution. The calculated effect on the electronic structure is seen as a shift of unoccupied states to higher energy and thus an increase in the calculated band gap. The calculated total and projected density of states (DOS) for the 1x1 unit cell of rutile are shown in Figure 3.2 for different values of the Hubbard U parameter. The valence band below the Fermi level (E_F=0 eV) is primarily composed of O states, and the conduction band above E_F is primarily composed of Ti states. The DOS plot clearly reflects the ionic nature of TiO_2 as such an electronic

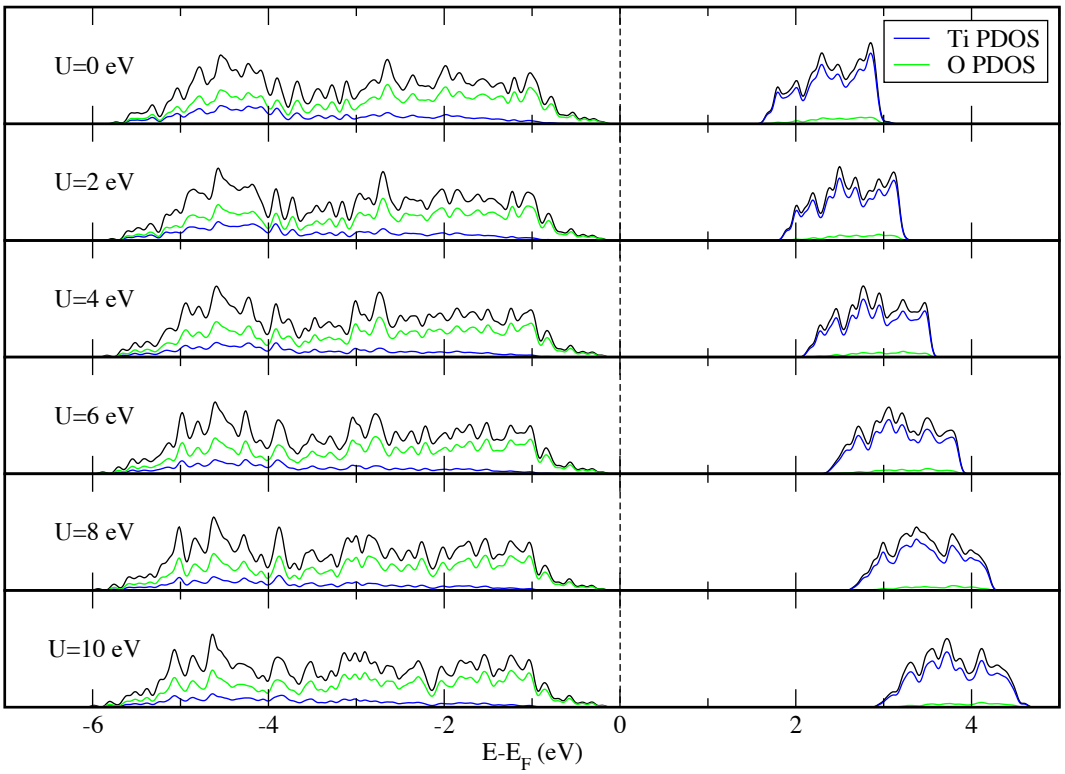

Figure 3.2: Total and projected density of states (DOS) plots for the 1x1 rutile unit cell. Blue lines represent the states projected onto Ti atoms, and the green lines represent the states projected on the O atoms. The Fermi level has been shifted to E=0. The atomic positions were optimized for each Hubbard U value, and a converged 8x8x12 $\vec{k}$-points mesh in the Monkhorst-Pack scheme was used to sample to the Brillouin zone.

structure is due to charge transfer from Ti to O. Also, the hybridization between Ti and O states in the valence band is indicative of the partial covalent nature. As the Hubbard U parameter is increased from 0 to 10 eV, there is clearly a widening of the band gap (Figure 3.2). Although at a value of U=10 eV the DFT+U approach correctly matches the experimental band gap, the method has its own set of drawbacks that become more exaggerated with an increasing U value. First, there is no universal recipe to constructing a Hubbard U Hamiltonian, so like hybrid functionals the method is no longer *ab-initio*. This method requires knowledge of the electronic

bandstructure in order to construct a Hubbard U Hamiltonian as the choice in the U value is parameterized by empirical data. Additionally, the computational expense during geometry optimizations increases as the Hubbard U is known to introduce multiple local minima in the potential energy surface to which the system can easily become trapped.[89–93]

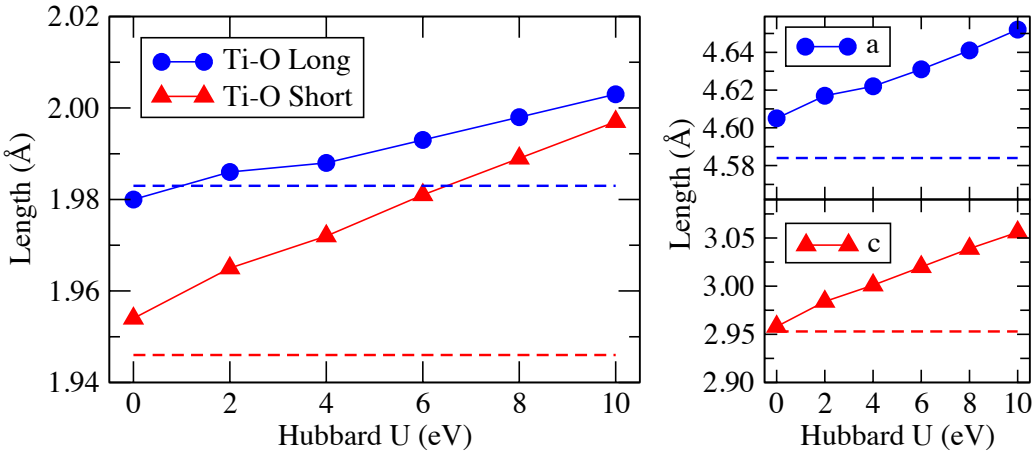

Figure 3.3: Optimized Ti-O bond lengths (left) and lattice constants (right) in Å from DFT+U calculations. Dashed horizontal lines indicate the experimental values, such as those shown in Figure 3.1.

Lastly, the improvement in calculation of the band gap comes at the expense of a less accurate description of the atomic structure. Figure 3.3 shows the effect of Hubbard U on the two characteristic Ti-O bond lengths and lattice constants. Geometry optimizations for the 1x1 rutile unit cell were performed at each Hubbard U value. The dashed horizontal lines show the experimental values for each of the four lengths. Clearly, an increasing Hubbard U value directly leads to a larger deviation from the experimental bond lengths. It is important to note that these deviations are substantially worsened in large surface supercell calculations where the atoms are not confined to the small dimensions of the 1x1 unit cell.

Hybrid functionals are not used in this study as the primary interest is the be-

havior of supported Pd_n clusters. Previous and recent studied have indicated that the gradient corrected functionals lead to electronic and magnetic properties of metal clusters that are in good agreement with observed behaviors.[28,31,34,35,94,95] As for the Hubbard U approach, there is clearly a tradeoff between an accurate description of the electronic band gap and the shortcomings of the method as described above. All results presented within the chapters of this PhD have been determined without a Hubbard U term. To examine if the band gap of TiO_2 would affect any calculated properties of Pd_n clusters, supplemental calculations were performed with the inclusion of U. The reader is referred to the Appendix for details. As shown in the Appendix, the inclusion of Hubbard U leads to no major differences in the results.

3.3 Periodic Slab Model

To simulate the rutile TiO_2(110) surface, a periodic slab with a thickness of four TiO_2 trilayers (12 atomic layers) was placed in a periodic supercell. This slab thickness has previously been shown to provide converged atomic adsorption energies,[96] and has been adopted as the standard model used in almost all recent TiO_2-supported cluster calculations.[34,97,98] The slab is shown in Figure 3.4. The surface consists of two types of Ti and two types of O atoms, which are labeled by their atomic symbol and coordination number (i.e., Ti_{5c} and Ti_{6c} for the fivefold and sixfold coordinated Ti atoms, respectively, and O_{2c} and O_{3c} for the twofold and threefold coordinated O atoms, respectively). The top layer is characterized by a "surface channel" formed by the bridging O_{2c} atoms that extend the furthest out of the (110) direction. The Ti_{5c} atoms form the center of the surface channel.

Because in this study the TiO_2 surface is used as a support for supported cluster calculations, a large surface must be used to ensure no lateral interaction between

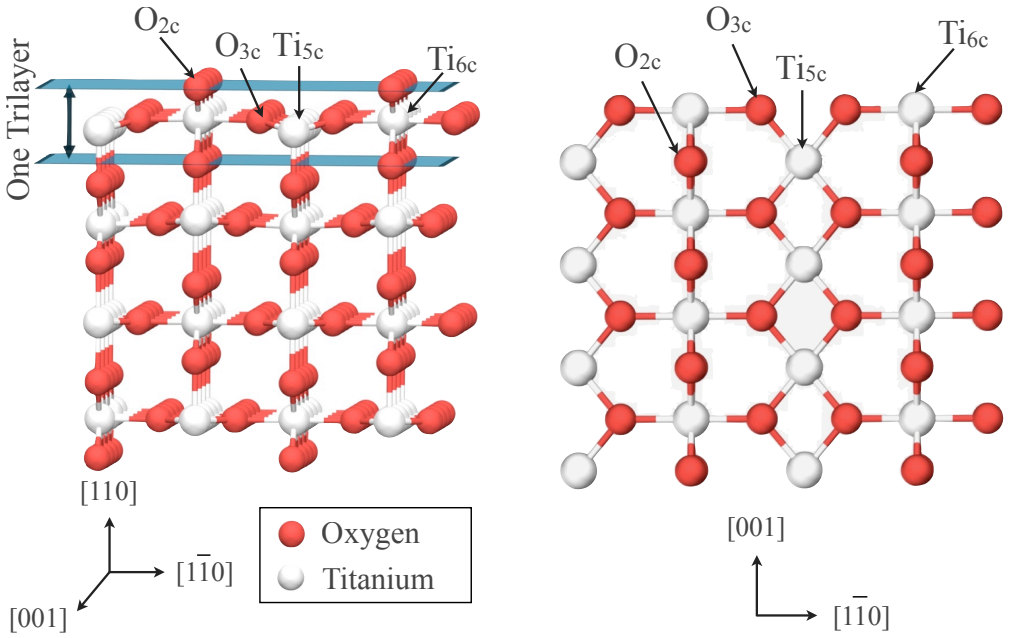

(a) Side view

(b) Top View

Figure 3.4: Ball and stick renderings of the slab model used to represent the rutile TiO_2(110) surface. For clarity, only the top trilayer is shown in (b). The four types of surface atoms are labeled by their atomic symbol and coordination number.

periodic images of supported species. A 4x2 surface supercell was chosen, which consists of four unit cells in the [001] and two in the [1$\bar{1}$0] direction. This results in a supercell with lengths of 13.1 x 11.9 Å, and is the default size used in all calculations within this PhD unless stated otherwise. The slab was separated by a vacuum layer equivalent to six trilayers (∼18 Å) in the [110] direction. The large vacuum layer ensures no "vertical" interaction between periodic images, particularly accounting for the additional height added by the Pd cluster. During all geometry optimizations, the top two trilayers were allowed to fully relax, while keeping the bottom two trilayers frozen in the calculated bulk coordinates. This is referred to as a 4(2) scheme in the literature as a total of four trilayers are used, two of which are held fixed. Within this scheme, both the surface and bulk properties of the TiO_2 support are effectively

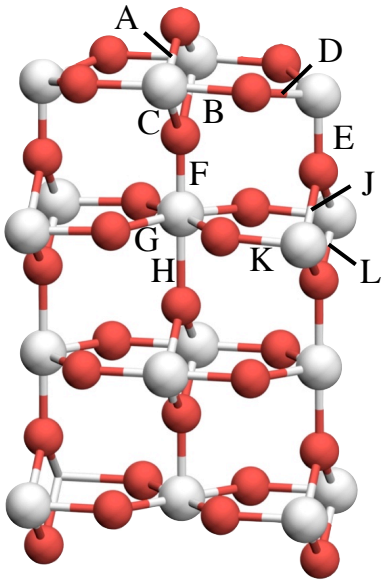

(a) Characteristic bond labels

Bond Lengths (Å)			
Bond Label	Expt.	Theor.	This Work
A	1.85	1.84	1.84
B	2.15	2.04	2.05
C	2.08	2.11	2.12
D	1.90	1.92	1.96
E	1.79	1.82	1.81
F	1.90	1.87	1.86
G	2.00	1.97	1.99
H	2.11	2.19	2.19
J	2.01	2.04	2.05
K	1.92	1.97	1.98
L	1.89	1.90	1.90

(b) Bond lengths corresponding to those labeled in part (a)

Figure 3.5: A comparison between the experimentally and previously reported theoretical bond lengths and the lengths calculated in this work. Experimental and theoretical values are those published by Lindsay et al.[100] and Thompson et al.,[96] respectively.

accounted for. Accounting for the relaxation of surface atoms has previously been shown to be necessary in predicting the adsorption site of even a single Pd atom.[99] Because the total energy is known to depend on the size of the supercell, all free cluster calculations were performed in a supercell with identical dimensions to the supercell used for the slab.

The optimized bond lengths for the TiO_2 surface have been verified to be within 5% agreement of previously reported high resolution LEED-IV experiments[100] and previously published theoretical[96] values. The ground state bond lengths, as determined by the periodic slab model described above, are reported in the table shown in Figure 3.5(b). The bond labels correspond to those shown for in Figure 3.5(a) for the four trilayer 1x1 surface.

3.4 Free Pd_n Clusters

The atomic, electronic, and magnetic properties of free Pd_n clusters have been studied both theoretically and experimentally by a number of groups.[3,9,59,101–104] This section is intended as a brief review of those studies and the properties of free Pd_n clusters as determined within the methods used in this PhD. The calculated structures for Pd_n clusters are shown in Figure 3.6. All sizes, except for the Pd atom, have spin triplet ground states, in agreement with previous studies.[9,59,102–104]

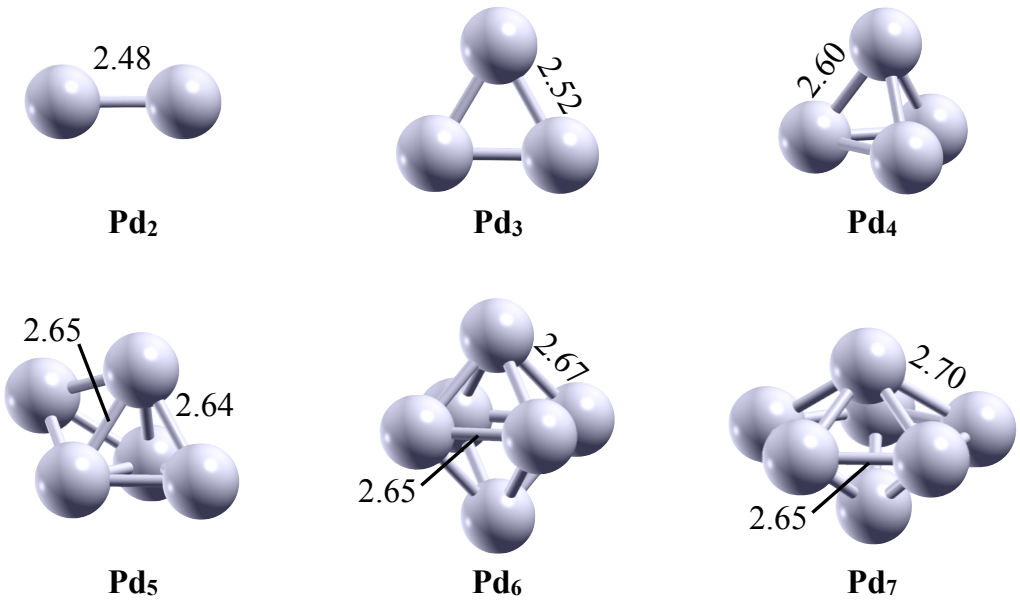

Figure 3.6: Ball and stick drawings of ground state free Pd_n clusters. Bond lengths are in angstroms.

For the Pd atom, the calculated energy difference between the singlet ground state $^1S(5s^04d^{10})$ and triplet excited state $^3D(5s^14d^9)$ is 0.90 eV, in good agreement with the experimental value of 0.82 eV.[105] For all other sizes, hybridization between s- and d- orbitals occurs and gives rise to two phenomenon. The first is a splitting of the d- orbital electronic states, which depletes otherwise fully occupied d- shell and gives

rise to the non-zero magnetic moments. The second is the compact structures as shown in Figure 3.6. The electronic states for the Pd_n clusters are shown in Figures 3.7 through 3.9. At all sizes, hybridization between s- and d- orbitals is clear, and the contribution by the p- states is rather small. With an increase in cluster size and the presence of more d- states, hybridization increases and shifts the s- states to higher binding energies. On the DOS, this is seen as the s- states pushed deeper below the Fermi energy with increasing size. Approaching the bulk limit, the s- and d- orbital hybridization will lead to a free electron-like s- band and a [relatively] narrow d-band.[106,107] The finite dimensions of clusters spatially confine electrons, forming discrete states rather than the electronic bands. While adding Pd atoms to a cluster does introduce more electronic states, the deepening of the s- states occurs to all of the sizes. This is seen in the DOS plots by comparing Pd_2 (Figure 3.7(a)), where a peak in occupied s- states lies between -0.5 eV and the Fermi level, to Pd_7 (Figure 3.9(b)), where more s- states are present, but all are shifted to -1 eV and below.

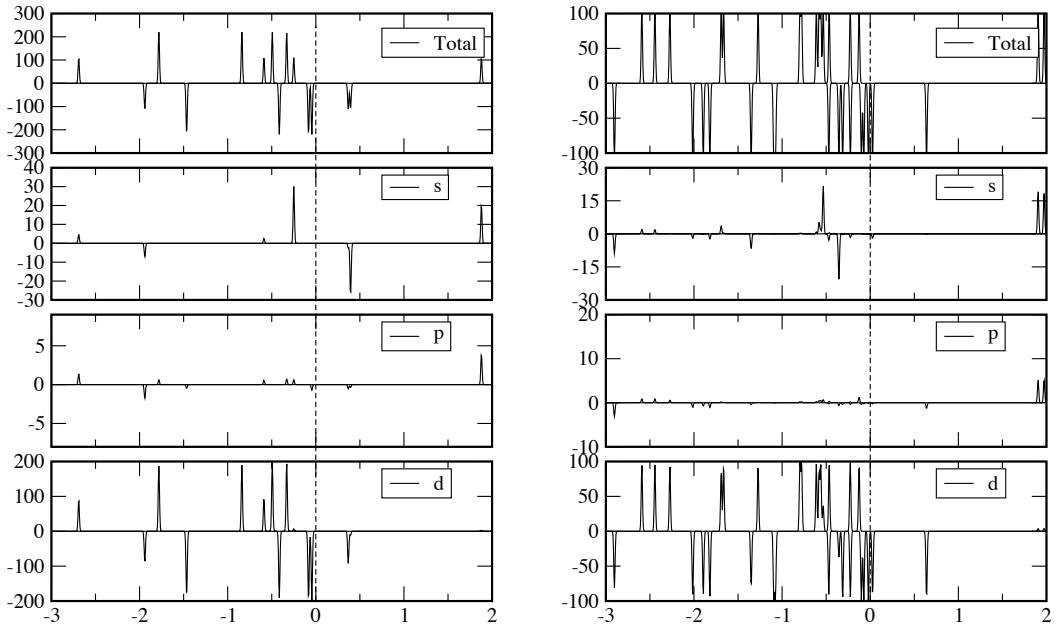

(a) Pd_2 (b) Pd_3

Figure 3.7: Density of states (DOS) plots for free Pd_2 and Pd_3 clusters. The top panel is the total DOS and the bottom panels are angular momentum decomposed DOS. The dashed, vertical line denotes the Fermi energy.

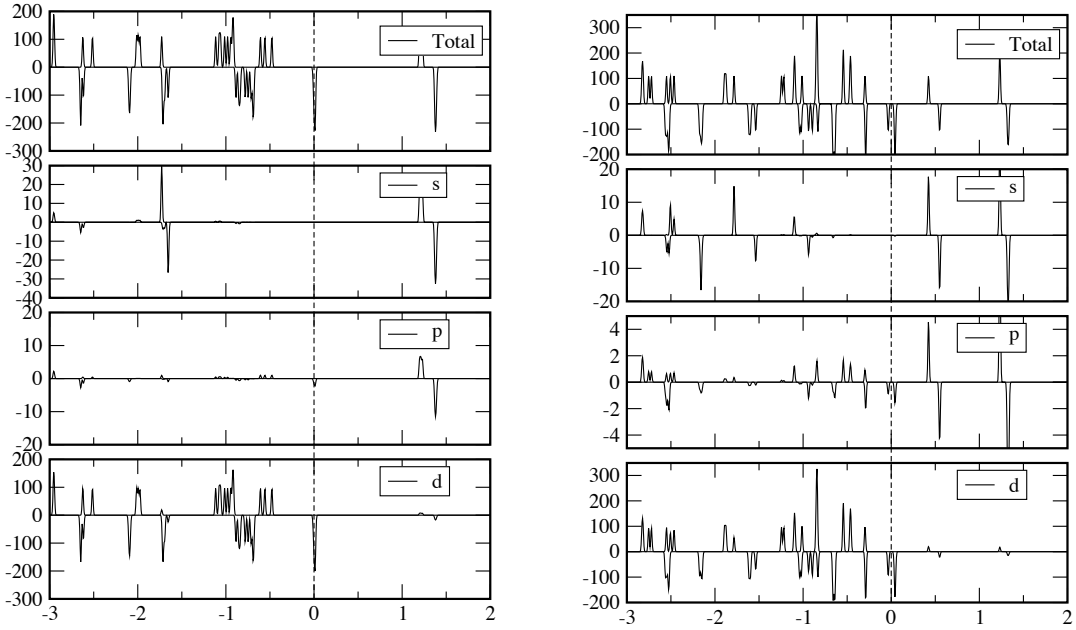

(a) Pd_4 (b) Pd_5

Figure 3.8: Same as Figure 3.7 but for Pd_4 and Pd_5.

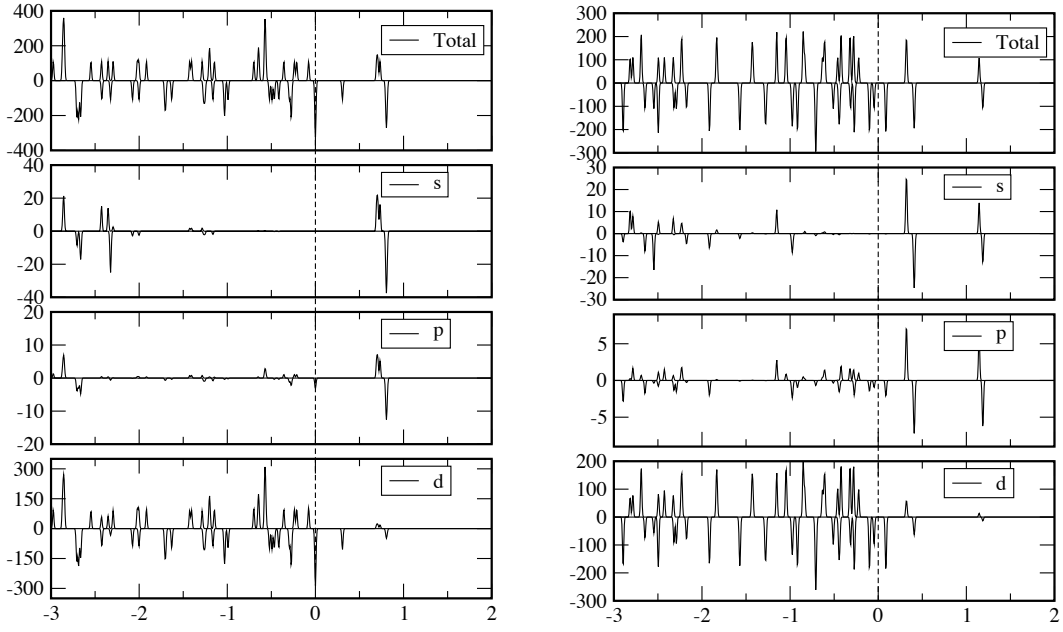

(a) Pd_6 (b) Pd_7

Figure 3.9: Same as Figure 3.7 but for Pd_6 and Pd_7.

4. The Effect of Oxidation on the Pd_4 Cluster Geometry

4.1 Introduction

One of the important findings in the numerous experimental and theoretical studies on the catalysis of free and supported clusters is that, for small clusters, the activity can change with size and that the activity of free clusters can be radically different from those of the supported species. These variations are partially rooted in the fact that the support can alter the geometrical structure of the cluster. Since the electronic structure is intimately linked to the geometry, the changed geometry can alter the reactivity. Further, the support can even enhance the activity by modulating the electronic structure through cluster support interactions. These effects are complemented by the fact that most oxidation reactions proceed via initially adsorbing oxygen, and that this adsorbed oxygen draws electronic charge from the supported species. The charging as well as the nature of metal oxygen bond can also affect the shape and electronic structure of the cluster. Consequently, understanding the role of support and oxidation on the electronic and geometric structure is vital to understanding the catalytic process and in designing effective catalysts. To gain an understanding into the roles and effects that the support and oxygen play, a comprehensive study is presented on the oxidation properties of a Pd_4 cluster supported on

the rutile TiO_2(110) surface.

One of the primary intents of this chapter is to introduce the strong tendency for oxygen to draw charge and the effect this has on the TiO_2-supported Pd_4 cluster. Additionally, as the adsorption of any species can lead to a deformation to the local surface structure to which it adsorbs, the nature of Pd_4/TiO_2 interactions is discussed with an emphasis on the nature of adsorbate induced reconstructions. As will be shown in this chapter, the Pd_4 cluster has an energetic preference to undergo a structural change upon adsorption, and this change modifies the nature of the cluster-support interaction. The importance of all these effects will be referred back to in chapters to follow. The overall theme of this chapter is to answer three questions: (1) What is the ground state structure of unoxidized, supported Pd_4 and are there competing geometries that could affect the observed behavior at finite temperatures? (2) What is the nature of cluster support interactions and do the Pd atoms primarily interact with the lattice O or the Ti sites? (3) How does the atomic structure change as successive O atoms are added to the cluster and what electronic features control the change? The answer to these questions is critical to a microscopic understanding of the catalytic phenomenon as these processes involve the addition and removal of O atoms. The emphasis on Pd_4 is twofold. First, studies on free clusters that indicate that Pd_4 is a highly stable species with a tetrahedral structure.[59] Second, the nature of the cluster-support interactions (e.g., cluster-induced surface deformations, the nature of charge transfer, trends in cluster binding energies, etc...) should be introduced in detail before continuing to the following chapters, and as will be shown, the Pd_4 cluster is the ideal template for such introduction. Ultimately, understanding the microscopic mechanism that results in structural changes for such a stable species is an important problem.

4.2 Electronic Structure Controls Reactivity

In a recent work, Kaden et al. investigated the CO oxidation by O_2 by Pd_n clusters containing between 2-25 atoms supported on the rutile $TiO_2(110)$ surface.[56] The experiments were performed within ultra high vacuum conditions (10^{-10} Torr), and the objective was to correlate changes in the electronic structure of supported Pd_n clusters with the catalytic production of CO_2. In these experiments, Pd_n cluster cations are mass selected and then deposited on rutile $TiO_2(110)$ via soft-landing deposition. This technique allows for the ultimate control of cluster size distribution, and the details of the technique can be found in a recent review by Popok et al.[108] Upon deposition, the clusters are exposed to O_2 followed by CO, and the catalytic oxidation of CO was carried out. The experiments were performed as temperature programmed reactions (TPR) to determine the activity as a function of increasing temperature. The catalytic activity of a cluster was determined by measuring the amount of CO_2 produced per TPR. To relate the cluster activity to the electronic features of the cluster, Kaden et al. probed the 3d core-level states of the Pd_n clusters through x-ray photoemission spectroscopy (XPS). Their results showed that the catalytic activity could be directly correlated with changes in the Pd 3d binding energy. In particular, clusters where the 3d level was higher than the value corresponding to a simple scaling with size, showed enhanced activity. The correlation between variations in the shift in Pd 3d binding energy and the concentration of CO_2 can be seen in Figure 4.1(a), taken from Kaden et al.[56].

The UHV experiments by the Anderson group also implemented Ion Scattering Spectroscopy (ISS) to probe the morphology of clusters mass-selected and deposited on the TiO_2 surface. Their technique is rooted on the premise that it is possible to determine the relative ratios of exposed surface atoms by measuring the kinetic

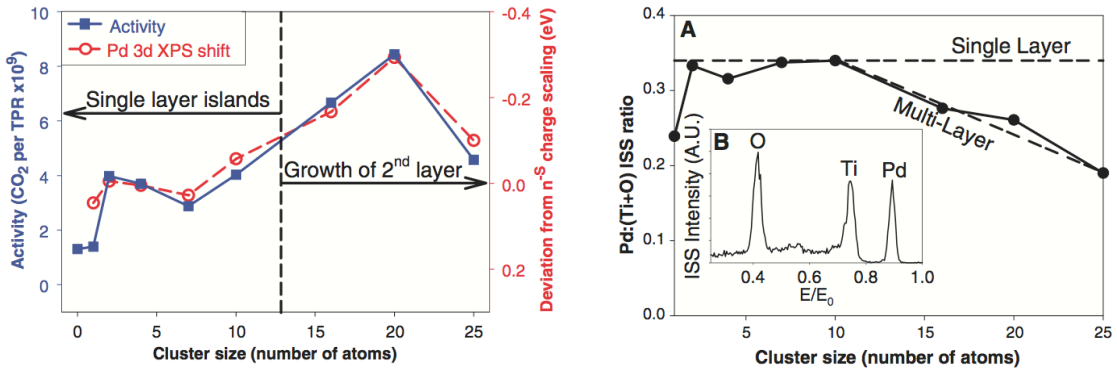

(a) XPS Data and CO_2 concentrations

(b) Ion scattering spectroscopy results

Figure 4.1: Figure (a) shows Xray photoelectron spectroscopy (XPS) data plotted with the amount of CO_2 produced at each cluster size. Figure (b) shows results from the ISS experiments from the UHV deposited cluster experiments by the Anderson group. A typical ISS spectra is shown in the inset. Such a spectra was taken at each cluster size and used to plot the data in the main portion of the figure, which shows the ratio of Pd sites to Ti+O sites.

energy of an impinging noble gas ion (e.g., He^+ ions) scattered from the Pd/TiO_2 surface. Because a collision suffered by the incident He^+ ion on a Pd vs. a Ti vs. an O site will each result in a scattered He^+ ion with different outgoing kinetic energy, the relative ratios of the He^+ ions with the three different kinetic energies is related to the concentration of each exposed surface species. Their results suggested that the clusters containing up to 10 Pd atoms are forming single layer structures and that a second layer develops as more Pd atoms are added. The planar structure for smaller species seems puzzling as the ground state atomic configuration of free (gas phase) Pd_n clusters are all compact structures. Additionally, Pd_n clusters continue to have compact structures while supported on alumina surface as indicated by recent studies within the Khanna group.[59]

A typical ISS spectra is shown in the inset of Figure 4.1(b). The ratio of exposed Pd to exposed Ti+O sites plotted as a function of size to determine changes in the cluster morphology. As seen in Figure 4.1(b), there is a decrease in the amount of

Pd sites exposed beginning at 10 atoms. At this size, the Pd:(Ti+O) ratio decreases linearly with increasing cluster size and has been interpreted by Kaden et al. as the formation of a second layer of Pd atoms.[56]

All this suggested that there are strong interactions between the palladium clusters and the TiO_2(110) surface that lead to the single layer structures observed in the UHV experiments. This conclusion is also supported by the earlier studies that observed Pd particles on TiO_2 in the SMSI state.[44,46,48] A microscopic understanding of the atomic and electronic structure of the deposited clusters is needed to understand these findings.

4.3 Theoretical Results

Geometry optimizations and total energy calculations have been performed within this PhD to determine the possibility of a three-dimensional Pd_4 cluster. The ground state structure was determined by starting from various initial configurations of the Pd_4 at various locations on the TiO_2 slab, and optimizing the geometry by moving atoms in the direction that would minimize the forces on the atoms. As palladium clusters are known to possess finite spin magnetic moments,[9,103] the ground state search also included investigation of various spin multiplicities. For determination of the ground state atomic configuration, the geometry with the lowest total energy is designated as the most stable. Higher energy isomers, which may co-exist with the ground state at finite temperatures, are also reported alongside the total energy relative to the ground state.

The results indicate a tetrahedral ground state for the adsorbed Pd_4 cluster as seen in Figure 4.2. The structure (including bond lengths) is nearly unchanged from the calculated free cluster geometry. The Pd_4 cluster sits in the surface channel made

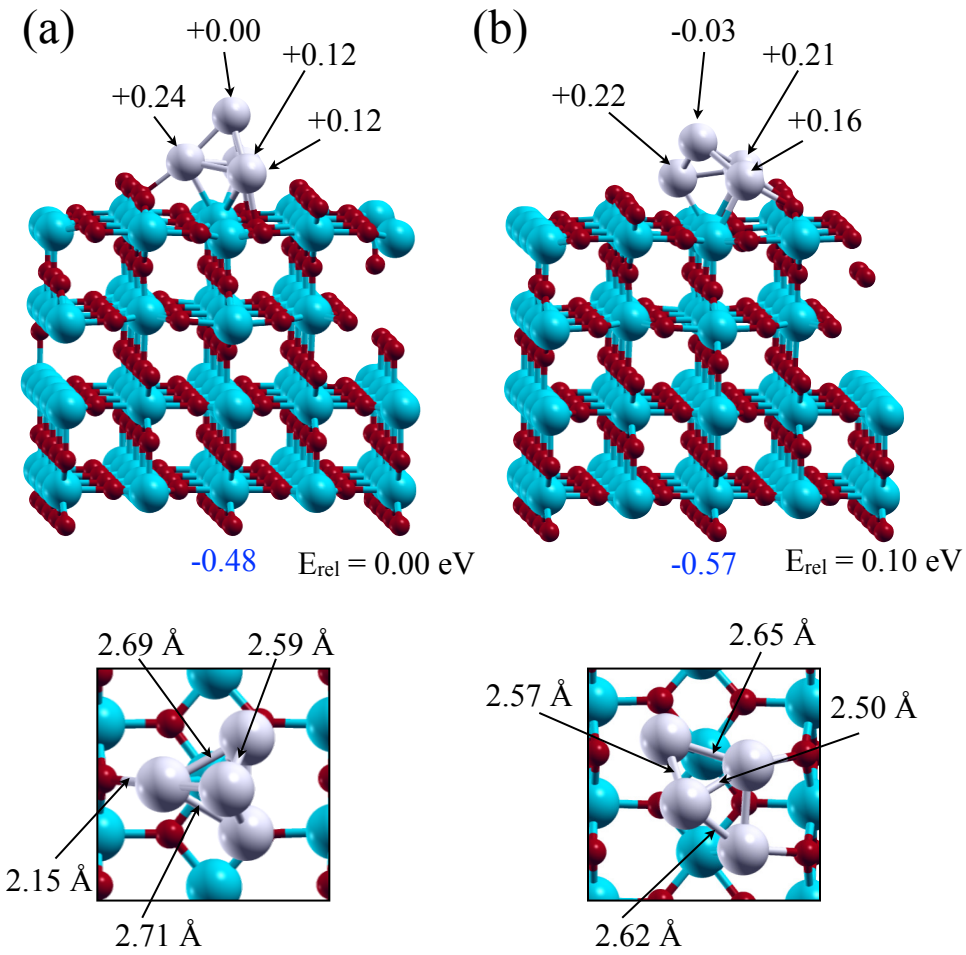

Figure 4.2: Ground state and higher energy isomer ball and stick drawings of the Pd_4 cluster on TiO_2. The positive and negative numbers in the top portion of the figure indicate the Bader charge on the Pd and O atoms, while the negative number below the surface indicates the Bader charge on the entire TiO_2 slab. The numbers on the bottom portion of the figure are bond lengths. Coloring scheme: Silver (Pd), Blue (Ti), and Red (O).

by the bridging O_{2c} atoms that protrude out of the $TiO_2(110)$ surface. Three Pd atoms are directly coordinated to the surface, and the base of the tetrahedral cluster is centered over a Ti_{5c} atom. The surface undergoes a relaxation in which several surface atoms are displaced from their initial positions. For example, by comparison with the unreconstructed surface, the Ti_{5c} atom protrudes out of the [110] plane

by a distance of 0.35 Å and shifts 0.11 Å in the $[1\bar{1}0]$ direction, centering directly beneath the base of the Pd_4 tetrahedral. The bridging O_{2c} atom nearest to the Pd_4 cluster, depicted with a drawn bond in Figure 4.2(a), is tilted towards the channel by 0.11 Å from its initial position. This leaves a Pd-O bond length of 2.15 Å on this side of the cluster, while the two Pd atoms on the other side of the cluster are each about 2.90 Å away from the O_{2c} atoms nearest to them. As the surface undergoes substantial relaxation, the energy required for the surface deformation was also calculated. This was done by comparing the total energy of the bare surface frozen in the atomic positions when the cluster is supported to the total energy of the relaxed, bare surface (see Equation 2.32 from Section 2.4.1). The calculated surface deformation energy was 1.27 eV for the ground state supported Pd_4 cluster. The ground state has a spin magnetic moment of 2.0 μ_B that is localized entirely on the Pd d-states. This indicates that the cluster maintains its free cluster geometry and spin configuration when deposited on $TiO_2(110)$.

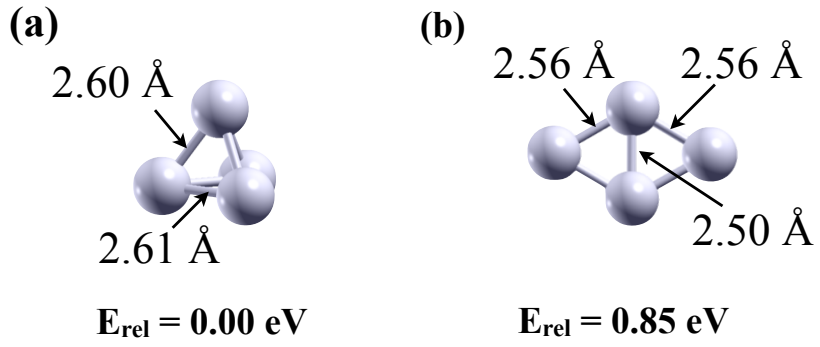

Figure 4.3: Ground state and higher energy isomer ball and stick drawings of the free (gas phase) Pd_4 cluster.

The ground state is followed by a pseudo-planar structure, which is only 0.10 eV above the ground state and is shown in Figure 4.2(b). Within the accuracy of the density functional approach this energy difference is small, and the pseudo-planar

structure can be considered as an isomer that co-exists with the tetrahedral structure. This pseudo-planar geometry also sits inside the surface channel; however, this isomer sits over two protruding Ti atoms. The cluster is partially flattened out on the surface in comparison to the tetrahedral ground state. This effectively leads to shorter bond lengths of around 2.23 Å between three of the Pd and neighboring O_{2c} atom pairs. The higher coordination between Pd atoms and surface atoms leads to the quenching of the magnetic moment of the cluster. The small energy difference between pseudo-planar and compact structure is quite striking for two reasons. First, the calculations on a free Pd_4 cluster show that a planar structure is almost 0.85 eV less stable than the compact structure, as shown in Figure 4.3(b). Second, the Pd_4 cluster maintains its compact structure when deposited on an alumina surface.[59] What features then stabilize the planar structure in the present case? What role does the planar structure play in oxidation reactions?

These questions were answered by investigating the effect of adding an O atom to the cluster. The focus on Pd_4 clusters with only a single O atom stems from the understanding that O-O bonds from adsorbed O_2 are expected to be activated (if not completely dissociated) at the Pd surface during oxidation. Adsorption of molecular oxygen at the Pd(111) surface occurs dissociatively and without an activation barrier.[109] The result is two atomically adsorbed O atoms at threefold hollow sites on the palladium surface.[109] Additionally, if an oxidation reaction is to take place (e.g., oxidation of carbon monoxide), one of the two O atoms will be removed leaving a single O atom on the cluster surface. Thus, Pd_4O clusters are likely to be stabilized under typical reaction conditions. To determine the ground state structure, geometry optimizations for 13 different conformations of an O atom and supported Pd_4 cluster were performed. The optimum binding site was found by relaxing the O atom, the Pd_4 cluster, and the top two trilayers of the support for all initial binding sites and

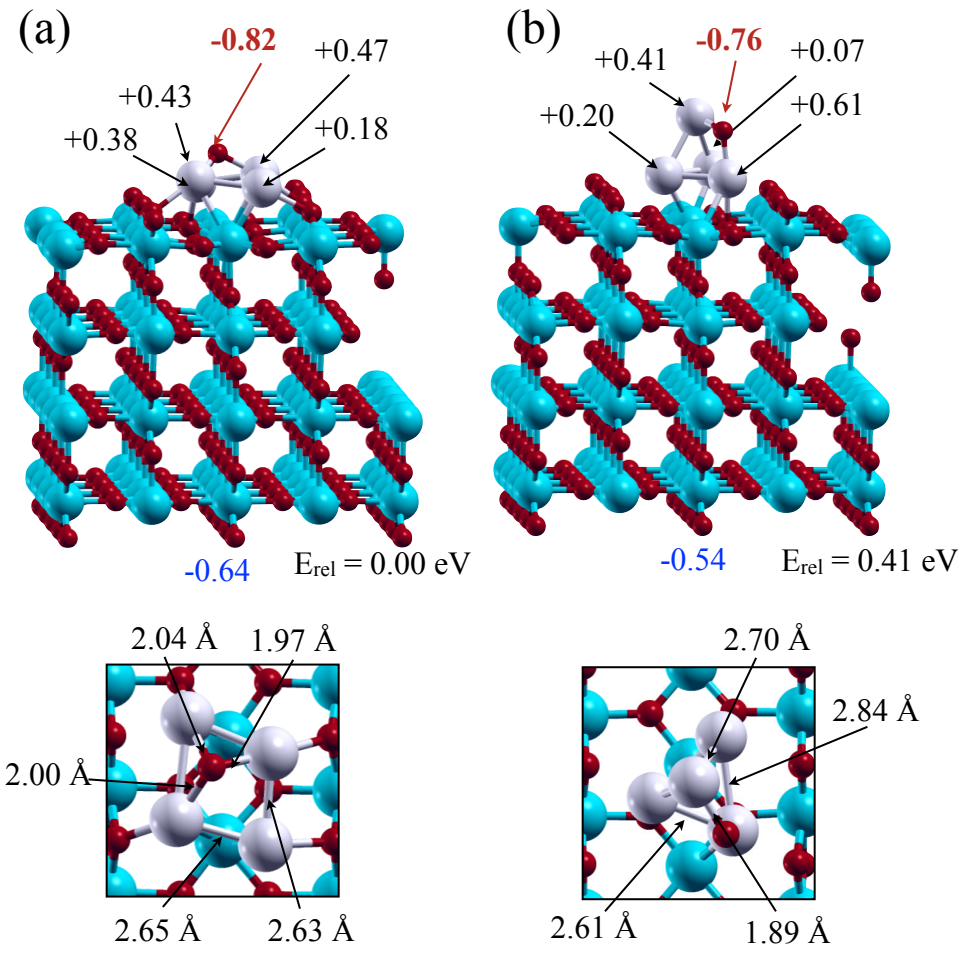

Figure 4.4: Ground state and higher energy isomer ball and stick drawings of the Pd_4O cluster on TiO_2.

then comparing the total energies. Initial geometries included O adsorption sites both on and off the Pd_4 cluster, and O adsorption on the Pd_4 cluster was always found to be more stable. In the free Pd_4 cluster, an O atom occupies a twofold bridging site leaving the structure compact. For the supported cluster, the studies indicate a planar ground state structure with the O atom occupying a threefold hollow site, shown in Figure 4.4(a). The adsorbed O atom is bonded to three Pd atoms with an average Pd-O bond length of 2.01 Å. Previous work by Todorova et al. indicates

that this is also the case for the Pd(111) surface, where the O atom from a dissociated O_2 molecule sits at a threefold hollow site with an average Pd-O bond length of 1.99 Å.[109] As seen in Figure 4.4(a), the Pd_4 cluster sits in the surface channel centered over two protruding Ti surface atoms. In comparison to the tetrahedral Pd_4 structure, the bond lengths between Pd atoms and the bridging O_{2c} atoms of the surface are shortened. That is, each of the four Pd atoms is coordinated to a single bridging oxygen atom, which is canted towards the center of the channel and thus the Pd_4 cluster. The calculated surface deformation energy of 2.18 eV indicates a much stronger surface deformation by the Pd_4O cluster compared to Pd_4. In the ground state of the supported Pd_4O structure, the adsorbed O is bound to three Pd atoms with an average Pd-O bond length of 2.01 Å. Does the planar structure survive as more O atoms are added?

To determine the possibility of another structural change, an additional O atom was added to the cluster. Geometry optimizations were performed using the same methodology as mentioned above for the single O atom, but by sampling 23 different conformations of two O atoms and a Pd_4 cluster. Conformations where one or both O atoms were adsorbed off the Pd_4 cluster were also sampled, and the results indicate a preference for at least one O atom to remain bound exclusively to the Pd_4 cluster. It should be noted here, that two supported Pd_4O_2 structures will be discussed. Both structures represent local minima in the potential energy surface, but one is 0.60 eV higher in energy than the ground state. The higher energy (less stable) structure is the lowest energy configuration in which both O atoms remain bound exclusively to the Pd_4 cluster, while in the other case one of the two O atoms spills over onto the TiO_2 surface. The latter is the calculated absolute ground state geometry, but the possibility of a high potential energy barrier for oxygen spillover requires both structures to be considered in detail. In the ground state structure, the Pd_4 motif

remains planar and adsorbs a single O atom at a threefold hollow site, as in the case of the supported Pd_4O cluster; however, the second O atom spills over to the neighboring, bare Ti_{5c} atom and binds with a Ti-O bond length of 1.72 Å and a Pd-O bond length of 2.18 Å. The structure is depicted in Figure 4.5(a). This Ti_{5c} atom is displaced out of the surface by 0.81 Å. The resulting surface deformation energy is 3.56 eV. The case where both O atoms remain bound to the Pd_4 cluster is shown in Figure 4.5(b), where the Pd_4 cluster possesses a pseudo-planar geometry. One of the O atoms is bound to three Pd sites while the other occupies a twofold bridge site. In this case, there is very little surface deformation that takes place to the TiO_2 support. The calculated surface deformation energy is 0.92 eV, the smallest deformation energy amongst the cases considered here. Since the ground state Pd_4 structure changes with a varying degree of oxidation, one of the central issues is what controls the geometry and the associated electronic structure changes.

4.4 Strong Metal Support Interactions: Pd-O or Pd-Ti?

The purpose of this section is to explain the effect of oxidation on the Pd_4 cluster and characterize the interactions between the Pd_4 cluster and the TiO_2 surface. As will be shown, these two are interconnected due to the effects of oxidation on the clusters atomic configuration and thus manner it interacts with the support. One of the primary results of this section pertains to the "strong metal support interaction" (SMSI) state and gives a molecular insight to the chemical and physical interactions that occur between palladium particles and a titania support. With that stated, the content of this section is first introduced by stating the experimental consensus on

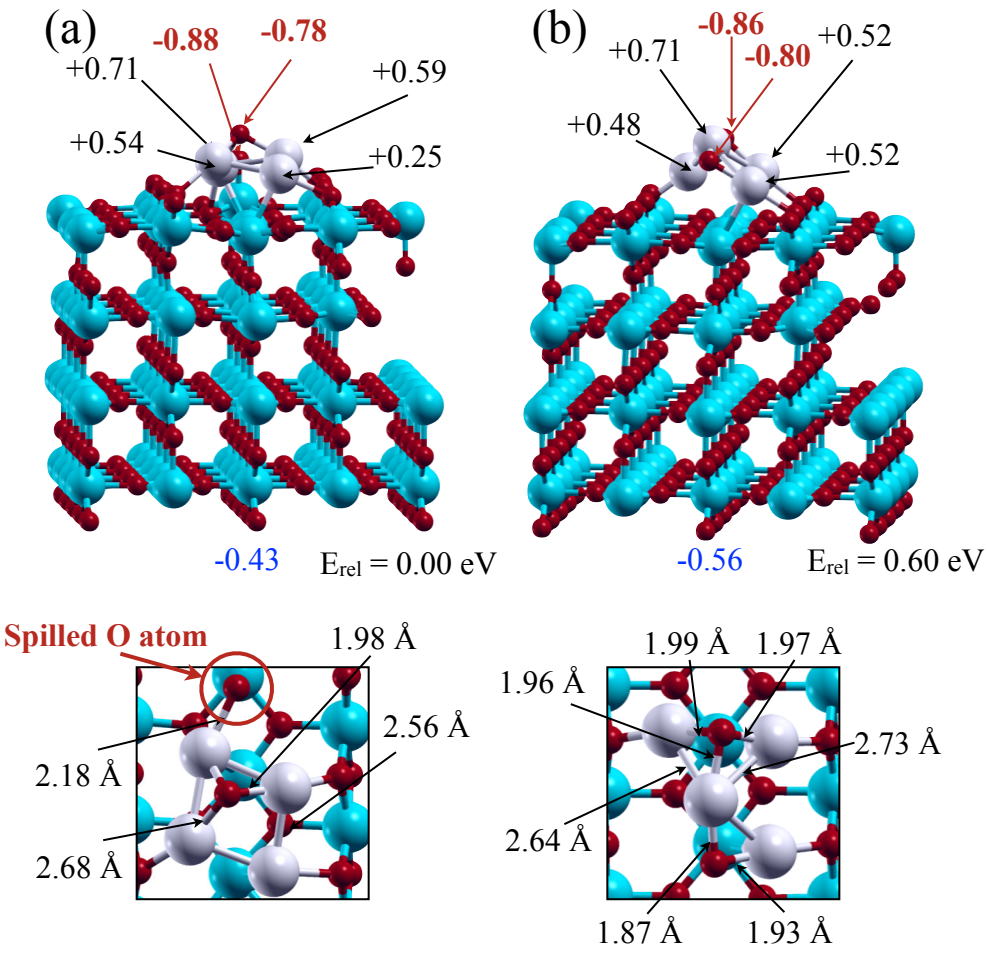

Figure 4.5: Ground state and higher energy isomer ball and stick drawings of the Pd_4O_2 cluster on TiO_2. The spilled O atom is highlighted in the ground state "oxygen spillover" geometry.

the SMSI state followed by a discussion of the results reported in the previous section (Section 4.3).

4.4.1 Experimental Consensus

The first experimental evidence of the strong metal support interaction (SMSI) state was reported by Tauster in 1978.[41] The effect was reported to occur "when some transition metals, supported on a reducible oxide, are heated in a reducing atmo-

sphere." The actual observation was a reduction in the supported transition metal's "sorption" (adsorption or absorption) strength of CO, O_2, and H_2. Why the reduction is "sorption" strength occurs is still a matter up for debate, however the most prominent explanations are the following:

1. Strong electronic interactions between metal particle and support
2. Alloy formation between supported metal particle and diffusive metal ions from the metal-oxide support
3. Encapsulation of the supported metal particle by diffusive metal ions from the support

Any of these could affect the sorption strength of the supported metal, yet experimental evidence claiming alloy formation[40,43,44,46,110] and metal encapsulation[47,111,112] have led to two popular schools of thought and are considered to be the most likely. Most of the SMSI literature is experimental, particularly with Pd or Pt particles supported on TiO_2, and an atomistic-level depiction of the nature of interactions between cluster and support is difficult. Specifically, whether supported Pd particles are interacting with Ti or O sites remains a matter of uncertainty.[32,33,99,113] The following sections are intended to provide a theoretical insight to the atomic-level nature of these interactions.

4.4.2 Theoretical: Supported Clusters

To examine the nature of bonding and the origin of cluster and surface deformations, a detailed analysis was performed on the charge transfer, binding energies, and electronic structure of the clusters and substrate. For the sake of clarity, the Pd_4, Pd_4O, and pseudo-planar Pd_4O_2 results are discussed first, while the Pd_4O_2 structure where

one oxygen spills over is discussed separately. First, the compact and pseudo-planar configurations of a Pd_4 cluster are discussed. For a free Pd_4 cluster, a planar structure is almost 0.85 eV higher than the compact geometry as shown in Figure 4.3. In bonding to the surface, however, only the Pd atoms forming the base of the tetrahedral are bound to the surface O sites. On the other hand, the pseudo-planar structure allows more coordination between Pd and the surface sites. This stabilizes the planar form making it only 0.10 eV higher than the compact ground state. An analysis of the electronic charge redistribution upon adsorption was carried out by a Bader charge analysis described in Section 2.4.2. Figure 4.2 shows the charges at various atomic sites with the number below the figure indicating the net charge on the TiO_2 surface (positive numbers indicate charge depletion while negative numbers indicate charge accumulation). Figure 4.2(a) and (b) show that while the compact Pd_4 transfers 0.48 e^- to the surface, the pseudo-planar cluster transfers 0.57 e^-.

The planar form is really stabilized via the addition of an O atom. In fact, the cluster reconstructions are driven by the accumulation of charge by adsorbed oxygen. In the case of Pd_4O, by adsorbing at a threefold hollow site the O atom maximizes wavefunction overlap and accumulates a Bader charge of 0.82 e^- (Figure 4.4(a)). This is the maximum amount of charge gained by the adsorbed O atom compared to all other sampled Pd_4O geometries. In free clusters, the ground state Pd_4O is a tetrahedral Pd_4 with O bound at a twofold bridging site. Such a structure for the deposited cluster is 0.41 eV higher in energy and allows only 0.76 e^- to be accumulated by the O atom (Figure 4.4(b)). In general, the results indicate that charge accumulation is maximized with a maximum number of Pd-O bonds and directly leads to the ground state structure, despite a substantial rearrangement of Pd atoms from their free cluster geometry. The same trend for pseudo-planar Pd_4O_2 species is observed. Here, one of the O atoms accumulates 0.86 e^- of charge

at a threefold hollow site, while at the opposite side of the cluster the second O atom accumulates 0.80 e^- at a twofold bridging site. The stability of this particular structure can be described by the following two mechanisms. First, of all the cases where both O atoms are bound to the Pd_4 cluster, the pseudo-planar Pd_4O_2 results in the maximum charge accumulation by oxygen. Second, the electron accumulation by the O atoms effectively creates two point charges interacting via a Coulomb potential. By adsorbing at opposite sides of the cluster with a mediating Pd site, these point charges are separated by 3.79 Å, and the Coulombic repulsion is minimized. Further, the Pd-O bonds stabilize the structure through polar, covalent interactions. This O-O separation is believed to play an important role in minimizing the total energy of the system and is the mechanism that unfolds the Pd_4 structure into a pseudo-planar geometry.

It is well known that the metal-O bond strength plays an important role in the catalytic oxidation of CO.[36] To this end, the binding energy of the O atom to the Pd cluster was calculated by taking the difference between the total energy of the ground state oxidized cluster and the sum of total energies of the unoxidized cluster and free oxygen atom. The results indicate that in the case of Pd_4O, the O atom binds with an energy of 4.98 eV. For pseudo-planar Pd_4O_2, the second O atom binds with an energy of 4.33 eV. In the latter case, the reduced oxygen binding energy is due to the competition of charge accumulation of the two O atoms, effectively weakening each Pd-O bond. In this respect, it may be interesting to examine if this binding can be further weakened by additional O_2 molecules.

Cluster support interactions play an important role in catalysis and this interaction is analyzed next. To estimate the strength of bonding, a comparison between the total energy of the deposited species and the total energies of the free Pd_4O_x motifs

and the free TiO_2 surface are determined by the following equation:

$$B.E.(Pd_4O_x/TiO_2) = E(Pd_4O_x) + E(TiO_2) - E(Pd_4O_x/TiO_2), \qquad (4.1)$$

where (x=0,1,2), and the Pd_4O_x cluster is considered to bind as a single motif. The results are reported in Table 4.1. There is a clear correlation between the number of Pd atoms directly coordinated to the surface and the binding energy, where a rough binding energy of 0.8 eV per directly coordinated Pd atom is observed. That is, for Pd_4 where three atoms directly coordinate to the surface, the cluster binds with an energy of 2.40 eV, while Pd_4O coordinates with four Pd atoms and binds with 3.21 eV. The pseudo-planar Pd_4O_2 structure represents an intermediate case where between three and four atoms are directly coordinated to the surface, yielding a binding energy of 3.03 eV. This correlation of binding energy and number of directly coordinated Pd atoms agrees with results previously shown for Pd_6 and Pd_{13} clusters supported on TiO_2 as reported by Murugan et al.[35] and Pd_{12} supported on TiO_2 as reported by San-Miguel et al.[33]

	Pd_4	Pd_4O	Pd_4O_2
Pd_4O_x binding energy (eV)	2.40	3.21	3.03
Charge from Pd_4O_x to surface (e^-)	0.48	0.64	0.56
Surface deformation energy (eV)	1.27	2.18	0.92

Table 4.1: A comparison of the cluster binding energy (Equation 4.1), charge transferred from the cluster to the surface, and the surface deformation energy for Pd_4, Pd_4O, and pseudo-planar Pd_4O_2 supported clusters.

To further probe the nature of interactions marking the Pd_4, adsorbed O, and the surface sites the total density of states (DOS) and the projected density of electronic states (PDOS) at various sites of the TiO_2 and deposited cluster were examined. Figure 4 shows the total and various local densities of states for Pd_4 on TiO_2, where the Fermi level has been set to E=0. The sharp peak of O states at about 1.3 eV below

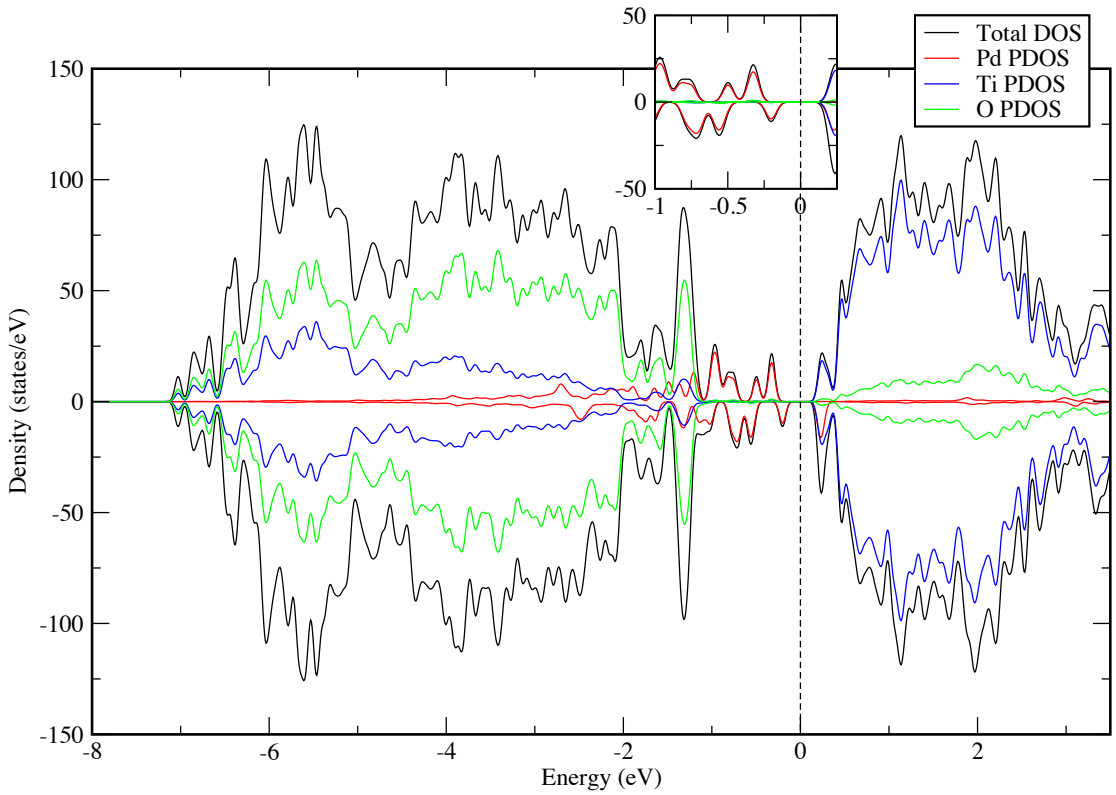

Figure 4.6: Total and projected density of states for Pd_4 supported on TiO_2. Top and bottom portions represent the spin up and spin down states, respectively. The Fermi level has been shifted to E=0. The inset shows the states near E_F.

the Fermi level originally makes up the top of the valence states for the TiO_2 surface. The insertion of Pd states between this peak and the bottom of the conduction states reduces the gap. In Figure 5, the DOS for (a) Pd_4O and pseudo-planar (b) Pd_4O_2 supported on TiO_2 is shown. There is a clear mixing of Pd d-states with the states of adsorbed O near the Fermi level, and an overall metallic character of the system.

As stated earlier, the deposited clusters induce deformations on the TiO_2 surface. Here, the deformation is shown to be rooted in the charge transfer between Pd and Ti+O surface sites, and hence calls attention to the results of the Bader charge analysis in Figures 4.2(a), 4.4(a), and 4.5(a). The results indicate that the more a cluster coordinates to the surface, the more charge it transfers to the surface. For

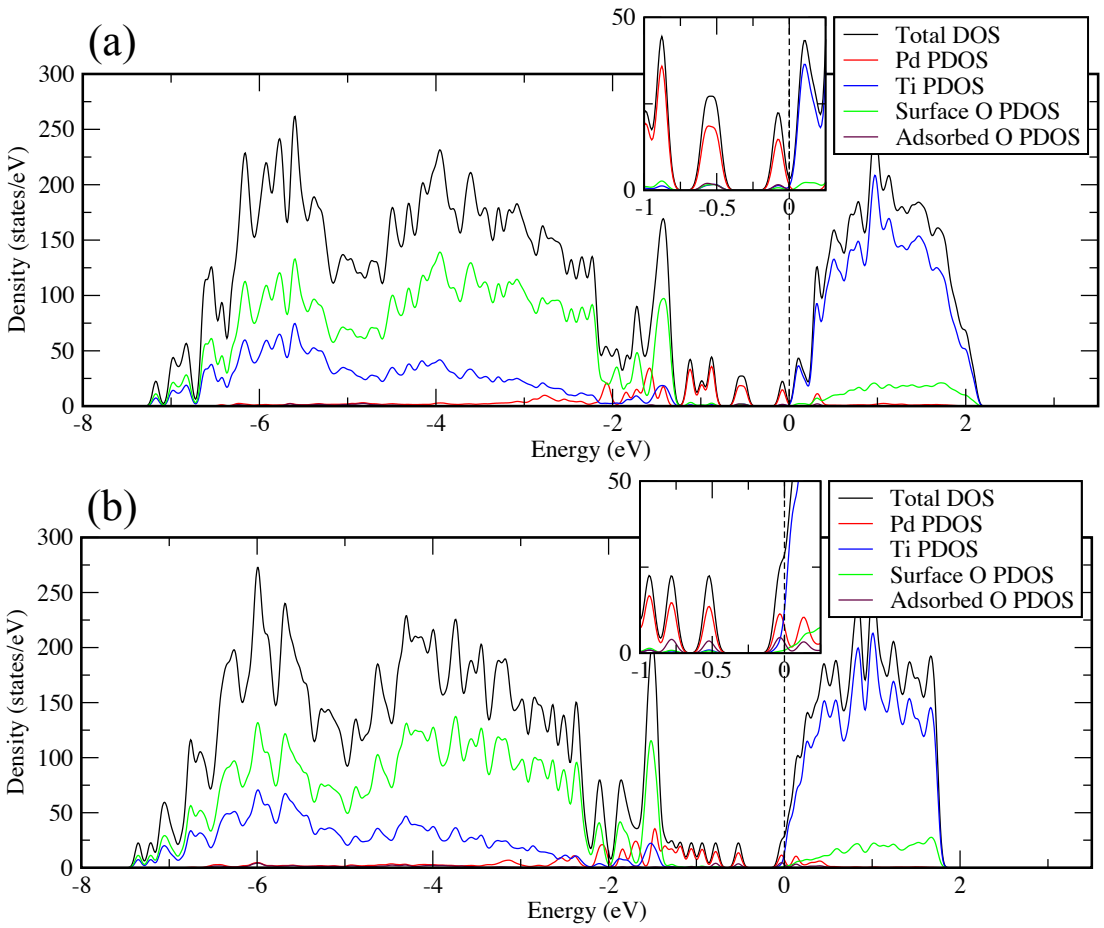

Figure 4.7: Total and projected density of states for (a) the Pd_4O and (b) the Pd_4O_2 cluster supported on TiO_2.

all three cases, Pd atoms readily donate charge, which is transferred almost entirely to the Ti and O atoms in the top trilayer of the surface. These atoms are resilient to a change from their bare surface charge state. This is indicated by a change in charge state of less than 0.06 e^- for all atoms except the Ti_{5c} atoms directly beneath the Pd cluster. Effectively, the Pd cluster is donating a small amount of charge to all of the neighboring bridging O_{2c} and in-plane O_{3c} atoms, resulting in the accumulation of charge by Ti atoms as well. The amount of charge accumulated by these Ti atoms governs the extent of Ti atom displacement and thus governs the

surface deformation energy. That is, for Pd_4, Pd_4O, and pseudo-planar Pd_4O_2 the two Ti atoms beneath the Pd cluster accumulate a combined 0.15, 0.21, and 0.07 e^-, respectively, and are displaced from their original position a combined distance of 0.42, 0.44, and 0.20 Å, respectively. By comparing the displacements for all atoms before and after Pd cluster deposition, the protrusion of these Ti atoms accounts for almost all of the surface deformation. The mechanism for surface reconstruction can be understood when taking into account the partially ionic and partially covalent nature of the Ti-O bonds. The Ti-O bonds are partially ionic, and the accumulation of charge by Ti results in the weakening of this ionic bond between the Ti atoms and nearest-neighbor O atoms. Supporting calculations of a free TiO_2 cluster reinforce this conclusion. The change in Ti-O bond length was monitored as charge was added to the system. It was found that the Ti-O bond length increases by 3% upon the addition of an electron to the TiO_2 cluster.

Next, the microscopic mechanism of the strong metal support interaction (SMSI) observed for some transition metals supported on reducible oxides is considered.[41] As indicated above, the Ti sites are displaced from their positions in the lattice by the charge transfer from lattice O sites, which depends on the degree of coordination between cluster species and support. In addition, there is minimal interaction between the Pd and Ti sites. This can be seen from the local density of electronic states at the Pd, Ti, and O sites shown in Figure 4.8. There is no appreciable mixing between Ti and Pd states.

4.4.3 Theoretical: Free Clusters

As a further confirmation to this, model electronic structure calculations on a free Pd-Ti dimer were carried out using the ADF code.[114] The molecule is bound with a

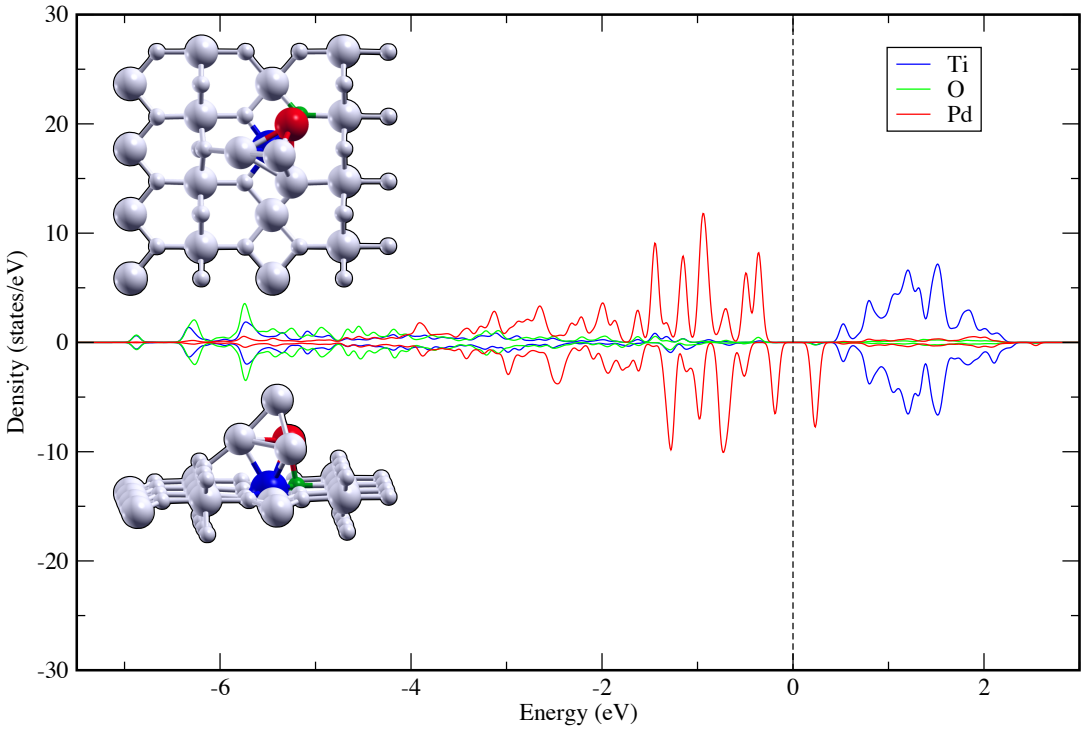

Figure 4.8: Local density of states for Pd_4 cluster supported on TiO_2 highlights the limited mixing of Pd and Ti states. Only the states of a single Ti, single O, and single Pd are plotted. The atoms which states are projected are colored in the ball and stick drawing, and the DOS plot is color coded similarly. The Fermi level has been shifted to E=0.

binding energy of 3.17 eV and a bond length of 2.20 Å. Figure 4.9(a) shows the one-electron energy levels and molecular orbitals of the PdTi dimer, and one can clearly identify the bonding orbitals. For instance, there is clearly Pd-Ti orbital overlap with s-orbital character between -1 and -1.5 eV as shown in the figure. Likewise, the states at -3 eV show d-orbital bonding between Pd and Ti atoms. Because the interest here is to know the effect of oxidation on the Pd-Ti bond, the next step is to examine the changes in bonding when oxygen is present. Figure 4.9(b) shows that in the oxidized structure, the Pd-Ti bond stretches to 2.66 Å, and the molecular orbitals no longer show any significant Pd-Ti bonds. Note that both O atoms are slightly closer to the Ti rather than Pd, and close inspection of the molecular orbitals shows Ti-O rather

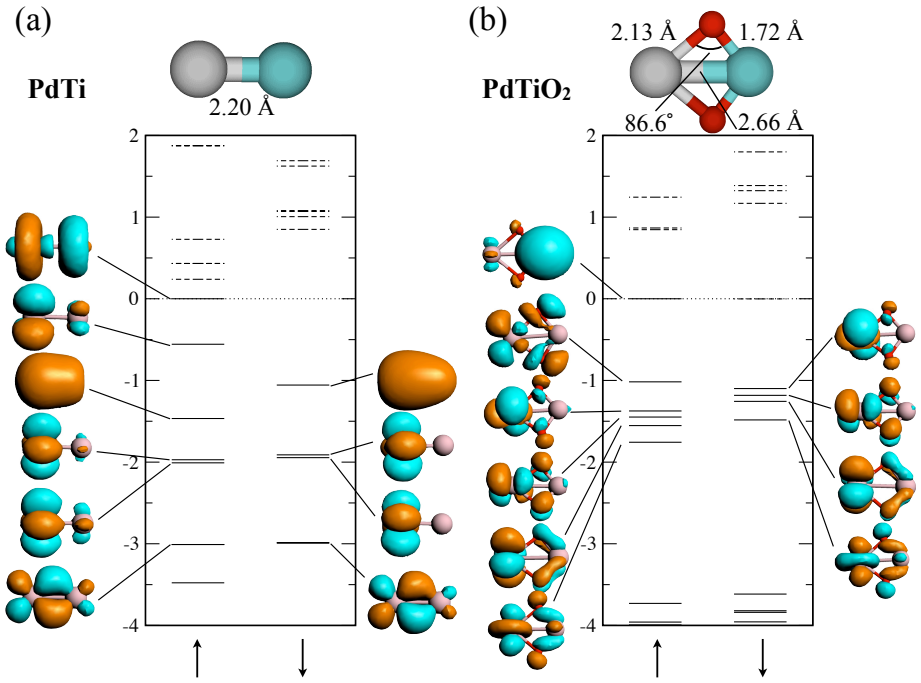

Figure 4.9: Electronic states and free cluster geometries of PdTi (left) and $PdTiO_2$ (right). The electronic energy levels and corresponding molecular orbital plots are shown. The Fermi energy has been shifted to E=0. Silver spheres represent Pd atoms, blue spheres represent Ti atoms, and red spheres represent O atoms.

than Pd-O orbital overlap. In fact, the electronic state in the spin up channel at -1 eV shows anti-bonding character between the Pd and the O atom. This model study on the PdTi dimer is helpful in understanding the cluster-support interactions. In regards to TiO_2-supported Pd clusters, the model study suggests that the Pd-Ti interactions are weak and have no direct relation to the large displacement of Ti out of the surface. Instead, the weakened Ti-O ionic interactions, due to Pd-to-O charge transfer, allow Ti ions to protrude and become mobile. This Pd-to-O charge transfer represents the first of two mechanisms in which the Ti-O ionic interactions are weakened and Ti atom surface protrusions occur. The second mechanism is described in the following paragraph. It should be noted here that in the prototypical case of Pt nanoparticles supported on $TiO_2(110)$, the SMSI state is observed as either encapsulation of Pt or

the formation of an intermetallic alloy by diffusive Ti ions.[48,111] In a similar fashion to what is described here, an appreciable charge transfer likely occurs between the near-surface Pt atoms and the surface O_{2c} and O_{3c} atoms, which results in similar weakening the Ti-O bond.

Next, the case for Pd_4O_2 with oxygen spillover is considered. The O atom that remains bound to the Pd_4 cluster accumulates 0.78 e^- of charge, while the spilled O atom accumulates 0.88 e^-. It is visible in Figure 4.5(a) that the Pd atom between the two adsorbed O atoms is coordinated to both oxygens and hence donates more charge than the other three Pd atoms. Following the binding energy equation stated earlier (Equation 4.1), the calculated Pd_4O_2 binding energy is 3.64 eV. The Ti_{5c} surface atom that the O atom is spilled onto is displaced from its original position by 0.81 Å. The mechanism behind such a large displacement is due to the Ti_{5c} atoms tendency to weaken Ti-O ionic interactions in order to donate charge to the spilled O atom. Considering the Bader charge of 0.88 e^- on the spilled O atom, one might expect the Ti_{5c} directly beneath it to undergo a dramatic change in charge state. However, the Bader analysis indicates the Ti atom depletes only 0.07 e^- more than it would in the bare surface. By undergoing such a large displacement, the Ti atom effectively de-coordinates from neighboring O atoms, which accumulate charge from the Pd atoms, and this results in a charge transfer of 0.88 e^- to the spilled O atom. Thus, the de-coordination of Ti to neighboring O atoms, in order to donate charge to the spilled O atom, represents a second mechanism of weakening Ti-O ionic interactions. The existence of oxygen spillover in Pd_4O_2 could also account for recent experimental findings in the group of Anderson on the catalytic oxidation of CO by TiO_2(110)-supported Pd_n clusters.[56] Oxidation of CO at 550 K by the oxidized Pd_n species generates CO_2, but the amount of CO_2 is much less than to account for the removal of all O atoms. Yet, the experiments do not see desorption of O_2 up until 600 K. Further,

the ISS experiments indicate that there are no adsorbates left on the Pd_n surface, suggesting that the remaining O atoms have spilled over onto the TiO_2 surface.

4.5 Conclusions

The work presented in this chapter demonstrates that the supported Pd_4 clusters on TiO_2 surface undergo significant geometrical and electronic changes as O atoms are added to the cluster. For the bare Pd_4 the studies indicate both compact and pseudo-planar configurations. It is shown that Pd_4O presents a planar structure while Pd_4O_2 presents two different possibilities, namely a pseudo-planar structure and oxygen spillover structure. This emphasizes the importance of interpreting ion scattering spectroscopy results when oxygen may be (and most likely is) present. For Pd_4O_2, the studies indicate that the most stable configuration corresponds to a spillover O that binds to a surface Ti site, and that these findings could account for some of the recent experimental observations. The studies also indicate a locally stable pseudo-planar Pd_4O_2 structure where both O atoms are bound to the Pd_4 cluster. There is significant interaction between the deposited clusters and the substrate, and structural changes in the deposited clusters can be related to the charging of the O atoms. Finally, the studies suggest that the microscopic origin of the strong metal support interaction may lie in two different mechanisms. In both cases, Ti-lattice O interactions are weakened and Ti atoms are displaced out of the surface. In the first weakening mechanism, the deposited Pd atoms donate charge to the surrounding lattice oxygen atoms, while in the second mechanism the Ti donates its charge to spilled over oxygen. Palladium clusters are important oxidation catalysts and the ability of the clusters to adapt to the deposited atoms is believed to play an important role in controlling the reaction barriers.

5. Enhanced Oxygen Binding through Surface Mediated Ionic Bonds

5.1 Introduction

The intent of this chapter is to introduce details of the long range interactions which are shown to take place on the TiO_2 surface. The previous chapter showed the energetic preference for one of two adsorbing O atoms on a Pd_4 cluster to adsorb in a spillover mode. Since the oxygen binding energy represents an important parameter in many catalytic oxidation reactions, the nature of oxygen binding to the Pd/TiO_2 system is presented. This chapter presents results on the interaction of a single Pd atom and a single O atom on TiO_2 as a model system to discuss these long range interactions. The results discussed in the present chapter have direct implications in the chapters to follow.

It has been demonstrated experimentally that single O atoms can be found at Ti_{5c} sites of the clean, stoichiometric TiO_2 surface via the dissociative adsorption of O_2 at an oxygen vacancy site of the non-stoichiometric TiO_2 surface.[54] To arrive at such a state, one O atom from a dissociated O_2 molecule fills the oxygen vacancy while the other O atom (O_{ad}) adsorbs at a nearby Ti_{5c} site.[38,115,116] As the results from this

chapter show, an O_{ad} atom binds to TiO_2 weakly, much weaker than the bond strength of a free O_2 molecule. This suggests that at temperatures high enough to overcome diffusion barriers, mobile O_{ad} atoms can re-combine to form hot O_2 molecules, which then undergo molecular desorption from the surface, an observation supported by experiments at temperatures above 410 K.[117] However, experiments also indicate that O atoms spilled over from a Pd particle, even farther away from cluster, remain bound at temperatures beyond that ($\sim$550 K).[40] Since the spillover atoms are primarily bound to surface Ti sites, it is puzzling that the presence of remote Pd sites can increase and as will be shown, more than double O binding to the Ti sites compared to single O atom. The results show that the presence of both spillover oxygen and Pd on the surface is related to the strong metal support interactions (SMSI). While the debate continues on whether Pd encapsulation or Pd-Ti alloy formation is the result of the SMSI effect, there is consensus that diffusive Ti ions are a necessary precursor to the manifestation of SMSI. Since both Ti and the adsorbed Pd are bound to O sites by donating charge, they are in positive charge states. Consequently, the Pd-Ti interactions, if any, are not expected to be strong.[34,113] In regards to SMSI, the question to be addressed is what initiates the migration of Ti sites to the surface and close to the Pd locations?

In this chapter a microscopic understanding of these issues is presented by considering a PdO molecule separated at various distances on a TiO_2(110) surface. The key issue is the increase in binding of both Pd and O atoms when adsorbed as the PdO molecule in comparison to individual atomic adsorption. The spillover oxygen corresponds to an O atom bound to the surface Ti_{5c} site as in a bare TiO_2 surface. Consequently, the binding energy of O as the Pd-O distance is increased from 2.00 Å (the ground state PdO separation of the deposited molecule) to 5.50 Å is examined. The studies show the existence of an ionic interaction between Pd and O sites

that is mediated by the lattice and operates even at large separation, thus providing a microscopic origin of the enhanced binding of the spillover oxygen. Also, these studies introduce a molecular mechanism that shows a direct correlation between the presence of spillover oxygen and the SMSI effect by determining the atomic/molecular rearrangements that are energetically feasible. To this end, the energy involved in replacing the Pd site by either (1) a Ti atom or (2) a TiO unit consisting of a Ti and a spilled over O atom is investigated. Surprisingly, the interchange of the Pd and "TiO" motifs requires the least amount of energy and this is proposed to be related to the nature and number of valence electrons.

5.2 PdO Molecule on TiO_2

First, the binding energies of a single O atom, a single Pd atom, and then a PdO molecule on the TiO_2 surface are considered. The studies indicate that when individually adsorbed, the O and Pd atoms bind to the bare TiO_2 surface with an energy of 1.69 eV and 1.52 eV, respectively. Both species interact primarily with a single surface site. The Pd atom binds directly atop an O_{3c} site, and the O atom binds directly atop a Ti_{5c} site in the center of the TiO_2 surface channel. To achieve equilibrium, atoms in the surface layers reconstruct in response to the adsorbing species. Specifically, adsorption of an O atom induces a protrusion on the lattice Ti_{5c} site to which it adsorbs. The protrusion pushes the Ti_{5c} atom out of the surface (surface normal direction) by a distance 0.82 Å, which also increases its bond lengths to the neighboring lattice O sites. The calculations indicate that by adsorbing at a single lattice O site, the Pd atom also induces a surface reconstruction, but displacements of the surface atoms are smaller compared to the case for O adsorption. A Bader charge analysis shows a charge transfer of 0.24 e^- from Pd to the surface atoms (net charge

of +0.24 e^- on Pd). The binding energy of 1.69 eV for a single O atom is rather low as should be expected for an O atom on a stoichiometric TiO_2, where Ti surface ions are highly coordinated and thus nearly saturated. Considering the fact that the calculated binding strength of a free O_2 molecule is 5.2 eV, the process where the two adsorbed O atoms combine to form an O_2 molecule and leave the surface is energetically feasible given enough energy to overcome diffusion barriers. (The calculated binding energy of an O_2 molecule in DFT in 6.56 eV, and the process where the two O_{ad} atoms combine to form a molecule and leave the surface remains energetically feasible.) This is consistent with experiments that indicate that O atoms on a free TiO_2 surface do desorb from the surface at finite temperatures.[117]

A Bader charge analysis indicates that the O atom accumulates 0.77 e^- of charge. The accumulation of charge by the O species is expected, but to understand the source of charge donation, the ionic nature of the TiO_2 surface should be considered. While one might expect the majority of charge to be transferred from the Ti_{5c} site that adsorbs the O atom, the results indicate that instead charge is donated collectively by Ti and O sites in the first two trilayers of the surface. If the Ti_{5c} site solely donated all 0.77 e^-, it would undergo a dramatic change in charge state that would likely propagate to neighboring lattice O sites. Here, Ti_{5c} decoordinates from the neighboring O sites by protruding out of the surface. This protrusion increases the distance between the Ti_{5c} atom and its lattice neighbors, allowing for very little change in charge state of the Ti itself and surrounding lattice O sites. As will be shown later, the sharing of the donated charge by Ti and O sites occurs in other cases too, and this can be looked upon as a resiliency of the lattice sites to undergo a change in their oxidation states.

Now the case of PdO on the TiO_2 surface is considered. The Pd occupies a site above three lattice O_{3c} sites, and the O_{ad} is bound atop a neighboring Ti_{5c} site. The

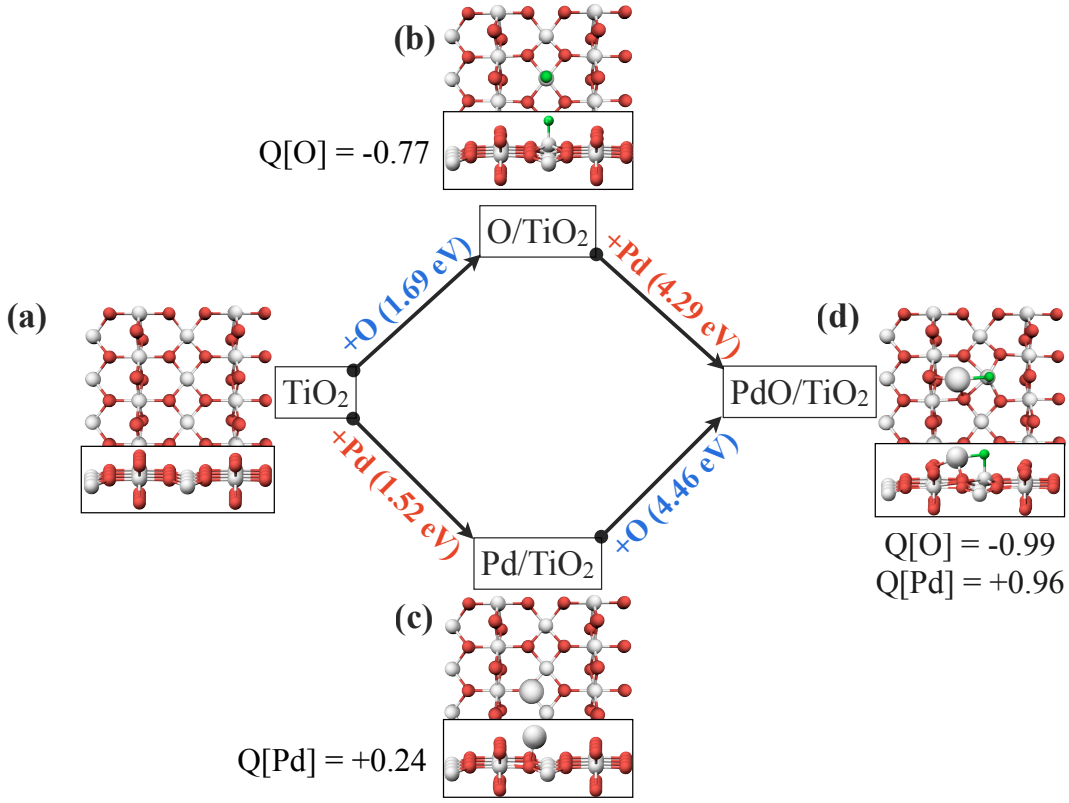

Figure 5.1: Top and side view drawings of the ground state structures for (a) clean, stoichiometric rutile TiO_2(110), (b) a single O atom on TiO_2, (c) a single Pd atom on TiO_2, and (d) a supported PdO molecule. For clarity, only the top trilayer of the TiO_2 slab is shown. The calculated binding energies are shown to highlight the binding energy enhancement of one surface species in the presence of the other (see text for details). The coloring scheme is as follows: lattice Ti (small silver spheres); lattice O (small red spheres); Pd (large silver spheres); and adsorbed O (green spheres).

bond length of the molecule increases from 1.83 Å in a free molecule to 2.00 Å for the adsorbed species. Since the catalytic activity of any oxidation reaction is governed by the binding energy of the O to the surface, the next step was to determine the amount of energy required to remove the O atom. The calculations indicate that the oxygen binding energy (OBE) is increased to 4.46 eV. Recall that a single O atom is bound by only 1.69 eV to the TiO_2 surface in the absence of Pd; the increase could be due to direct, covalent PdO bonding. As a free PdO molecule has a binding energy of

3.30 eV, the increase in binding could be roughly accounted for by the PdO binding energy. Such a proposition is consistent with the finding that the energy required to remove the Pd atom also increases from 1.52 eV for a single Pd atom to 4.29 eV for the PdO, and the increase in the binding of Pd and O are exactly the same at 2.77 eV. Thus, the presence of an O surface species enhances Pd binding, and likewise the presence of a Pd surface species enhances O binding. The calculated ground state structures and corresponding binding energy calculations are summarized in Figure 5.1. Beginning with the clean, stoichiometric TiO_2 surface (Figure 5.1(a)), two paths that lead to the PdO/TiO_2 structure (Figure 5.1(d)) are considered. In one path, Pd adsorbs on the O-doped TiO_2 surface (a $\rightarrow$ b $\rightarrow$ d), and in the other path, O adsorbs on the Pd-doped TiO_2 surface (a $\rightarrow$ c $\rightarrow$ d). Since the Pd and O atoms in PdO are bound by a covalent bond, the next step was to examine whether the binding energy of O could be altered by increasing the Pd-O separation and thus decreasing direct orbital overlap.

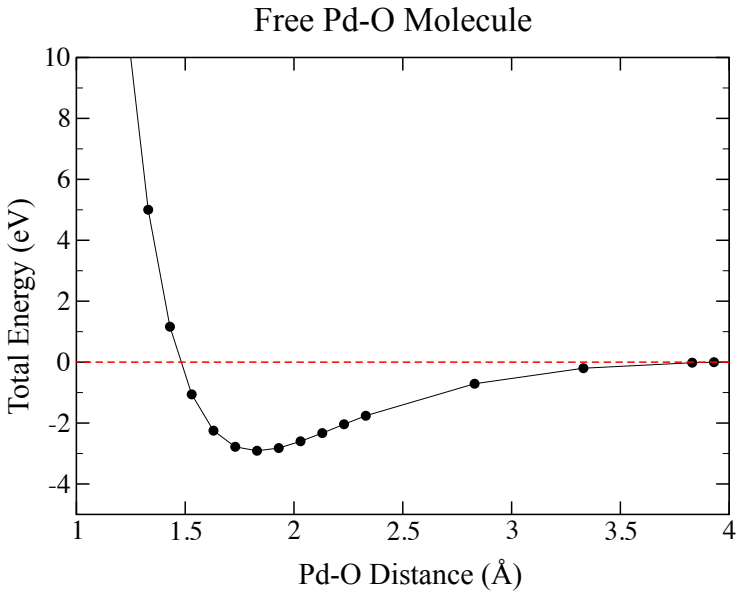

Figure 5.2: Total energy vs. Pd-O separation distance for a free PdO molecule.

To investigate the origin of the OBE enhancement, the first step was to examine if the covalent bonding in a free PdO could account for the bonding on surface. To this end, the change in binding strength as the PdO distance was increased was investigated. Recall that a free O atom binds only at a Ti_{5c} site, and thus the O was placed on Ti_{5c} sites farther from the Pd atom leading to PdO separations of 3.85 Å and 5.50 Å. Because covalent bonds are highly localized, one would expect that the O binding energy would drop to its value on a bare surface for larger separation. This concept is reinforced when considering the interaction energy of a free PdO molecule. Figure 5.2 is a plot of the total energy of a PdO molecule as a function of Pd-O separation. The minimum at 1.83 Å indicates the ground state bond length of the molecule, and the tail of the energy curve shows that the PdO molecule is essentially non-interacting by about 3.5 Å. Thus, there should be no more covalent interactions in a free PdO molecule at such large Pd-O separations. However, the calculations indicated that in comparison to O individually adsorbed on the bare TiO_2 surface, the increase in O binding energy was 1.79 eV even at a separation of 5.50 Å. This suggests that the Pd and O sites are probably bound by interactions that are appreciable at larger separations. One possibility was to consider an ionic interaction between the Pd and O sites as Coulomb contributions to the energy, which decrease slowly with distance $(1/r)$, can be large even at larger separation. Recall that without a Pd species present an O atom accumulates 0.77 e^- of electronic charge from the surface. For the ground state configuration of PdO, the studies indicate that the presence of Pd leads to an O atom accumulating 0.99 e^-. What is more interesting is that this charge is almost entirely donated by the Pd site which is left with an opposite charge in similar magnitude of +0.96 e^- leaving the underlying surface almost neutral. In this configuration, Pd-O separation is only 2.00 Å, and the overlap of the charge density and the surface deformations would alter the ionic contribution. One would,

however, expect Coulomb terms to dominate as PdO is farther separated. To this end, a comparison between the Coulomb attraction and the calculated enhancement in oxygen binding energy as a function of Pd-O separation is presented. The results, which are summarized in Figure 5.3, show three different geometries corresponding to Pd-O distances of 2.00, 3.85, and 5.50 Å. The latter two cases are less stable configurations compared to the ground state, and the feasibility of long range spillover will be discussed later. The results indicate that even at large Pd-O distances the OBE enhancement is substantial. Alongside the OBE enhancement plot are the magnitudes of the Coulombic potentials calculated for the three Pd-O distances. The atomic charges used in the Coulomb potential equation were determined by Bader charge analyses and are shown in the inset above the ball and stick drawings.

Clearly, there is a convergent behavior between the two curves indicating that at a Pd-O distance of 5.50 Å the OBE enhancement is strictly a result of Coulomb interactions. However, at smaller Pd-O distances two additional factors may affect the calculated oxygen binding energy, and thus give rise to the shaded region between the two curves. The first factor, likely to have an impact at only short distances, arises from the likelihood of chemical bond formation between Pd and O. The second factor pertains to adsorbate-induced deformations. Recall that each species induces a local deformation to the surface structure. At large Pd-O separation (e.g., 5.50 Å), the O and Pd induced surface deformations are well separated. Thus, the binding energies of O and Pd are the sum of: (1) the binding energies in their isolated cases (1.69 eV and 1.52 eV, respectively) and (2) the Coulomb interaction contribution. When Pd and O are in close proximity of each other (e.g., 3.85 Å or less) the adsorbate-induced surface deformations are also in close proximity. This results in an O atom bound to a surface structure that is deformed by Pd adsorption and vice versa. This coupled with the overlap of charge densities modifies the pure ionic term.

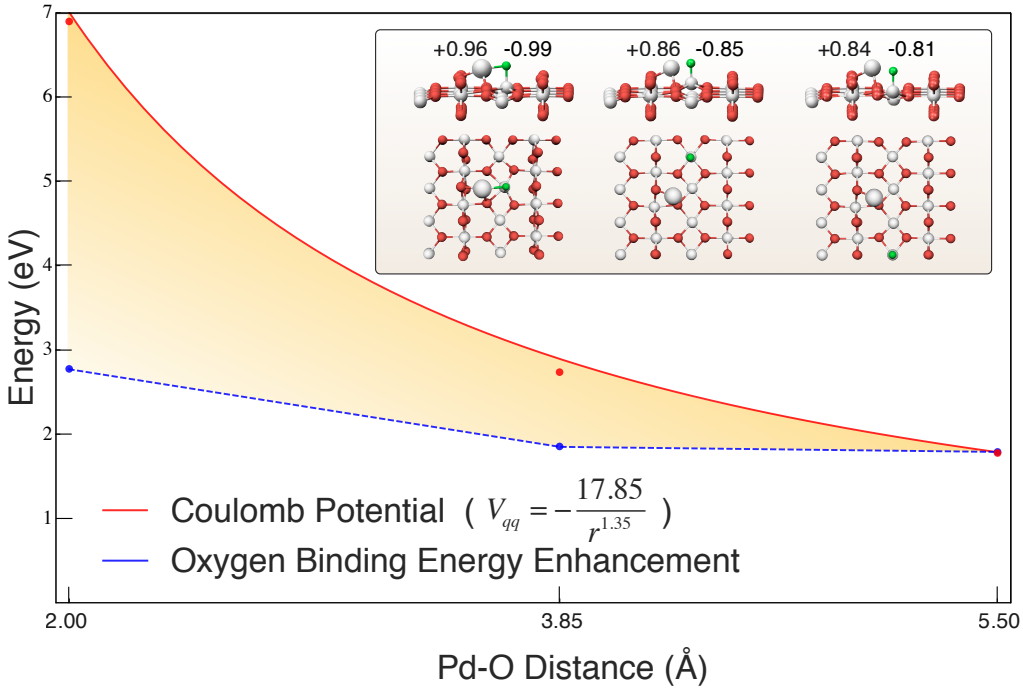

Figure 5.3: The blue points are the calculated oxygen binding energy (OBE) enhancement over the OBE of a single O atom on the surface (1.69 eV). The dashed, blue lines are shown only as a visual guide to the eye. The red points are the calculated electrostatic interactions between the supported Pd and O species, and the red curve is a least-squares fit of the data. The inset shows side and top views of the geometries with three different Pd-O distances. The inset also shows the calculated atomic charges on Pd (positive numbers) and O (negative numbers) atoms that were used to calculate the electrostatic interactions.

This concept is reinforced when considering the energetic cost of deforming the surface structure. To quantify this energetic cost, Equation 2.32 from Section 2.4.1 is used. The calculated surface deformation for the individually adsorbed O atom is 3.47 eV. The calculated O-induced surface deformation at Pd-O separation of 5.50 Å is 3.67 eV, indicating a very similar reconstruction. At Pd-O separations of 3.85 Å and 2.00 Å, the O-induced deformations are 3.83 eV and 5.04 eV, respectively. Essentially, the closer the Pd-O distance the more the two species-induced deformations spatially overlap. The result is a shift in the oxygen binding energy, which gives rise to the shaded region between the two curves in Figure 5.3. There was some concern as to

whether the inclusion of a Hubbard U term into the Hamiltonian would change the results presented here. As shown in Appendix A, upon inclusion of a U term the results remained qualitatively the same.

As stated earlier, individual Ti and O lattice sites are unlikely to undergo major changes in charge state. In fact, the adsorbate-induced deformations can be considered a mechanism to avoid undergoing a major change in charge state. The resiliency to a change in charge state is further reinforced when considering the charge on the Pd and O atoms at the three distances of separation. First, recall how the Pd atom is left in a $+0.24$ e^- charge state when adsorbed individually. As shown in the inset of Figure 5.1, in all three cases where O is present the Pd charge is at least $+0.84$ e^-. The large charge buildup at the Pd site is an effect of two phenomena. First, at the three Pd-O distances shown here, the O atom accumulates at least 0.81 e^-, driven entirely by its tendency to accumulate electronic charge. Second, because the Ti and O lattice sites are resilient to undergo a change in charge state, the source of electronic charge is the Pd atom, even at a distance of 5.50 Å. Essentially, the adsorbed O atom accumulates charge from the Ti_{5c} site to which it binds, leaving the surface layers in a slightly charged state. However, when Pd is present it serves as the source of charge, and at all three Pd-O distances it accounts for nearly all of the charge accumulated by O.

Returning to the idea of long range spillover, it should be noted that oxygen spillover has been observed by STM imaging at distances up to several nanometers away from TiO_2-supported Pd nanoparticles.[110] To investigate the potential barrier for single O atom diffusion on a surface with Pd present, a climbing image nudged elastic band (NEB) calculation was performed.[118] The reaction path contains the O atom diffusing from the Ti_{5c} site nearest the Pd atom to a neighboring Ti_{5c} site in the [001] direction. In the NEB calculation, the initial and final configurations

correspond to structures with Pd-O distances of 2.00 Å and 3.85 Å, respectively. The results indicate a maximum potential energy barrier of 1.14 eV for an O atom to cross over to a neighboring Ti_{5c} site.

In the STM experiments by the Bowker group,[48] another important feature is observed. As oxygen continues to spillover from the Pd nanoparticles to nearby titania sites, new titania layers form. The titania layer growth occurs fastest near the Pd particle compared to other parts of the surface indicating oxygen spillover is a major contributing factor.[110] Growth can even occur in the form of titania overlayers, leading to surface structures where Pd particles may become encapsulated.[48,111,112,119]

While in Chapter 4 the weakening of the ionic contribution of Ti-O surface bonds is discussed, here using a PdO molecule on the surface gives insight to the molecular mechanism of how the SMSI state might occur. Specifically, this model system can be used to understand how a Pd atom might become encapsulated by titania overlayer growth. Note that Pd encapsulation could be initiated by a Pd atom substituting a Ti site on the surface. Consequently, the energetic feasibility of exchanging Pd site with other atoms/motifs on the surface was examined. First, the energetic cost of an exchange between the Pd and a surface Ti site was considered. The state with sites exchanged was 1.99 eV less stable than the original configuration. An alternate possibility was to exchange Pd by another unit. As mentioned before, the addition of an O atom displaces Ti_{5c} surface site beneath it and de-couples it from the surface. Therefore, a geometry optimization on a configuration where the Pd atom and the TiO unit were swapped was performed. The two structures are shown in Figure 5.4. For clarity, red and blue wireframe meshes are drawn as cages surrounding the ball and stick models of the Pd atom and the TiO unit, respectively. Interestingly, the total energy of the swapped structure (Figure 5.4(b)) is only 0.29 eV less stable than the ground state structure (Figure 5.4(a)).

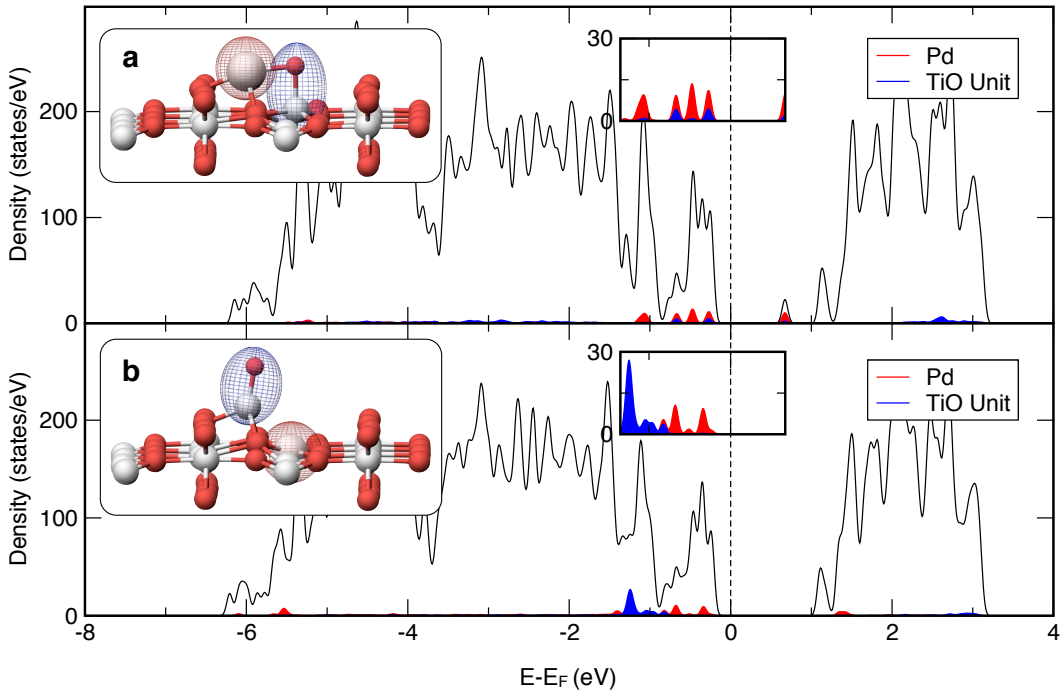

Figure 5.4: Total (black lines) and projected (colored regions) density of states plots for geometries where (a) PdO is supported on TiO_2 and (b) Pd swaps positions with a neighboring TiO site (i.e., Pd atom encapsulation). For the projected DOS, the red regions correspond to states of the Pd atom (drawn inside of a red wireframe mesh) while the blue regions correspond to states of the TiO unit (drawn inside of a blue wireframe mesh). The Fermi energy (E_F) is shifted to 0 eV.

This energy difference is strikingly small, especially when considering such a drastic change in geometry. However, upon further inspection it can be seen that many of the criteria that defined stability of the ground state structure are still met. First, the valence electron count at each site remains the same in both cases. Second, the Ti atom in the TiO unit remains highly coordinated to O sites (three lattice O sites as well as the single O atom of the TiO unit). Along the ball and stick drawings of Figure 5.4, the total and projected density of states (DOS) plots are shown. The total DOS is shown in black outline, while the projected DOS for the Pd atom and TiO_2 unit are shown in the red and blue shaded regions, respectively. The insets show an

expanded view of the region where most of projected states lie. Clearly, the majority of the Pd and TiO valence states lie within 2 eV below the Fermi level and the total DOS are similar. All this indicates that the interchange of the TiO and Pd may be the starting point of the encapsulation of the Pd site.

The low energy cost in interchanging TiO and Pd sites raises an interesting issue. Both TiO and Pd atom have a similar valence pool of 10 valence electrons and contain d-states. Recent studies indicate that such pairs can exhibit similar electronic features.[120] For example, Pd^+ and ZrO^+ with 9 valence electrons have recently been found to exhibit similar reactivity and fragmentation products when reacted with CO and ethylene. Theoretical studies indicate that these similarities could be assigned to the occupation and presence of d-states in the electronic structures of the two species that have same number of valence electrons.[120] The present studies indicate that motifs with d-states and with same number of valence electrons seem to be interchangeable.

5.3 Conclusions

The results of this chapter present studies that indicate that O sites on a TiO_2 surface exhibit enhanced stability in the presence of Pd atoms. For PdO, the Pd donates a charge that is transferred to the O sites with the underlying surface remaining almost neutral. These interactions bring out a new class of ionic interactions that are mediated by the surface and could be classified as surface mediated ionic bonds. In this case, what is surprising is that TiO_2 is a well-known semiconductor with a large band gap of 3.0 eV. Yet, the surface mediates to transfer the charge from Pd to O even at large separations. This transfer is stimulated by the surface sites that resist any major change in their oxidation states and hence merely act to help transfer the

charge. Finally, the studies indicate the energetic cost of interchanging the Pd and TiO that have similar valence pool is lower than interchanging Pd and Ti. Further work is needed to develop these findings into useful guiding principles that could provide insight into the microscopic mechanisms of SMSI.

6. Adsorption of Pd_n (n=1-7) on Stoichiometric TiO_2(110)

6.1 Introduction

In this chapter, a systematic study of the atomic, electronic, and magnetic moment of Pd_n (n=1-7) clusters supported on a TiO_2 (110) surface is presented. As Pd_n clusters are oxidation catalysts, the effect of adding one and two O atoms on the electronic and magnetic character is investigated. These investigations are partly designed to offer insight not only to the oxidation behavior of supported Pd_n clusters, but also into the recent experimental observations on the growth characteristics. These include the STM experiments by Goodman and co-workers on the morphology of clusters on TiO_2 surfaces[121,122] as well as UHV experiments by Kaden et al. described in Chapter 4.[56] Recall that the ion scattering experiments indicated that clusters containing 4 and 7 atoms were planar while clusters containing more than 10 atoms were bi-planar. The studies presented within this chapter are directed towards offering a fundamental insight into some of these experimental findings. The basic issues addressed are the following: (1) The ground state atomic configurations, electronic structure, and magnetic properties of the supported palladium clusters and if the clusters containing 10 atoms or less are calculated to be planar. (2) The effect of adding an O atom on the atomic and electronic structure and the strength of bonding of the O atom. (3) The

ground state of the clusters with two O atoms and whether both O atoms occupy sites on the Pd_n clusters or the O atoms spill over to the substrate. The particular interest in strength of oxygen bonding has direct implications in the efficiency of Pd_n clusters as oxidation catalysts. The fundamental information gained in this work is believed to constitute a first step towards developing a coherent picture of the CO oxidation by Pd_n clusters.

Before discussing the issues fundamental to oxidation and catalysis such as active sites and oxygen binding strength, the geometries and binding energies of bare, supported Pd_n clusters are discussed along with a discussion of the cluster-support interactions that drive these systems to their lowest total energy. A wide variety of initial geometries (over 200 unique geometries) were fully optimized to obtain the equilibrium structures of the TiO_2(110)-supported bare and oxidized Pd_n clusters. The equilibrium structures were found by comparing total energies of all optimized structures. For each structure spin-polarized calculations were performed to determine the possibility of Pd_n clusters maintaining their free cluster magnetic spin moments. The choice of initial Pd cluster geometries included the calculated free cluster and isomer geometries, and each was sampled at multiple locations on the TiO_2 slab. When sampling oxidized cluster geometries, multiple oxygen adsorption sites on both the calculated ground state as well as energetically close Pd_n cluster geometries were attempted. To determine whether there is a preference for oxygen to adsorb on the TiO_2 slab instead of exclusively on the Pd_n cluster, Ti surface sites were also sampled for adsorbed oxygen.

6.2 Cluster Geometries and Binding Sites

First, the Pd atom on the TiO_2 surface will be discussed, as it is found to form a set of energetically similar binding sites to which the remaining sizes bind to the surface. A ball and stick drawing of the rutile $TiO_2(110)$ surface model is shown in Figure 6.1 to indicate the possible binding sites for the Pd atom.

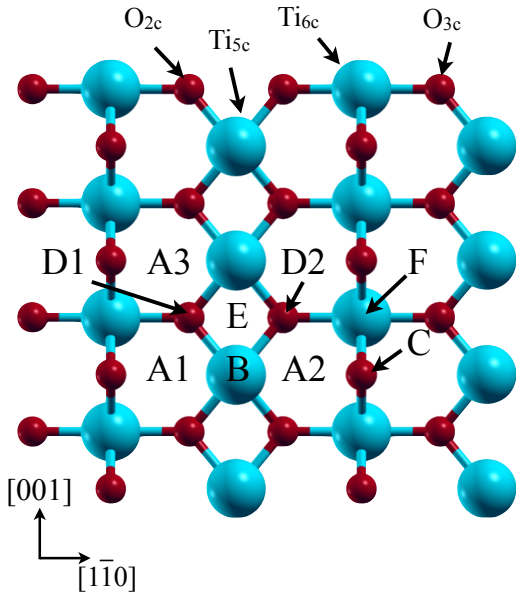

Figure 6.1: Labels for possible binding sites of the 4x2 rutile surface. The two types of Ti and two types of O atoms are labeled along with six different possible binding sites (labeled A-E). Sites labeled with the same letter (e.g., A1, A2, A3) are equivalent by symmetry. The blue spheres represent Ti atoms, and the red spheres represent O atoms.

The Pd atom favors a binding site in the surface channel directly atop an in-plane O_{3c} site, which is in agreement with previous theoretical studies.[34,123] The Pd atom also binds to several other sites with a comparable strength. Table 6.2 shows a list of binding energies for the Pd atom at the sites shown in Figure 6.1. Pd atoms have an energetic preference to bind with close proximity to lattice O sites rather than lattice

Site	Binding Energy (eV)
A	1.48
B	1.25
C	1.04
D	1.52
E	1.36
F	1.48

Table 6.1: List of Pd atom binding energies corresponding to the sites shown in Figure 6.1.

Ti sites. As discussed for the case of Pd_4 in Chapter 4, this is due to the charge on each atomic species. Within the lattice, Ti and O sites obtain positive and negative charge states, respectively, as bonding within the TiO_2 surface is partially ionic. At this stoichiometric TiO_2 surface, Pd atoms always donate charge to the surface and as a results are left in a positive charge state.

One of the important issues in characterizing cluster-support interactions pertains to the mobility of single atoms on the surface. The similar binding energy between the atop O_{3c} (site D) and hollow O_{3c} (site A) sites suggests that single Pd atoms may be mobile along the [001] direction of the TiO_2 surface. To this end, climbing image nudged elastic band (NEB)[124] calculations were performed to determine the diffusion pathways and diffusion barriers of a Pd atom on the surface. The results of the NEB analysis indicate virtually no diffusion barrier (maximum energy difference from ground state of only 0.05 eV) to move along the [001] direction. Interestingly, Pd diffusion is not entirely straight with respect to the surface channel direction. Figure 6.2(a) shows five "snapshots" of the minimum energy diffusion pathway that is curved towards the center of the channel to maximize Pd-O and minimize Pd-Ti interactions. This gives further support to the conclusion that Pd atoms prefer interaction with lattice O rather than lattice Ti sites. The extremely small energy differences of the five different positions on the surface are likely easily overcome during experiments,

which occur at finite temperatures.

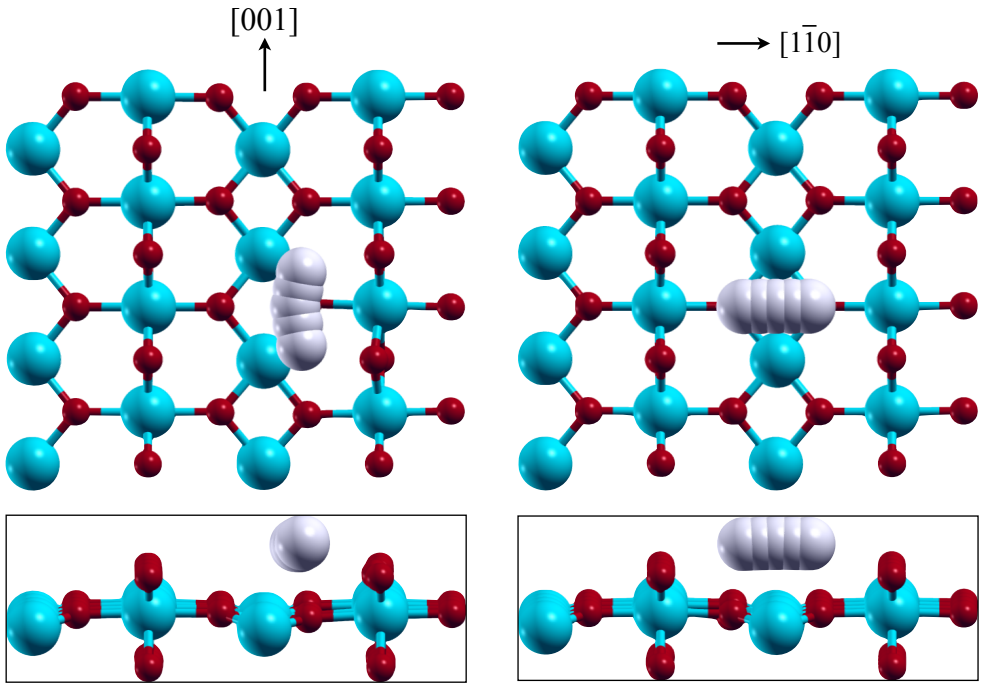

(a) Diffusion in surface channel direction (b) Diffusion across surface channel

Figure 6.2: Top and side views of the Pd atom diffusion pathways on the rutile surface in both the [001] and [1$\bar{1}$0] directions. Each figure contains five "snapshots" of the climbing image NEB calculation.

Pd atom diffusion across the center of the surface channel is also likely to occur if the pathway contains Pd diffusion directly over a Ti_{5c} hollow site shown in Figure 6.2(b). This diffusion contains virtually no energetic barrier (maximum barrier height of only 0.08 eV). On the other hand, crossing directly over a Ti_{5c} atom at the center of the surface channel, corresponding to pathway A1 $\rightarrow$ B $\rightarrow$ A2 from Figure 6.1, requires an activation energy of 0.27 eV due to direct Pd-Ti interaction. A Pd atom may even pass between two O_{2c} bridging atoms (binding site shown in Figure 2(h)), migrating to an adjacent TiO_2 surface channel. Thus, there is a large set of energetically similar Pd atom binding sites that are most likely to be observed at finite temperatures and help in the diffusion of the Pd atoms.

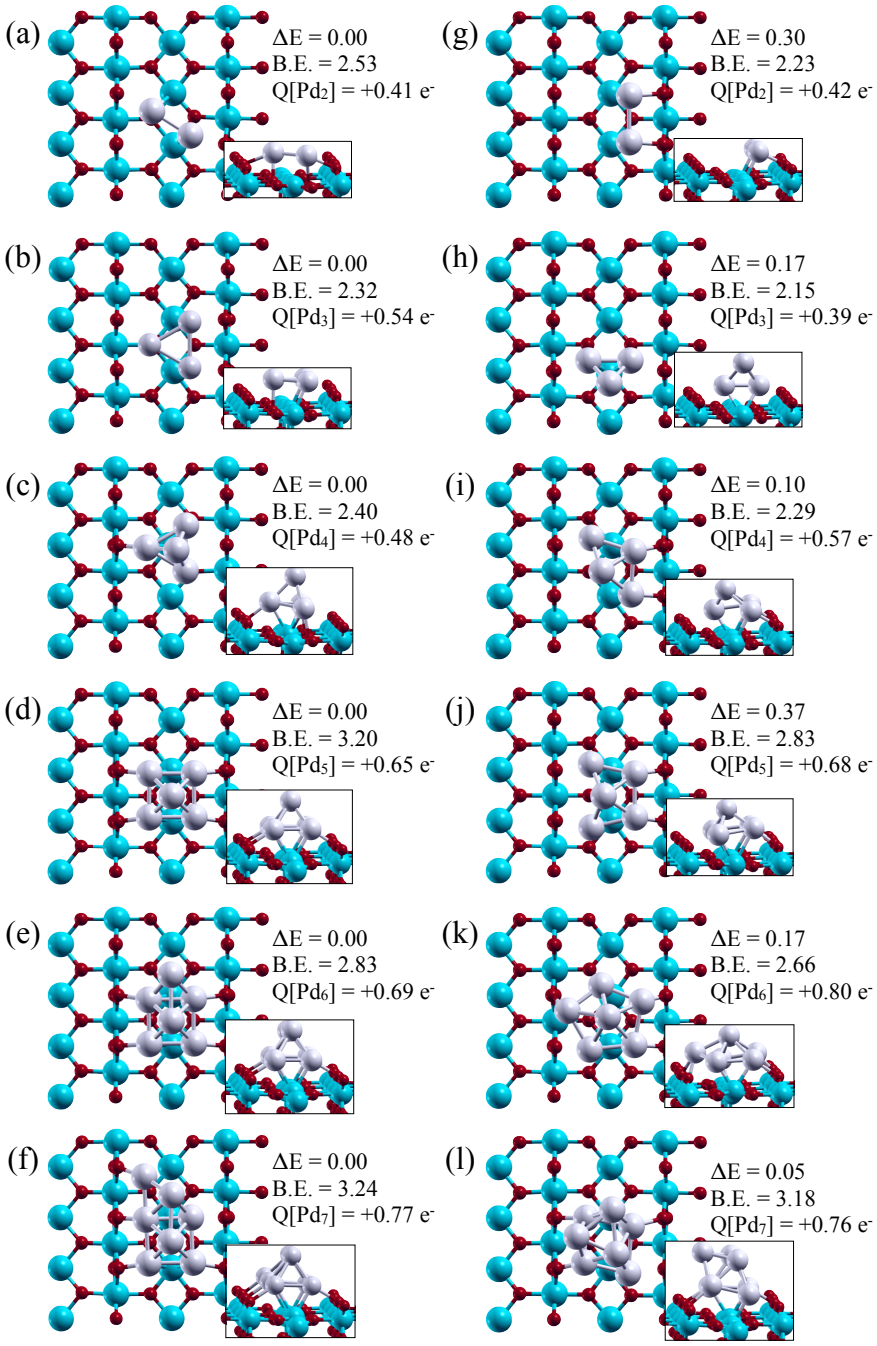

Figure 6.3: Ground state (left column) and near-lying isomers of Pd_n (n=1-7) clusters supported on the rutile TiO_2(110) surface. For clarity, only the top layer of the TiO_2 surface is shown. The silver spheres represent Pd atoms, the blue spheres represent Ti atoms, and the red spheres represent O atoms.

The ground state geometries and nearest energy isomers were determined by geometry optimizations of over 50 unique initial starting positions and are depicted in Figure 6.3. Beside each subfigure, the relative energies and Pd_n cluster binding energies are reported. Also reported is the charge on the entire Pd_n cluster, which was determined by a Bader charge analysis. In general, the results indicate that the ground state Pd_n cluster geometries are driven by either one or both of the two possible mechanisms: (1) intra cluster Pd-Pd interactions, due to s- and d- orbital hybridization, which favor close packing and lead to the compact structures of free Pd_n clusters, and (2) cluster-support interactions between Pd and lattice-O sites, which favor planar arrangements. Many of the clusters undergo only minor changes from their calculated free cluster geometries.

The calculated ground state structures of Pd_n (n=2-7) clusters appear as the addition of a single Pd atom to the Pd_{n-1} structure along the surface channel [001] direction. The exception to this trend occurs at n=4,6 where the fourth (sixth) Pd atom forms (contributes to) a second layer of the cluster. Considering the high mobility of Pd atoms along the [001] surface direction, these trends suggest cluster growth would occur in a Volmer-Weber[125] (formation of 3D islands) rather than a Stranski-Krastanow fashion[126] (formation of complete layer before 3D islands). This result is in agreement with STM experiments in the Goodman group.[121,122]

As the experiments are carried out at finite temperatures, energetically close-lying isomers likely coexist with the ground state. Structural isomer geometries that are close-lying in energy are shown in Figure 6.3(g-l). In general, these isomer geometries differ only slightly from the ground state structures, and in some cases only a small Pd-Pd bond length increase (e.g., Pd_2, Pd_4, Pd_5) or change in cluster orientation with respect to the surface (e.g., Pd_3) destabilizes the structure. Both of these destabilizing mechanisms point towards the governing idea that the ground state structure can be

considered as the balancing of the two competing forces mentioned earlier, namely Pd-lattice O and Pd-Pd interactions. In regards to cluster growth, knowledge of whether Pd_n clusters sit in the TiO_2 surface channel or on top of bridging O atom rows may elucidate details of previously reported results. Take the ground state and energetically close-lying isomer Pd_2 structures, for example. These structures are shown in Figures 6.3(a) and 6.3(g) and differ by their rotational orientation with respect to the surface and their Pd-Pd bond lengths of 2.66 Å and 2.73 Å, respectively. While both of these bond lengths are slightly longer than the calculated free cluster bond length of 2.48 Å, the Pd-lattice O interactions mentioned above help stabilize the slightly elongated structures. On the other hand, a Pd_2 structure that sits on top of the surfaces bridging O atoms, where both Pd atoms bound to adjacent bridging O_{2c} sites (two adjacent F sites from Figure 6.1), causes Pd-Pd separation to reach 2.78 Å and is 0.68 eV less stable than the ground state. This behavior is also seen at larger sizes, and geometry optimizations on Pd_n (n=3-7) cluster structures where some Pd atoms are bound atop or between two bridging O_{2c} atoms were at least 0.9 eV less stable than their ground states. This result indicates that while single Pd atoms may bind at bridging O_{2c} sites, larger clusters bound at bridging O_{2c} sites forces a large enough separation of Pd atoms to destabilize the structure.

Fundamental to understanding cluster growth on surfaces and available active sites per cluster is the size at which clusters transition from two- to three-dimensionality. Recall, the UHV deposited cluster experiments by the Anderson group which implemented Ion Scattering Spectroscopy (ISS) to probe the ratio of exposed Pd atoms with respect to Ti+O surface ions.[56] To this end, several geometry optimizations on planar configurations of the clusters were performed. As seen in Figures 6.3(i-k), the Pd_n (n=4-6) clusters possess structures where all Pd atoms could possibly be exposed in an ion scattering experiment. However, truly planar structures, in which all atoms

are directly coordinated to the surface, were calculated to be highly unstable (at least 0.9 eV higher than their ground states) for sizes n=5-7.

6.3 Spin Excitation Energy

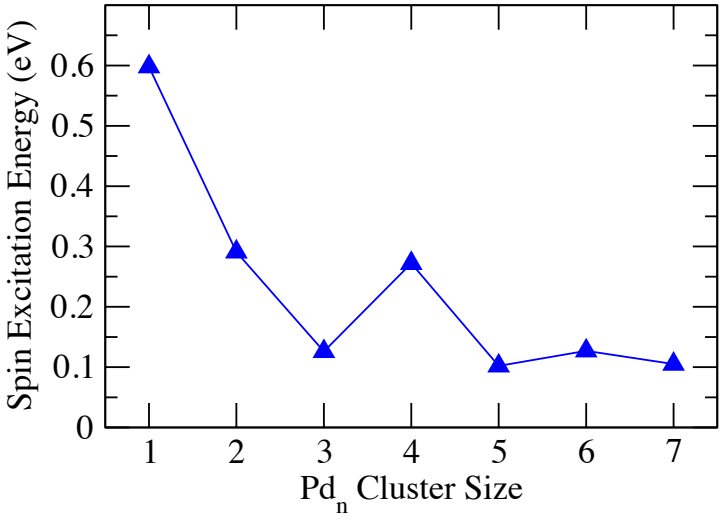

Figure 6.4: Spin excitation energy for $Pd_n/TiO_2(110)$ as a function of cluster size

Unlike the bulk metal, small Pd_n clusters have been found to possess finite spin magnetic moments.[3,9,101] Note that in a Pd atom, the 4d shell is completely full and followed by empty 5s states. The hybridization between s- and d- states in clusters coupled with a narrow "d-band" stabilizes a magnetic state.[103,127] Previous studies have indicated that the spin can have a determining effect on the reactivity with oxygen. For example, previous studies in the Khanna group have shown that the reactivity of gas phase Al_n^- clusters with an even number of electrons is strongly correlated to the spin excitation energy from the singlet ground states to the triplet excited states.[128] This is because the ground state of an O_2 molecule is a spin triplet and any weakening of the O-O bond requires filling of the minority spin states that

form the lowest unoccupied orbitals in the free O_2 molecule.[128] The present work shows that the spin moment for the deposited Pd_n clusters is primarily localized on the Pd sites. It is then interesting to explore if the spin excitation energy that controls the reactivity of gas phase clusters can also affect the behavior of supported clusters, where spin exchange may occur at the cluster-support interface. The spin ground state of the supported clusters varied between spin singlet and spin triplet, thus the spin excitation energy is calculated as the magnitude of the energy difference between the two spin states. As shown in Figure 6.4, the highest spin excitation energy of 0.60 eV occurs at Pd_1. If the spin excitation energy is a major factor in controlling the ability of supported clusters to activate an O_2 molecule, this may explain the results from the UHV experiments by the Anderson group that indicate the Pd atom exhibits the lowest activity for CO oxidation.[56] The effect of spin excitation on reactivity has yet to be shown for supported clusters, and requires further experimental verification before concluding that it is, in fact, a parameter critical in controlling the oxidation behavior of Pd_n clusters.

6.4 Oxygen Binding Sites and Binding Energies

The focus on Pd_n cluster with a single O atom stems from the understanding that O-O bonds from adsorbed O_2 are expected to be activated at the Pd surface during oxidation. This concept was first introduced in Chapter 4 and is now discussed for other cluster sizes. As will be shown for Pd_nO_2 (n=2-7) clusters, all ground state atomic structures have O-O bonds entirely broken, and in many cases at the extremities of the Pd_n cluster. Additionally, if an oxidation reaction is to take place (e.g., oxidation of carbon monoxide), one of the two O atoms may be removed leaving a single O atom on the Pd cluster surface. Thus, Pd_nO clusters are likely to be stabilized

under typical reaction conditions. The ground state structures were determined from over 60 geometry optimizations and the results are summarized in Figure 6.5(a-g). To account the possibility of an O atom stabilizing a higher energy Pd_n cluster, both the ground state and higher energy Pd_n motifs were included as initial configurations in Pd_nO optimizations.

The results indicate that O atoms prefer adsorption at threefold sites where wavefunction overlap and charge accumulation by the adsorbed O are maximized. Clearly, there is an exception to this trend at smaller sizes Pd_n (n=1-2) which do not contain threefold sites. For Pd_2, the adsorbed O binds at a twofold bridging site and accumulates the least amount of charge in the entire series (Figure 6.5b). For Pd_1, an oxygen spillover geometry, shown in Figure 6.5(a), is strongly preferred (by 1.3 eV) compared to a geometry where O adsorbs directly atop the Pd atom. The case for O atom adsorption on Pd_1 will be discussed in more detail in Section 6.6, where it is compared to O_2 adsorption. For cluster sizes Pd_n (n=3-7), the preference for O atoms to adsorb at threefold sites is visible in Figures 6.5(c-g). For these structures, the Pd-adsorbed O bond lengths are always near 1.98 Å and thus mimic the Pd-O bond lengths for O adsorbed on the Pd(111) surface.[109] At this distance, three equivalent Pd-O bond lengths can be formed without substantial deformation to the Pd_n cluster.

Adsorbed O atoms prefer to remain in the center of the TiO_2 surface channel, as visible in Figures 6.5(a-g). In other cases, where the O adsorbed close to the bridging O_{2c} rows (either laterally left or right) the geometries were always less stable than those with O atoms aligned in the center of the surface channel. As determined by a Bader charge analysis, the bridging O_{2c} lattice sites accumulate charge through the Ti-O lattice ionic interactions and repel the similarly charged adsorbed O atoms. By O adsorbing in the center of the surface channel, this repulsion is minimized. The Pd_nO clusters retain their unoxidized geometries, with the exception of Pd_4, which has

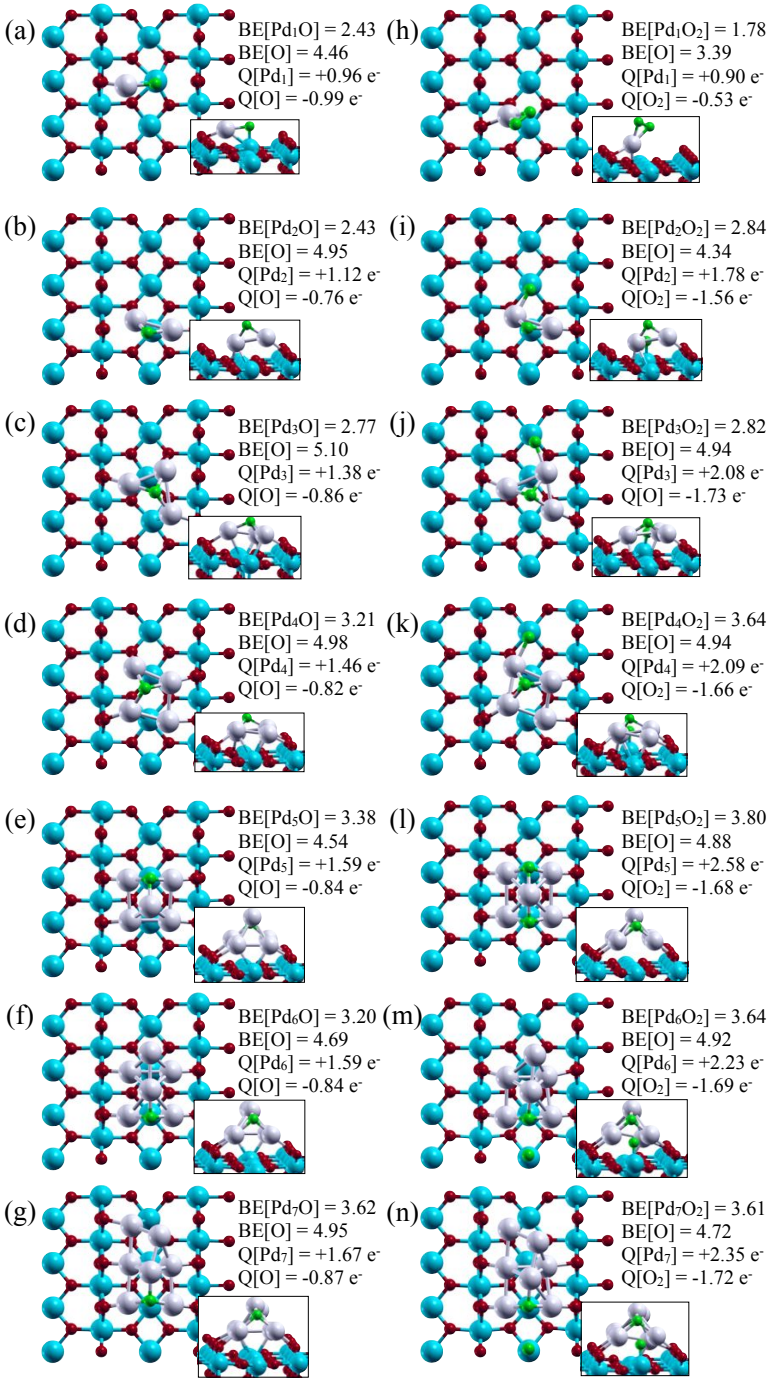

Figure 6.5: Ground state structures of TiO_2-supported Pd_nO (left column) Pd_nO_2 (right column) where n=1-7. The silver spheres represent Pd atoms and the blue spheres represent Ti atoms. The adsorbed O atoms are drawn as green spheres to differentiate from the lattice O atoms (red spheres).

previously been discussed in detail (Chapter 4). The stabilization of the planar Pd_4 structure shown in Figure 6.5(d) is due, in part, to these same repulsive interactions between surface and adsorbed oxygen. The other factor that contributes to stabilizing the planar Pd_4 structure is the opening of a threefold site that is centered in the TiO_2 surface channel. For O to adsorb at a threefold site on a tetrahedral Pd_4 motif, such as the one shown in Figure 6.3(c), the O atom is bound in close proximity of bridging O_{2c} atoms and was calculated to be 0.6 eV less stable than the ground state. This is indicative of the repulsive interactions that constrain adsorbing O atoms to the center of the surface channel.

In Figure 6.5, the charge accumulated by the adsorbed O atom and the charge depleted by the Pd_n cluster is also reported. Clearly, the Pd_n clusters donate more charge than the O atoms accumulate, indicating that charge is still donated towards the Ti and O sites of the support. As discussed in Chapter 4, the degree of coordination between Pd_n cluster and lattice O of the support is correlated to the amount of charge transferred from to the support. As for charge accumulated by the adsorbed O atom, the behavior is similar for all sizes except Pd_1. For n=2-7, charge is donated by the O-adsorbing Pd sites, while for Pd_1 the O accumulates charge from both Pd and a neighboring Ti_{5c} site, which it is also bound to. The spillover fashion that the O binds to the Pd_1/TiO_2 system with, allows for the maximum amount of charge (-0.99 e^-) to be accumulated.

6.5 Cluster Binding: Stability or Reactivity?

There is a well-known relation between a metal-O bond strength and the metals ability to perform a catalytic oxidation reaction.[36] From an energetic viewpoint, the more weakly a cluster binds an O atom the more active the cluster should be as a catalyst,

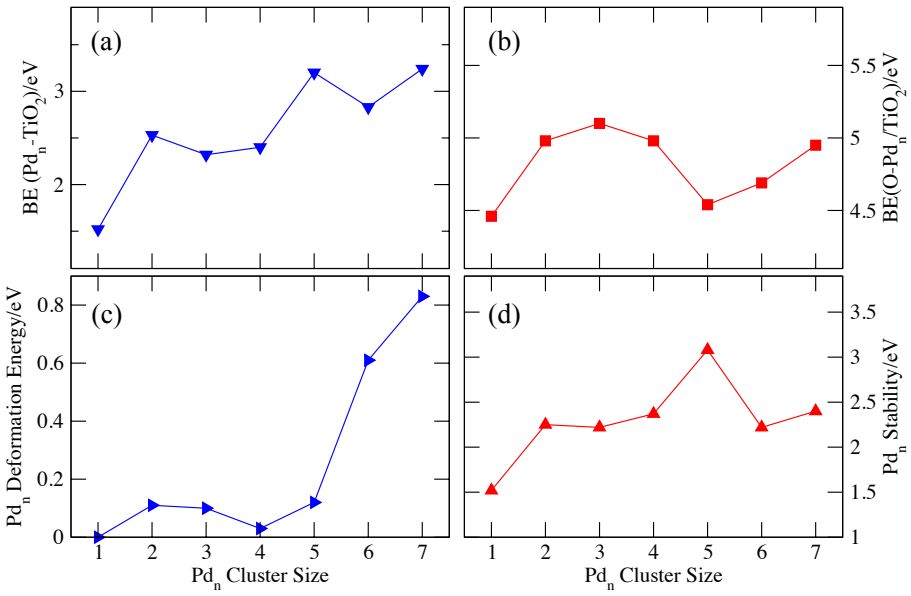

Figure 6.6: Plots of the (a) Pd_n cluster binding energy to the surface, (b) O binding energy to the supported Pd_n cluster, (c) Pd_n cluster deformation energy, and (d) Pd_n cluster surface stability.

as it will lead to CO oxidation to be a more exothermic. In supported clusters, one question yet to be answered pertains to the relation between metal-O binding energy and a supported clusters stability on a surface. Would the thermodynamics of an oxidation reaction favor a cluster that is strongly or weakly bound to the surface?

The plots in Figure 6.6 show the correlation between (a) the unoxidized Pd_n cluster binding energy to the surface and (b) the O binding strength to the Pd_n cluster. Excluding Pd_1, the results indicate that the weakest O binding energy occurs at Pd_5, the same size with a peak in Pd_n cluster binding energy. The enhanced binding of the supported Pd_5 cluster directly translates to a weaker oxygen binding energy. The inverse relationship between oxygen binding energy and Pd_n cluster binding energy holds for all sizes but Pd_1 and Pd_7. As already discussed, Pd_1 is a special case where the O atom binds differently than all other sizes and the spin excitation energy may play a major factor. On the other hand, it is quite surprising that the

trend falls apart at Pd_7. This motivates one to rethink the idea of cluster stability on the surface. In free clusters, the atomization energy of an n-atom cluster is the energy gained by binding n atoms together and is considered a marker of the inherent energetic stability of a cluster. In supported clusters, there are two contributions to stability: the cluster binding energy to the surface Figure 6.6(a) and the intra-cluster stability, which may can negatively affect a cluster's inherent stability if a cluster is deformed upon adsorption. This perturbation is referred to as the cluster deformation energy and is calculated by Equation 2.31 from Section 2.4.1. The results are shown in Figure 6.6(c) and reflect the structural deformations that most clusters undergo when binding to the TiO_2 surface. The largest deformation occurs at Pd_7, where the cluster undergoes a geometrical deformation that costs 0.83 eV in order to be accommodated into the TiO_2 surface channel. This introduces the notion of a supported cluster's "surface stability", calculated as the difference between the Pd_n binding energy and the Pd_n deformation energy. The surface stability is shown as a function of Pd_n cluster size in Figure 6.6(d) and clearly is inversely related to the oxygen binding energy. This stated, a cluster's surface stability can be considered as a lack of affinity toward O atom binding, but despite a low affinity O adsorption will still take place because of an O atom's strong tendency to accumulate charge. Further, the amount of charge accumulated by O remains relatively constant for the various cluster sizes. Essentially, charge accumulation by O is inevitable as it drives the system to a lower total energy, and while the amount of charge transferred is important, it holds a low critical value in determining how strongly O atom binds to a cluster. A Pd_n cluster's surface stability, however, holds high critical value as it is strongly inversely related to the O atom binding energy.

6.6 Pd_nO_2 Clusters

The addition of an second O atom to Pd_nO resulting in Pd_n clusters oxidized by two O atoms leads to intriguing behavior for cluster sizes n=2-7. The ground state structures are depicted in Figure 6.5(h-n). For all cluster sizes, Pd atoms donate charge while O atoms accumulate charge. In fact, the accumulation of charge by O atoms governs the geometries of the Pd_nO_2 clusters as the two negatively charged O sites try to be far separated. Recall that for Pd_4O_2, the interaction between the O sites leads to stabilization of a planar Pd_4 structure with one of the O atoms occupying a position bound to the cluster while the other O atom locates on a Ti site in a spillover mode. The analysis of the charge distribution showed how a repulsion between the O sites, that each accumulate nearly an electron of charge, could account for the structure. The following paragraphs will show how the accumulation of electronic charge by oxygen continues to govern the ground state atomic structure at other sizes as well.

Recall the experiments by Kaden et al.,[56] which show that a single Pd atom exhibits the lowest efficiency for oxidation of CO to CO_2. The present studies indicate that of all the cluster sizes considered here the Pd atom is the only case where the O-O bond of the absorbed O_2 is not broken. The O-O bond length is mildly stretched from its calculated free molecule bond length of 1.23 Å to 1.34 Å, however, indicating a minor activation. So, while the Pd site does activate the O-O bond, there is an additional barrier for the CO to convert into CO_2 as it involves breaking the O-O bond. As previously stated, the single Pd atom also has the highest spin excitation energy, which suggests that the spin state might be playing a role in low activity. For sizes n=2-7, on the other hand, both O atoms are well separated and atomic configurations where O-O bonds were still intact (distance of 1.40 Å or less) were on average 1.79 eV less stable than the ground state. More importantly, for all sizes

n=2-7, oxygen adsorbs in a spillover geometry. It is important to add that, as shown in Figure 6.5(l), Pd_5 possess a geometry where both O atoms bind to the cluster. This structure is energetically degenerate (only a 0.06 eV energy difference) with a structure where one O atom spills over. This feature is probably linked with the weakest binding of O to Pd_5 amongst Pd_nO clusters. By comparing the Pd_nO and Pd_nO_2 ground state structures, it is evident that the Pd_n clusters undergo minor atomic rearrangement upon addition of a second O atom. Thus, one O atom still prefers to bind at a threefold hollow site on the Pd_n cluster, while the second oxygen atom spills over to the nearest Ti_{5c} site. For Pd_nO ground state structures, atomic configurations where the O atom was initially bound to a Ti_{5c} site instead of the Pd_n cluster were also tested. The O atom prefers to bind to the Pd_n cluster for all cases except Pd_1, where it binds at the Pd-Ti interface. On the other hand, all ground state structures in the Pd_nO_2 series have one O atom spilled over to the neighboring Ti_{5c} site except for Pd_1, which has an intact O_2 molecule. The dissociation of molecular oxygen requires electronic charge transfer from the Pd_n cluster to the antibonding orbital of the O_2 molecule. Shown alongside the structures in Figure 6.5(h-n) is the charge on both the Pd_n cluster and the O_2 molecule. For Pd_1O_2, only 0.53 e^- are transferred from the Pd atom to the O_2 molecule. This weakens the O-O bond, as seen by the increase in O-O distance by 0.11 Å, but is not enough charge transfer to completely break it.

The result indicating oxygen's tendency to adsorb in a spillover mode was quite surprising, especially at large sizes where binding at two peripheries of a cluster would minimize the Coulomb repulsion between O atoms. To investigate this in more detail, the incremental oxygen binding energy as function of cluster size is plotted. The plot is shown in the upper panel of Figure 6.7, while in the lower panel the amount of charged transferred to the O_2 molecule is shown. There is a clear correlation between

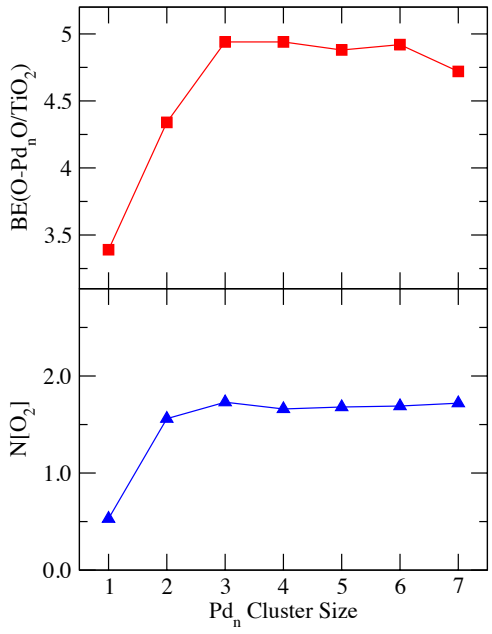

Figure 6.7: Upper panel: Binding energy of O to Pd_nO/TiO_2 in eV. Lower panel: Total charge accumulated by the O_2 molecule in e^-.

the two data, indicating that charge accumulation by oxygen is related to the oxygen binding strength. The weakest binding energy occurs at Pd_1, where both O atoms compete for charge accumulation from the same Pd atom. The next weakest occurs oxygen binding energy occurs at Pd_2. At this size, there is still a competition of charge accumulation between the two O atoms, however not as dramatic as for Pd_1. Beyond Pd_2, both the oxygen binding energy and charge on O_2 saturate to around 5.0 eV and 1.70 e^-, respectively. The similar oxygen binding energies for Pd_n cluster sizes n=3-7 arise from the similar oxygen adsorption configurations at these cluster sizes. At these sizes, one O atom binds at a threefold hollow site (the same threefold hollow site occupied by a single O atom in the Pd_nO/TiO_2 geometries), and the other O atom spills over to a neighboring Ti_{5c} site.

The existence of oxygen spillover is consistent with the UHV deposited cluster experiments on the catalytic oxidation of CO by $TiO_2(110)$-supported Pd_n clusters.[56]

It is found that the oxidation of CO at 550 K by the oxidized Pd_n species generates CO_2, but the amount of CO_2 is much less than to account for the removal of all O atoms. Yet, the experiments do not see desorption of O_2 up until 600 K. In fact, there are no adsorbates left on the Pd_n surface, suggesting that the remaining O atoms have spilled over onto the TiO_2 surface. Since the binding energy of the spilled over O atoms is less than that of the O atoms on the Pd_n cluster, one might wonder why the spillover O atoms are not involved in CO oxidation. It is believed that the O adsorbed on the Ti_{5c} sites may be expected to have a higher barrier for oxidation than those located on the Pd clusters.

6.7 Conclusions

The studies summarized in this chapter indicate that Pd_n clusters supported on stoichiometric $TiO_2(110)$ have geometrical structures that are governed by the Pd-Pd interactions that favor a compact geometry and Pd substrate interactions that favor Pd atoms occupying sites above the lattice O sites. This can lead to isomers (as in case of Pd_4) that favor compact or more open structures. For a single O atom, the oxygen binding energy changes with cluster sizes and is inversely related to the supported clusters stability. For the addition of O_2, it is shown that for a single Pd atom, the O-O bond is stretched from its free atom value. On the other hand, all the remaining clusters lead to structures with a broken O-O bond. One of the O atoms favors a position over the Pd_n cluster while the other occupies sites above a lattice Ti atom representing a spillover O atom. Further, spillover oxygen may be less susceptible for CO oxidation because of a larger barrier. The experimental work by Kaden et al. suggests that Pd_4 and Pd_7 probably have planar configurations when supported on the stoichiometric surface. For Pd_4, the studies do indicate a planar

isomer that is only 0.10 eV less stable. As the experiments are carried out at finite temperatures, it is feasible that planar configuration can be seen in the experiments. For Pd_7, a bi-layer ground state is found with a first layer of 5 atoms and 2 atoms occupying a second layer. The structures of the Pd_n clusters are highly sensitive to the environment and the addition of O does have a significant effect on the electronic and geometric structure. This softness is believed to be key to the interest in small clusters where the control over properties by size and environment can enable tunable catalytic features.

7. Adsorption of Pd_n (n=1-7) on Non-Stoichiometric TiO_2(110)

7.1 Introduction

The motivation in studying the non-stoichiometric surface is to provide a more accurate representation of the experimental TiO_2 surface. Ion bombardment or thermal annealing leads to surface defects known to be bridging O_{2c} vacancies,[26,38,39,129] and the periodic slab model would have to contain such vacancies to more closely match the experiment. Note that oxygen vacancy sites are known to react with residual water at the surface, even in UHV conditions, which can convert oxygen vacancy sites to sites containing a hydroxyl group.[39,130] This motivation is further compounded by previous studies have indicated that oxygen vacancies may affect both cluster nucleation by enhancing binding at the vacancy site and cluster catalysis by modifying the electronic properties of the cluster.[52,97,131–136] Take, as an example, the combined theoretical/experimental studies on MgO(001) supported gold clusters by Landman and coworkers.[133] In the case for MgO, a missing oxygen atom results in "trap electrons", highly localized electron pairs remaining exactly at the vacancy site.[131] The trap electron did, in fact, affect the cluster nucleation and cluster catalysis by enhancing the binding of Au clusters (Au_8 binding energy enhanced by over 2.00 eV) and promoting the activity of Au clusters by leaving them in negatively charged states.[133]

In regards to reactions with oxygen, negatively charged clusters should, at least in a general sense, be more reactive with oxygen as they can readily donate more electronic charge than neutral clusters. This is all, however, contingent upon the nature of cluster support interactions at oxygen vacancies, and the nature oxygen vacancies certainly differs between MgO and TiO_2. A detailed investigation of these interactions is necessary to understand the critical parameters for clusters on the reduced TiO_2 surface.

The results of this chapter show that in the presence of oxygen vacancies, the Pd_n clusters can bind to the surface in a variety of configurations. The configurations can most simply be grouped as *at* or *away from* the vacancy site, but whether or not the cluster binds at the vacancy leads to further differences in the cluster's electronic and geometric properties. Also, the results in this chapter show that the presence of oxygen vacancies allows the clusters to obtain a wider range of charge states (including negative charge states) compared to those obtained on the stoichiometric surface. Initially, this could be interpreted to suggest a wider range of oxygen atom binding energies as well. The calculations, however, show a general trend indicating that the calculated oxygen binding energy is larger compared to the case for Pd_n clusters supported on the perfect surface. As will be shown, the large oxygen binding energy is a consequence of not the charge state of the cluster, but the binding site to which oxygen prefers to adsorb. Within this chapter, a systematic study of the atomic and electronic structures of Pd_n clusters on the TiO_2 surface marked with oxygen vacancies is introduced. The key results of this chapter build on the previous chapters' discussions, specifically on the importance of charge accumulation by oxygen, oxygen spillover geometries, and surface mediated ionic bonds.

7.2 Theoretical Description of the Reduced TiO_2 Surface

In this study, the defect site is simply a missing O_{2c} atom from the surface layer. The structure of the reduced surface is shown in Figure 7.1(a). The 4x2 surface supercell contains eight bridging O_{2c} atoms, and removing a single O atom results in a bridging oxygen vacancy concentration is 12.5%. This is near the typical experimental concentrations where 7-12% of the unit cells containing bridging oxygen vacancies.[38,54] The system undergoes an energetic penalty upon the removal of an O_{2c} atom and this quantity, referred to as the vacancy formation energy, is calculated by the following equation:

$$E_{vf} = E(def) + \frac{1}{2}E(O_2) - E(perf), \tag{7.1}$$

where $E(def)$ and $E(perf)$ are the total energies of the defective and perfect (stoichiometric) surface, respectively, and $E(O_2)$ is the total energy of an O_2 molecule. Within the methods used here, the vacancy formation energy was calculated to be 3.49 eV, in good agreement with previous theoretical studies.[97,115] Because these calculations are periodic, the vacancy sites can interact with other periodic images producing artificial forces within the system and perturbing the total energy calculation. This is particularly troublesome for small surface cell calculations. Figure 7.1(b) shows the vacancy formation energy from previous studies and the present study, and indicates that the methods used in this study produce a converged formation energy with respect to cell size. The converged behavior of the curve indicates the oxygen vacancies are no longer interacting when they are separated by at least ~9 Å, which is achieved with 6 surface unit cells in a 2x3 surface scheme.

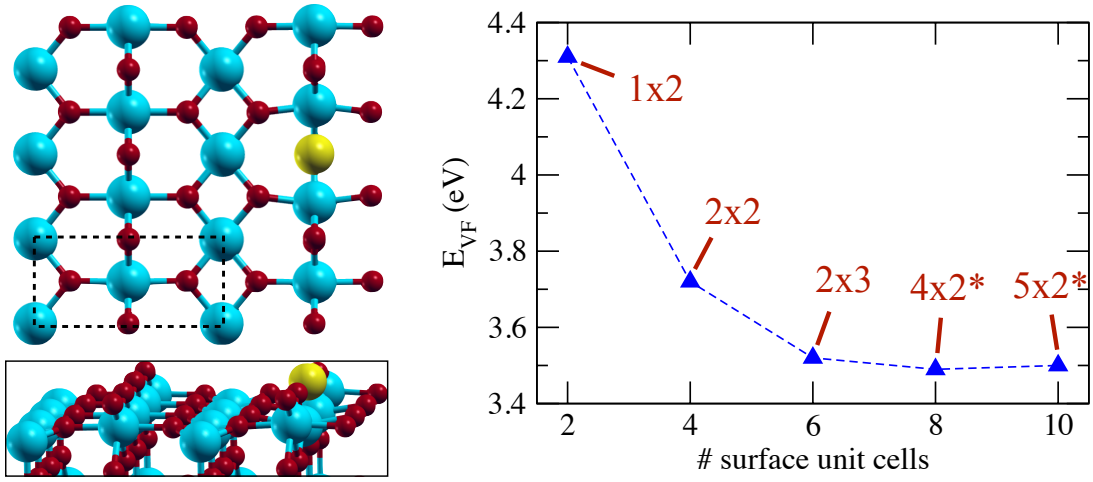

(a) Reduced TiO_2 Surface

(b) Oxygen vacancy formation energy.

Figure 7.1: Figure (a) shows a ball and stick drawing of the reduced TiO_2 surface in a 4x2 surface supercell. The oxygen vacancy site is depicted by a yellow sphere and a dashed box is drawn around the 1x1 unit cell. Figure (b) shows the oxygen vacancy formation energy as a function of surface size. The exact surface scheme used in the calculation is shown above the data points and the x-axis is the resulting number of surface unit cells. The two data points marked with asterisks are energies calculated within this study. Other data points were taken from Wu and Chretien, where identical computational methods as the one used in this study were employed.[97,115]

The presence of an oxygen vacancy, formally, leaves two electrons at the surface. In a partially ionic and partially covalent system such as TiO_2, these electrons are localized at 3d orbitals of nearby Ti atoms.[131,137] To this end, different magnetic spin states were calculated to determine the effect of the oxygen vacancy on the magnetic structure. Similar to the stoichiometric surface, the singlet and triplet spin states for a surface with a single oxygen vacancy are roughly energetically degenerate (0.05 eV energy difference). In the spin triplet case, the unpaired electrons are delocalized on Ti 3d orbitals surrounding the vacancy, thus leaving the local surface structure with an excess of electronic charge.

The presence of an oxygen vacancy also has an effect on the atomic structure. Near the vacancy site, the local lattice structure undergoes a distortion in which the

positions of under-coordinated Ti atoms near the vacancy site are slightly shifted toward O sites. The calculated distortions are apparent when considering the change in bond lengths from the reduced surface. Table 7.1 contains the characteristic bond lengths of the perfect surface and the reduced surface. The most change occurs for bonds labeled C, F, and H. As can be seen in Figure 3.5(a), a decrease in length for bonds C and H and an increase in length for bond F results in an increased Ti-O coordination for Ti atoms near the oxygen vacancy site. All three are Ti-O bonds and are oriented in the surface (110) direction. Hence, the lattice reconstructions primarily take place vertically (atomic positions shifting toward or away from the surface layer) rather than laterally.

Bond Lengths (Å)		
Bond Label	Perfect Surface	Reduced Surface
A	1.84	n/a
B	2.05	2.03
C	2.12	1.96
D	1.96	1.96
E	1.81	1.81
F	1.86	2.18
G	1.99	1.97
H	2.19	2.03
J	2.05	2.05
K	1.98	2.01
L	1.90	1.90

Table 7.1: Characteristic bond lengths calculated for the perfect and reduced titania surface. The column labeled perfect surface indicate the bond lengths for a surface without oxygen vacancies and is the same as found in the table shown in Figure 3.5(a). The column labeled reduced surface indicates the bond lengths directly at/beneath the vacancy site.

7.3 Pd_n clusters on Reduced TiO_2(110)

To obtain the equilibrium structures of Pd_n (n=1-7) clusters supported on the reduced TiO_2 surface, the same approach as described for the stoichiometric surface was taken. All of the geometries sampled for the stoichiometric surface were sampled for the reduced surface as well. In addition, geometries containing Pd atoms at the oxygen vacancy site were included to determine if there was any preference to bind at or near the vacancy.

The first objective, which is of primary interest when calculating adsorption energies and ground state geometries of clusters on the reduced surface, is to test whether or not the clusters bind preferably at the vacancy sites as this is likely to modify the cluster's electronic structure. The results indicate that, in general, the Pd_n clusters do not have a strong energetic preference of binding at the vacancy site. The caveat here is that for both Pd_2 and Pd_3 the lowest energy ground state structure is at the vacancy site, but both cluster sizes have energetically close-lying (in reference to their ground state) binding energies for sites away from the vacancy. These similar binding energies suggests that in experiments, which occur at finite temperatures, both of the sites may be available for cluster binding. On the other hand, while both Pd_4 and Pd_7 have ground states away from the vacancy site, they also have binding sites close-lying in energy with at least one Pd atom at the vacancy site. For the remaining sizes the preference to avoid the vacancy is clearly more energetically favored. By binding at the vacancy site, Pd_1 is 0.24 eV less stable compared to its ground state; likewise for Pd_5 and Pd_6, binding at the vacancy site results in less stable structures (0.67 eV and 0.79 eV higher in energy, respectively) compared to their corresponding ground states. In Figure 7.2, the calculated ground state geometries (left column) and higher energy isomers (right column) are shown. In the left column, all cluster

sizes (except n=2,3) show binding *away* from the vacancy site; while in the right column, all sizes (except n=2,3) show binding *at* the vacancy site. For cluster binding away from the vacancy, the geometries are characteristically similar to those on the stoichiometric surface (Figure 6.3). This suggests that the same intra-cluster interactions (Pd s- and d- orbital hybridization) and cluster-surface interactions (Pd and lattice-O interaction) that collectively stabilize the ground state structures on the stoichiometric surface also play a role in stabilizing the ground state structures on the reduced surface.

Cluster binding at the vacancy site, whether stable or unstable, results in atomic structures characteristically different than their gas phase or stoichiometric-adsorbed geometries. Interestingly, all of these structures are highly planar as shown in Figure 7.2(h-n). At the vacancy site, the electronic structure of the clusters is modified, which gives rise to the planar structures. Recall from the discussion of gas phase Pd_n clusters in Section 3.4 that s- and d- orbital hybridization causes (1) compact geometries in Pd_n clusters and (2) a splitting of the d- orbital electronic states, which results in partially depleted spin down d- states and thus non-zero spin magnetic moments. Also, recall that with an increasing cluster size the s- states are shifted to higher binding energies and thus appear deeper below the Fermi energy; while bulk palladium contains a free electron-like s- band that is shallow compared to the Pd d- band.[106] The key difference is that in compact clusters, the s- orbitals are localized as they are in gas phase clusters, while in bulk palladium the s- orbitals form a delocalized band due to enhanced surface interactions, and this delocalized band is indicative of a metallic-like structure.

For supported Pd_n clusters, the nature of s- and d- orbital hybridization is different depending on whether the clusters are bound at or away from the vacancy site. This difference leads to two types atomic and magnetic character. For clusters bound *away*

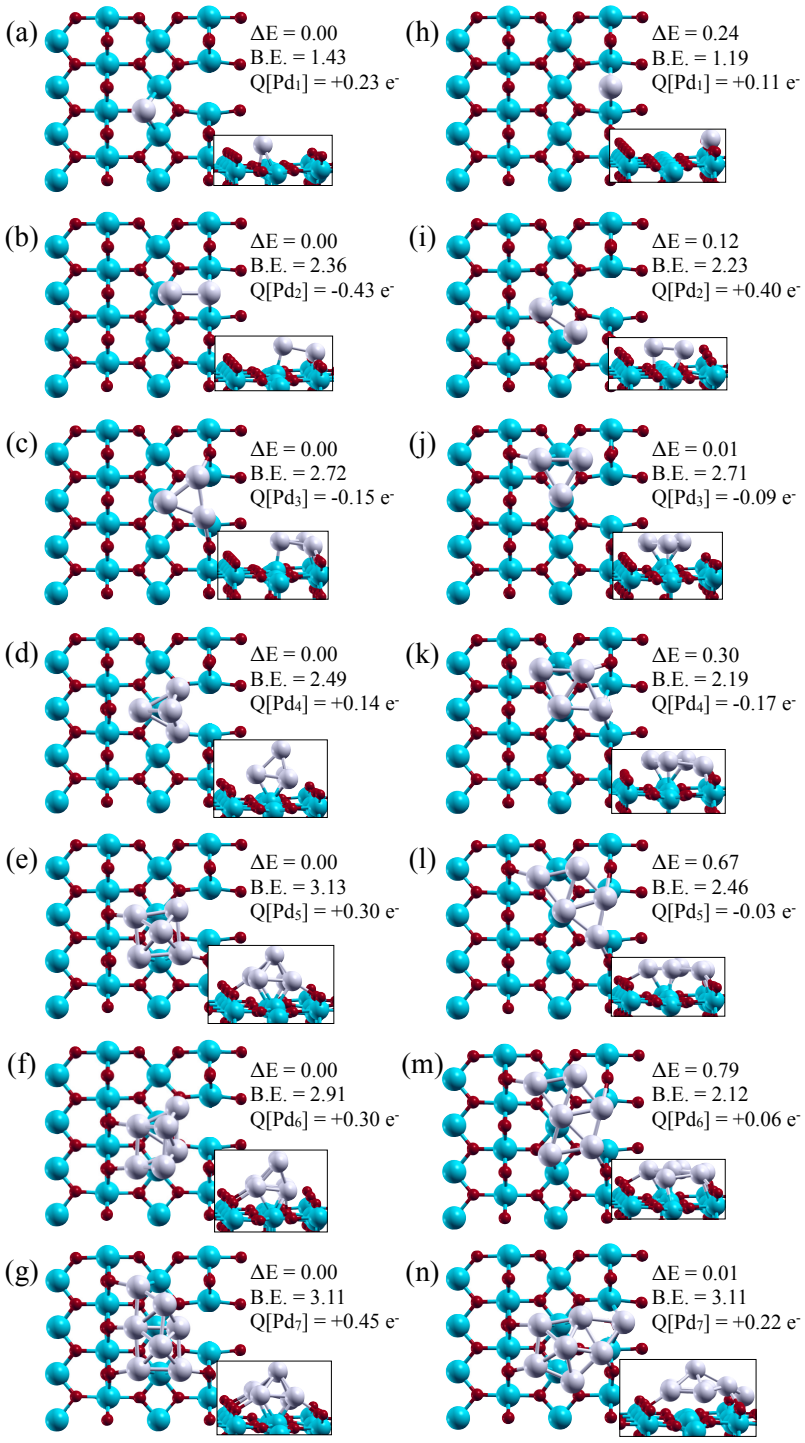

Figure 7.2: Ground state and isomer structures of reduced TiO_2-supported Pd_n where n=1-7. The silver spheres represent Pd atoms and the blue spheres represent Ti atoms. The vacancy site is in the same position as the yellow sphere in Figure 7.1(a), but now appears as a blank space (more clearly visible for Pd_n cluster not bound at vacancy).

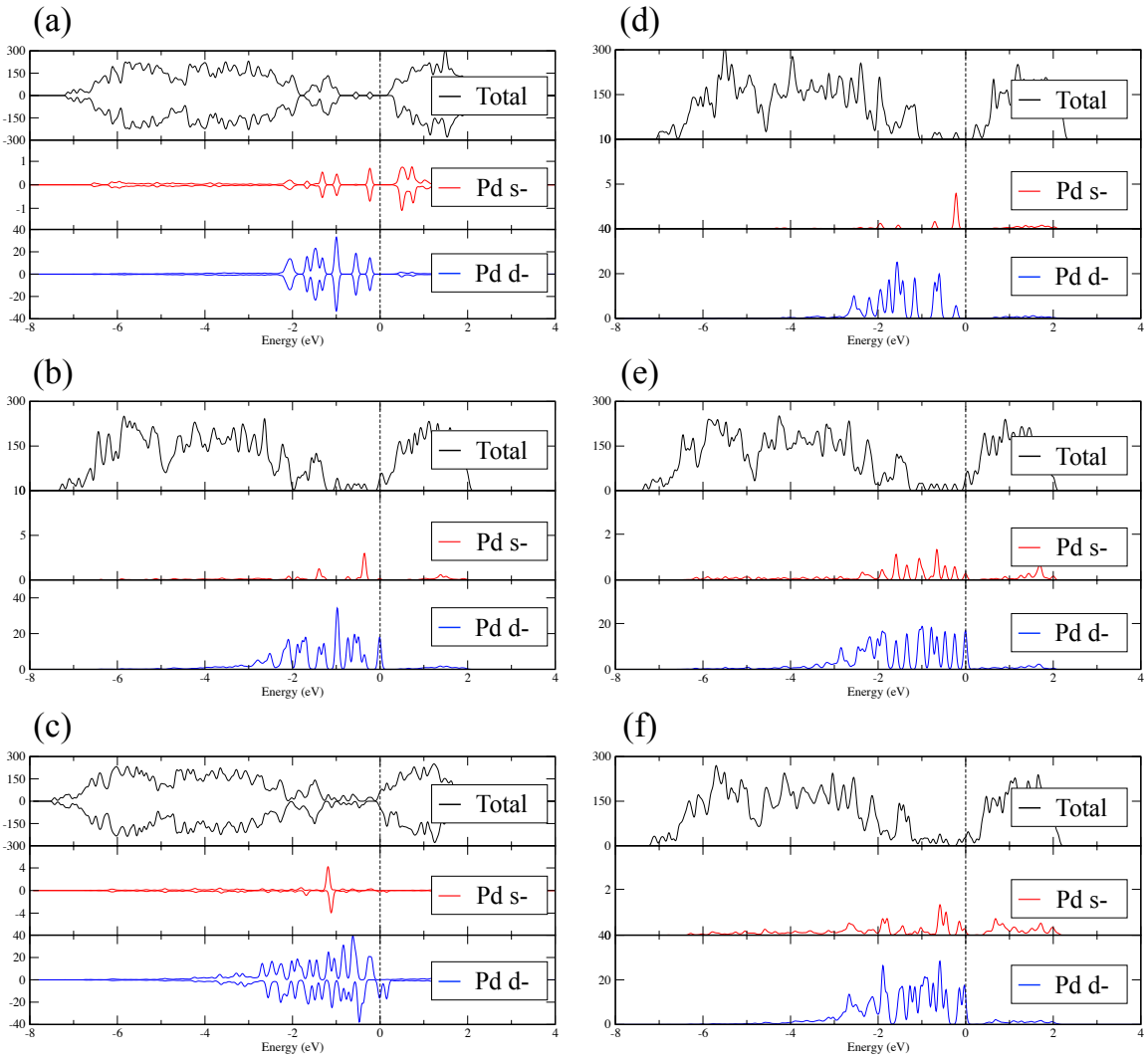

Figure 7.3: Density of states plots for Pd_n (n=2-4) on the reduced surface where clusters are bound away from (a thru c) and at (d thru f) the oxygen vacancy site. The black, red, and blue lines correspond to the total, Pd s-, and Pd d- states, respectively.

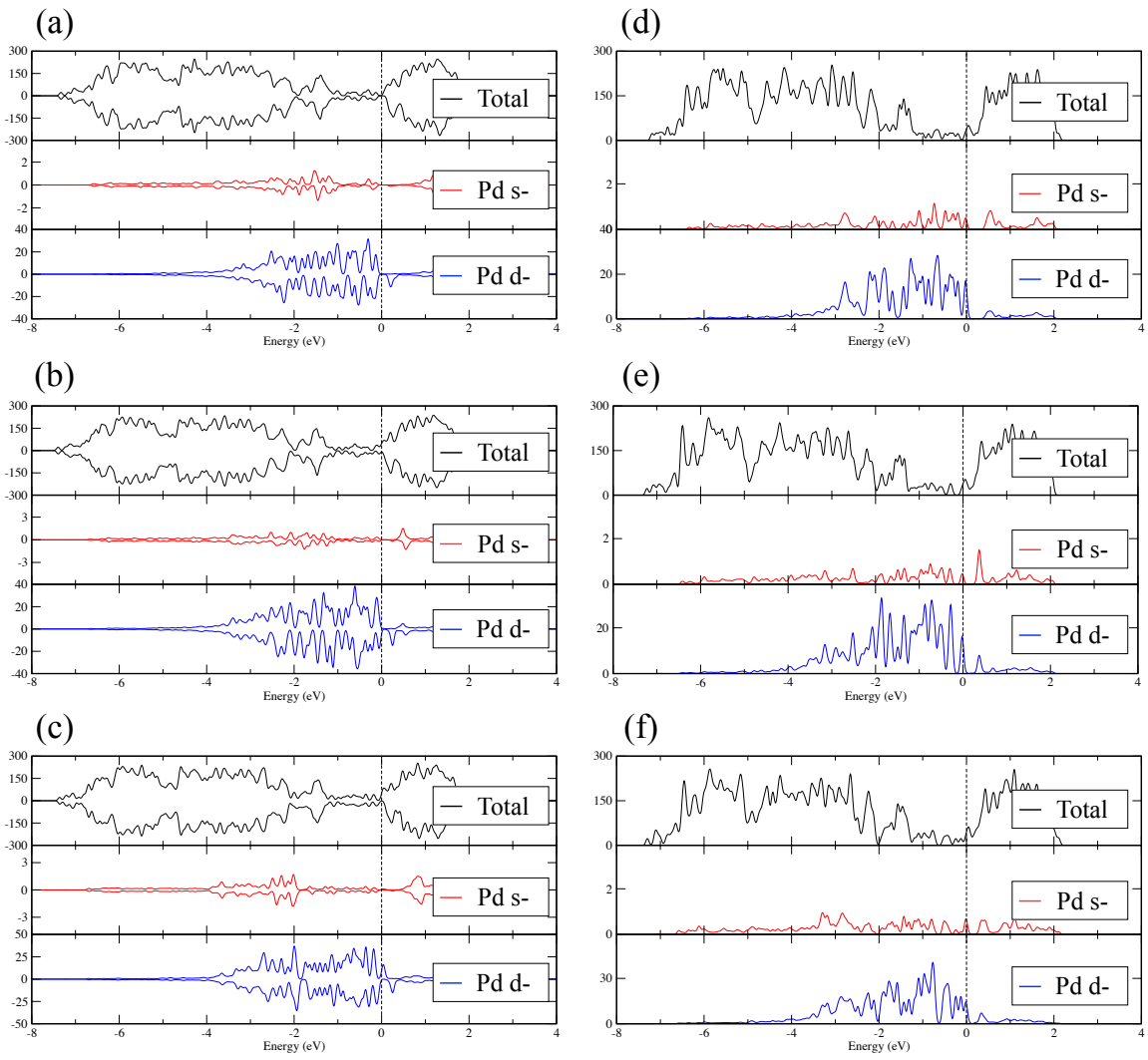

Figure 7.4: Density of states plots for Pd_n (n=5-6) on the reduced surface where clusters are bound away from (a thru c) and at (d thru f) the oxygen vacancy site. The black, red, and blue lines correspond to the total, Pd s-, and Pd d- states, respectively.

from the vacancy site, the s- states form a localized set that shifts to high binding energies with increasing clusters size, similar to gas phase Pd_n clusters. For clusters bound *at* the vacancy site, a shallow "band" of s- states forms, indicating a more metallic-like behavior which becomes more delocalized with increasing cluster size. The total and angular momentum decomposed DOS for Pd_n (n=2-7) is shown in Figures 7.3 and 7.4. The plots on the left side correspond to clusters bound away from the vacancy site, and those on the right side correspond to clusters bound at the vacancy site. At small clusters sizes (e.g., Pd_2), the localized nature of the s- states is apparent regardless of cluster binding site. Yet, with even a slight increase in size (e.g., Pd_3 and Pd_4), the different features begin to emerge for clusters bound at the vacancy. The Pd s- states in Pd_4, for example, form a sharp peak at about 1 eV below the Fermi level (see Figure 7.3(c)) when the cluster is bound away from the vacancy in a compact, tetrahedral geometry. On the other hand, the flat Pd_4 cluster bound at the vacancy site contains Pd s- states that are clearly more delocalized as the sharp peaks become more diffuse (see see Figure 7.3(f)). Finally, at the largest sizes (Pd_5 thru Pd_7), the clusters away from the vacancy feature a set of s- states that shift collectively, while the clusters at the vacancy feature s- states that continue to form a delocalized band. The clusters bound at the vacancy possess an electronic structure reminiscent of bulk palladium where the s- states form a wide, shallow band and the d- states remain relatively localized.[106,107] Interestingly, the similarities extend beyond the electronic structure and are reflected in the geometric and magnetic character as well. First, nearly all of the planar geometries shown in Figure 7.2(h-n) possess the hexagonal symmetry found in the stable (111) facet of the bulk palladium fcc structure. Second, the differing nature of orbital hybridization between clusters bound at and away from the vacancy leads to different magnetic character. For Pd_n clusters bound at the vacancy, the clusters are stabilized by the pairing of spin up

and spin down electrons resulting in spin magnetic moments of 0 μ_B; while almost all clusters away from the vacancy possess spin moments of 2 μ_B, as in the case of adsorption on the stoichiometric surface.

Referring to the results of the previous chapter, Pd_n cluster binding to the stoichiometric surface always resulted in charge transfer from Pd to the surface atoms and thus positive charge states on the cluster. The amount of charge transferred increased with an increasing cluster size, because larger clusters were more coordinated to the surface atoms that accepted charge. On the reduced surface, a wider variety of Pd_n charge states were calculated, and binding at the vacancy results in either negative or near neutral charges on Pd atoms. Even when the atomic structure was characteristically the same as it was on the stoichiometric surface (e.g., n=1,4-7), less charge was donated from Pd_n to the surface. For the sizes that preferably bind at the vacancy (n=2,3), charge was transferred from the surface to the Pd_n cluster. The observation that not all cluster obtain negative charge states indicates a qualitative difference between oxygen vacancies at the TiO_2 surface in comparison to those at the MgO surface that was discussed in the introduction of this chapter. The trap electrons produced as a result of an MgO oxygen vacancy are highly localized. Thus, cluster binding at an MgO vacancy always leads to charge transfer toward the cluster. On the other hand, oxygen vacancies on TiO_2 leads to an excess of electronic charge that is near the vacancy site, but less localized than an MgO oxygen vacancy. As a result, the charge state of Pd_n may be negative, but this is not necessarily the case.

The excess of electronic charge near a TiO_2 vacancy site has an strong effect on oxygen binding. Several of the previous chapters have highlighted the strong tendency for oxygen to accumulate charge, even to the extent of structurally modifying the Pd_4 geometry (Chapter 4) or adsorbing at the interface made by the Pd_n cluster and the underlying TiO_2 surface as a "spillover" mode (Chapter 6). Considering the excess of

electronic charge on the reduced surface, one might expect oxygen atom binding at the Pd-Ti interface to be feasible. As will be shown in Section 7.5, this is in fact the case. It should be noted here, however, that the total energy of the system is always lowered when an O atom is back at the vacancy site thus "healing" the vacancy. Despite this, there are two reasons why a Pd_n cluster and an O atom could co-exist as two surface species even in the presence of a nearby oxygen vacancy. The first is the possibility that the Pd_n cluster is already bound at the vacancy site, presenting a steric hindrance. The second pertains to the energetic barrier for an O atom to diffuse into the vacancy site. There is a barrier associated with the process of an O_{ad} atom inserting into an oxygen vacancy, thus healing it. This barrier is calculated by a NEB analysis to be 0.81 eV. This barrier is substantial, even at finite temperatures. More importantly, the presence of even a single Pd atom should increase this barrier due to enhanced oxygen binding via the surface mediated ionic bonds discussed in Chapter 5. As this will certainly change the energetic barrier for an O atom to diffuse on the surface, a short digression must be taken to discuss the details of healing an oxygen vacancy in the presence of a Pd atom.

7.4 "Healing" a Bridging Oxygen Vacancy

The energetic barrier for an O_{ad} atom to heal an oxygen vacancy was calculated to determine the feasibility of a single O_{ad} atom on the surface in the presence of an oxygen vacancy. There are two factors of concern here, both of which will certainly be affected with the presence of Pd. The first factor is the barrier for healing a vacancy when an O_{ad} atom is bound to a Ti_{5c} site directly adjacent to the vacancy. As just discussed, this barrier was calculated to be 0.81 eV when Pd is not present. The second factor is O_{ad} diffusion along the surface channel, a process which obviously

must occur in order for the first factor to be relevant. For the reduced surface, this process corresponds to O_{ad} diffusion from a Ti_{5c} site that is one lattice constant away from the vacancy to a Ti_{5c} site adjacent to the vacancy. The barrier corresponding to this process was determined to be 1.16 eV, in good agreement with previous theoretical[39] and experimental[38] studies. One the stoichiometric surface, where Ti_{5c} sites are indistinguishable, the barrier was calculated to be slightly less at only 0.82 eV. Nevertheless, these large barriers suggest that O_{ad} atoms are immobile on the reduced surface.

There is an important difference to O_{ad} mobility on the stoichiometric compared to the reduced surface that becomes evident when comparing the binding strength of O_{ad} to each of these surfaces. The binding of O_{ad} to stoichiometric TiO_2 was calculated to be 1.69 eV. This relatively weak binding occurs because all surface atoms are fully coordinated and the TiO_2 stoichiometry is conserved. On the other hand, binding of O_{ad} to the reduced surface, where Ti sites near the vacancy are under-coordinated, was calculated to be 5.25 eV. This huge gain in binding energy is a reflection of the instability of the oxygen vacancy surface. Recall the energetic penalty of forming an oxygen vacancy is 3.49 eV. This penalty is essentially accounted for in the binding energy calculation for O_{ad} on the reduced surface. That is, the difference between these two energies yields 1.76 eV, much closer to the O_{ad} atom binding energy on the stoichiometric surface. The consequence of such a huge binding energy is a limited diffusion for O_{ad} when adsorbed on the reduced surface.

Considering the long range ionic bonds introduced in Chapter 5, the presence of even a single Pd atom should modify both O_{ad} diffusion on the reduced surface and the energetic barrier to heal an oxygen vacancy. The barrier for O_{ad} to heal an oxygen vacancy when Pd is co-adsorbed on the surface was determined by a NEB analysis. The reaction pathway is shown in Figure 7.5(a) as a series of five steps optimized

within the NEB calculation, and the energies at each step of the NEB analysis are shown in the upper panel of Figure 7.5(b). The initial state is 0.43 eV higher in energy than the final state, but the calculated barrier for O_{ad} to diffuse away from Pd and fill the vacancy is 1.62 eV. This large barrier likely limits the mobility of O_{ad} to diffuse into the vacancy. At the initial reaction step, the O_{ad} is bound directly atop the Ti_{5c} site adjacent to the oxygen vacancy. As a result of this, the Ti_{5c} protrudes out of the surface by a distance of 0.8 Å in reference to its bare surface position. The plots in the lower panel of Figure 7.5(b) show the distance between this Ti_{5c} atom and the O_{ad} as well as the distance between Pd and O_{ad}. Thru reaction step 3, the Ti_{5c} remains protruding and maintains coordinated to the O_{ad} atom by a distance of 1.7 Å. But immediately after crossing the activation barrier the Ti-O distance jumps to 3.0 Å, and the Ti_{5c} atom begins to return to its original, bare surface position. The dashed, vertical line in Figure 7.5(b) is intended to emphasize the discontinuous behavior immediately after the system crosses the activation barrier. The Pd-O distance increases more continuously throughout the reaction. The result of the NEB analysis gives evidence to support the existence of an O_{ad} bound to a Ti_{5c} site adjacent to the oxygen vacancy without actually healing it, as long as Pd is present.

7.5 Pd_nO Clusters on the Reduced TiO_2 Surface

With justification that Pd and O can co-adsorb on a surface that contains a nearby oxygen vacancy, the Pd_nO clusters on reduced TiO_2 can now be discussed. The equilibrium structures were determined by the same procedure as without oxygen and geometry optimizations were performed where Pd_n clusters were either initially at or away from the oxygen vacancy site. Additionally, geometry optimizations included

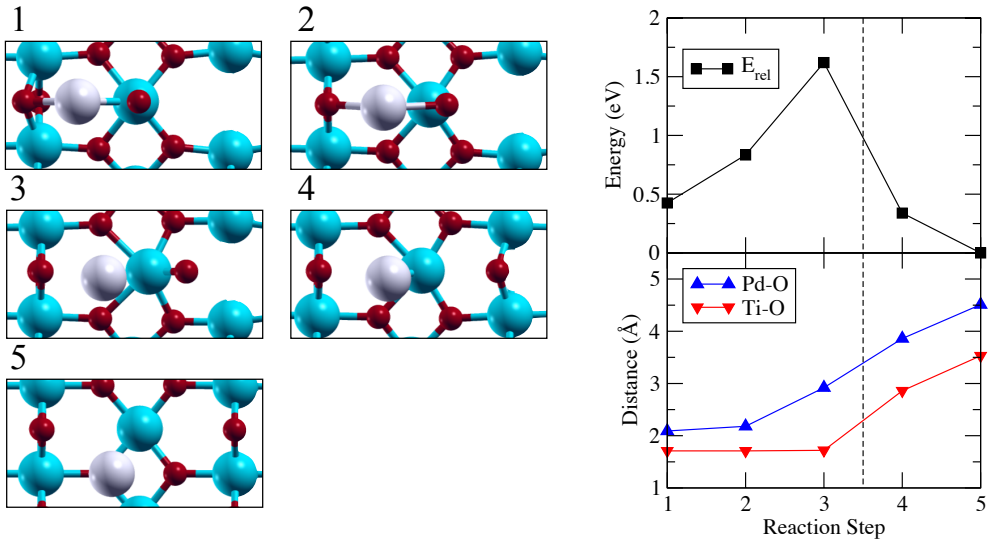

(a) NEB Reaction Pathway (b) NEB Barrier and Bond Lengths

Figure 7.5: Results of the NEB analysis for the diffusion of an O_{ad} atom into the vacancy site. Figure (a) shows each step of the 5 image reaction pathway. In Figure (b), the upper panel shows in the relative energy (black squares) of each state, and the bottom panel shows the distances of separation between Pd and O_{ad} (blue triangles pointed up) and Ti_{5c} and O_{ad} (red triangles pointed down).

configurations where the O atoms were both on and off the Pd_n clusters. The resultant geometries are shown in Figure 7.6. It is important to note here that for *all* geometries, the structures are *less stable* than if the oxygen vacancy is healed. Specifically, the structures shown in Figure 6.3 (Pd_n clusters on the stoichiometric surface) all resulted in a lower total energy than those shown here. To this end, the relative energy difference between these clusters and those of Figure 6.3 is reported beside each subfigure as E_{rel}. The figure is divided into two groups: Parts (b) thru (g) correspond to the lowest energy configurations where Pd_n clusters are away from the vacancy, and the vacancy is not healed. Parts (i) thru (l) correspond to the lowest energy configurations where the Pd_n cluster is at the vacancy site. For Pd_6 and Pd_7, geometries where Pd_n was at the vacancy were not convergent because the Pd_nO cluster's dimensions exceeded the dimensions of the surface supercell. In all cases, O

adsorption at the Pd-Ti interface is energetically favored, and the Pd_n motifs undergo little change in atomic configuration when compared to the case without oxygen.

An important feature to highlight here is that while the atomic configurations shown in Figure 7.6 are indicative that O energetically prefers to adsorb in a spillover mode, there is a wide variety of atomic configurations that could possibly exist in an experiment. In the experiments by Anderson, the deposited clusters are oxidized by introducing molecular oxygen into the vacuum.[56] The Pd_n clusters then dissociatively adsorb the O_2 molecule resulting in two atomically adsorbed O atoms. One factor that is not included in the present study is that O atom diffusion on the Pd_n cluster may be limited to due high diffusion barriers. This stated, the cluster configurations shown in Figure 7.6 assume that O mobility on the Pd_n cluster is high, and that O atom adsorption at the Pd-Ti interface is a result of this high mobility. For each cluster size, configurations with O bound exclusively to the Pd_n cluster were calculated and *always* resulted in higher total energies.

As shown beside each subfigure, the amount of charge transferred by Pd_n does not entirely account for the charge accumulated by the O atom. This behavior is in direct contrast with the clusters supported on the stoichiometric surface where Pd_n charge states were larger in magnitude than O charge states; recall that Pd_n donated charge to adsorbed O atoms and to lattice O atoms. On the reduced surface, charge accumulation by the adsorbed O atom occurs partially from Pd_n and partially from the excess of electronic charge associated with the oxygen vacancy. The behavior is more clearly seen by comparing the charge state on a given Pd_n cluster when it bound at the vacancy compared to being bound away from the vacancy. Smaller positive charges occur on Pd_n clusters bound at the vacancy sites.

The binding energy between O and Pd_n/TiO_2 is reported beside each subfigure. In all cases, binding is strong due to direct interaction with the reduced surface and

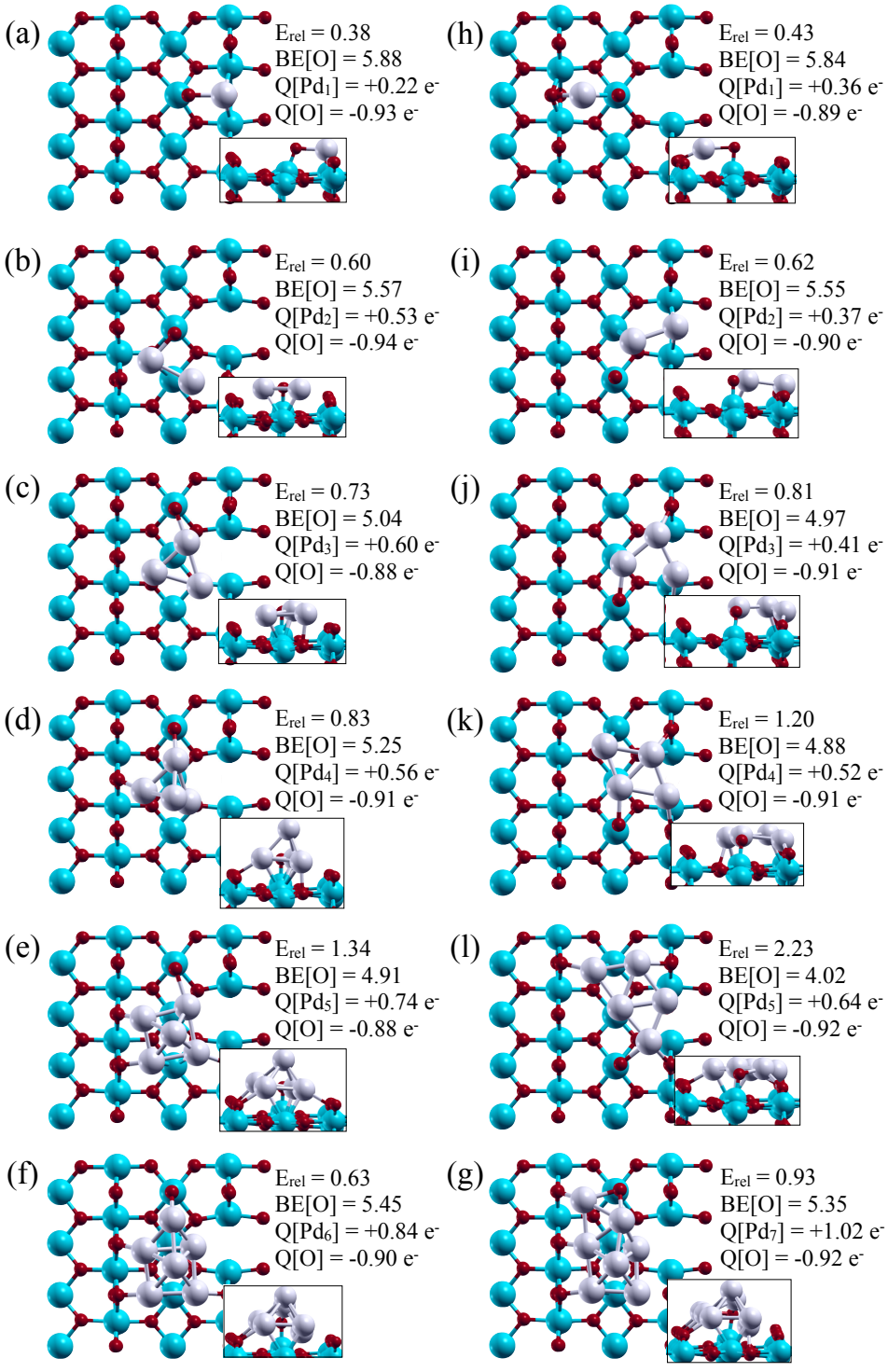

Figure 7.6: Ball and stick drawings of Pd_nO clusters on reduced TiO_2. The figure contains lowest energy configurations for Pd_n and O on the reduced surface when the vacancy is not healed. The figure contains configurations where Pd_n is bound both away from and at the vacancy site.

Pd_n cluster. As seen in Figure 7.6, the oxygen binding energy is almost always weaker when Pd_n is bound at the vacancy. The exception is Pd_1, but the binding energy differs by only 0.04 eV between the two cases. This calls attention to a deeper look at what controls the oxygen binding energy. For Pd_4, the oxygen atom binds with 0.37 eV less energy when the cluster is bound at the vacancy site (Figure 7.6(k)). This is due to a higher total energy for system to be in that configuration. Yet, the existence of such a configuration is not entirely unreasonable. Recall that bare Pd_4 binds at the vacancy site with a cluster binding energy only 0.30 eV less than if it were away from the vacancy. This difference is not large enough to rule out the possibility of Pd_4 binding at a vacancy site, and if it does bind at the vacancy, the result is a more weakly bound oxygen. The reason for this is clear when consulting the oxygen binding energy equation from Equation 2.34. A higher total energy for Pd_nO/TiO_2 translates to weaker oxygen binding. As stated earlier, configurations where O was bound exclusively to the Pd_n cluster *always* resulted in higher total energies. Also stated earlier was that O atom diffusion on the Pd_n cluster may be limited to due high diffusion barriers. If the mobility of O on Pd_n clusters is in fact limited, this may be a mechanism to achieve weaker oxygen binding. Determining the O mobility is out of the scope of the present work, but holds an important value for prospective research.

7.6 Pd_nO_2 Clusters on the Reduced TiO_2 Surface

Lastly, the case where two O atoms are at bound to Pd_n/TiO_2 is considered. The equilibrium geometries were determined by the same method as described in previous sections. The results of the geometry optimizations are shown in Figure 7.7. As in the case for Pd_nO, *all* geometries shown here are *less stable* than if the oxygen vacancy

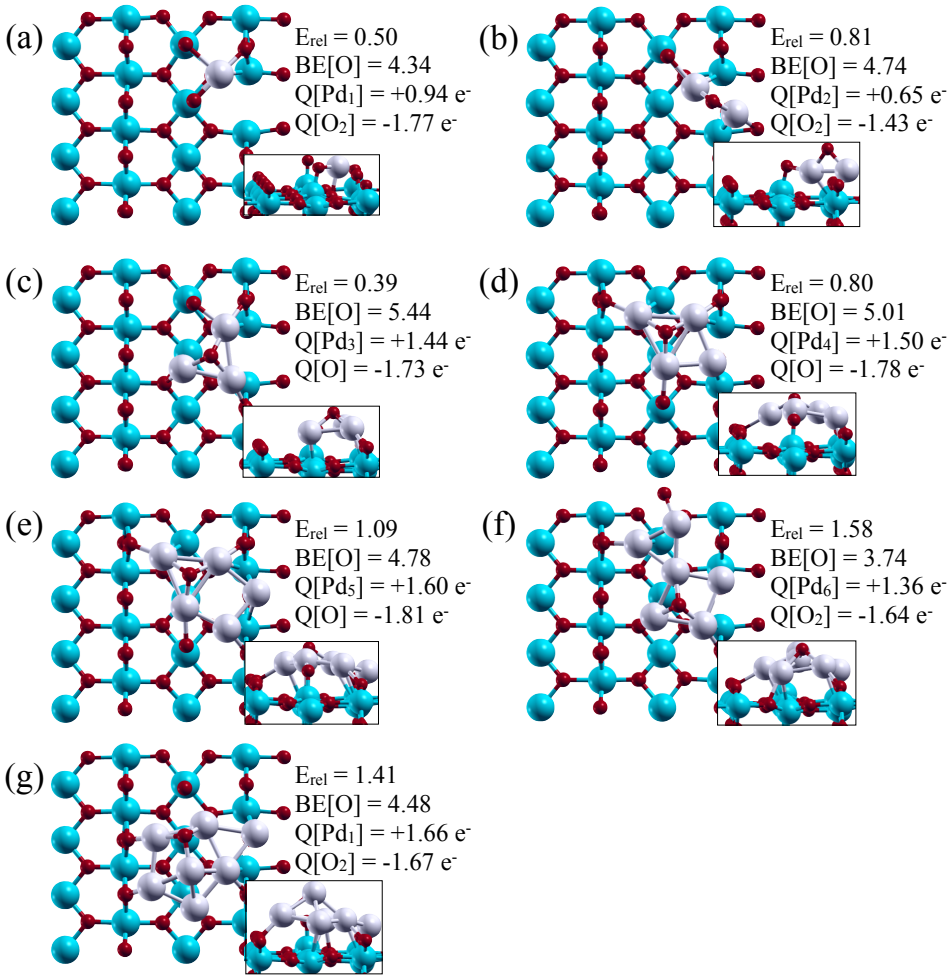

Figure 7.7: Ball and stick drawings of Pd_nO_2 clusters on reduced TiO_2. The figure contains lowest energy configurations for Pd_n and two O atoms on the reduced surface when the vacancy is not healed.

is healed. That is, the structures shown in Figure 6.5(a-g) (Pd_nO clusters on the stoichiometric surface) all resulted in a lower total energy than those shown here, and the relative energies are reported beside each subfigure. As described earlier, several factors justify the possibility of configurations where the vacancy is not healed.

During the geometry optimizations, if the Pd_n motif was initially away from the vacancy, the optimization often led to a configuration where the oxygen vacancy was healed. However, in some cases both O atoms remained exclusively on the Pd_n

cluster. Such geometries were at least 1.0 eV higher in energy, which as discussed previously, may be interpreted as weakly bound oxygen if the mobility of O on Pd_n is limited. As seen in Figure 7.7, all sizes except Pd_1 possess geometries where one O atom is bound exclusively to the cluster and the other O atom is bound in a spillover mode. This is characteristically the same as Pd_nO_2 on the stoichiometric surface shown in Figure 6.5(h-n). In fact, there are many similarities between Pd_nO_2 on the stoichiometric and reduced surface. In all cases, the energy is minimized when the O-O bond is broken. The adsorption sites for O atoms bound to the Pd_n cluster always occurred at threefold hollow sites, where all three Pd-O distances are nearly equivalent. The adsorbed O atoms remain in the center of the TiO_2 surface channel to minimize Coulomb repulsion with the bridging O_2c sites. There are two main differences between the characteristics of Pd_nO_2 on the stoichiometric and reduced surfaces. The first pertains to the charge on oxygen. On the stoichiometric surface, charge accumulation by O_2 increased with cluster size but saturated at about 1.7 e^- at size n=3. The availability of charge associated with the oxygen vacancy on the reduced surface allows for a comparable amount of charge accumulation at all sizes. This gives support to the conclusion that oxygen binding to Pd_n clusters on the reduced surface is enhanced as charge transfer readily occurs from the surface sites or the Pd_n cluster. The second difference pertains to the atomic configuration and binding configuration of the Pd_n motif. Of course, with the presence of an oxygen vacancy, cluster binding at the vacancy site is now possible. However, beyond that, the Pd_nO_2 structures on the stoichiometric surface were planar up to n=4, but reverted to three dimensional motifs for sizes n=5-7. On the reduced surface the clusters form highly planar structures that, apart from the fragmenting that can be seen in Figure 7.7(e-f), are similar to the bare Pd_n clusters bound at the vacancy site from Figure 7.2(h-n). The electronic structure of the stoichiometric supported

Pd_n clusters differed from their compact alternatives mainly by the formation of a delocalized s- band rather than a discrete set of s- states. This electronic configuration is said to responsible for weak binding in small Pd_n clusters[104] as the clusters no longer form close-packed structures, and it may be this that causes the fragmenting of the clusters seen especially for sizes n=5,6.

7.7 Conclusions

The studies in this chapter indicate that Pd_n binding on the reduced surface can occur in two entirely different manners. While Pd_n binding away from a vacancy site is the lowest energy configuration at most sizes, binding at the vacancy is at most 0.8 eV less stable and in some cases preferred. Cluster binding at the vacancy produces an entirely different electronic structure, that more closely resembles the formation of an s- orbital band seen in bulk palladium. Moreover, the effect of this modified electronic structure is manifested in the atomic configuration of the vacancy-bound Pd_n clusters, where the hexagonal symmetry seen for bulk palladium is mimicked within the cluster geometries. Binding of atomic oxygen is strengthened on the reduced surface due to an excess of electronic charge. This has a direct effect of Pd_nO geometries in that O prefers adsorption at the Pd-Ti interface rather than exclusively on the Pd_n clusters. Binding of molecular oxygen is in many ways similar whether the clusters are supported on the stoichiometric or reduced surface. The primary difference is that Pd_n clusters are highly planar and that the weak intra-cluster binding may result in cluster fragmentation. This chapter provides a more realistic simulation of the experimental conditions, where bridging oxygen vacancies are known to exist. The formation of highly planar species for Pd_n clusters bound at the vacancy sites can be interpreted as evidence that supports the ISS experiments

by Anderson.[56]

8. Conclusions and Prospectives

The studies within this PhD provide a theoretical description of the stability and oxidation of Pd_n (n=1-7) clusters on rutile TiO_2. The study on bare Pd_n clusters indicates that the atomic configurations undergo only small changes upon adsorption with respect to the gas phase configurations. Yet, in the presence of even a single adsorbed oxygen atom, the strong tendency for oxygen to accumulate charge while minimizing Coulomb repulsion with other nearby oxygen sites, can lead to structural changes. All this occurs in attempt for the Pd_n cluster to open a threefold Pd site at the center of the TiO_2 surface channel, at which an oxygen atoms prefers to bind. A change in Pd_n cluster configuration causes the cluster to interact with the surface differently, which can enhance cluster-surface binding and surface deformations. The study on Pd_n with two oxygen atoms indicates the preference for one oxygen atom to adsorb in a spillover mode, and is shown to be energetically preferred for all sizes except the Pd atom. The Pd atom poses a special case in its oxidation properties, mainly because of the lack of electron charge it is able to donate. The studies indicate, however, that additional factors may contribute to the lack of oxidation for Pd_1 (e.g., spin excitation energy), but experimental verification is necessary before confirming such conclusions.

The studies on the TiO_2 surface marked with oxygen vacancies indicate no strong preference for the Pd_n cluster to bind at the vacancy site, but that such a binding configuration should be energetically feasible at finite temperatures. Also shown is

that the electronic, magnetic, and atomic configurations of clusters bound at the vacancy greatly differ from those away from the vacancy, or those in the gas phase. The primary difference in atomic configuration is that binding at the vacancy site leads to planar species. Considering the experimental studies by the Anderson group, which propose the Pd_n clusters are planar up to a size of n=10 atoms, this may suggest that the clusters are indeed binding at the vacancy sites. The local electronic structure of the reduced TiO_2 surface is marked by an excess of electronic charge, which modifies the way that the Pd_n clusters oxidize. Mainly, single oxygen atoms prefer to bind in a spillover mode rather than at threefold Pd sites. Further, when a second oxygen atom is introduced the adsorption reverts back to one oxygen atom bound exclusively to the cluster and the other remaining bound in a spillover mode.

The presence of spillover oxygen is calculated to be energetically favored for almost all cluster sizes whether at the perfect or reduced surface. These studies provide a molecular insight to the interactions that take place between Pd and a spillover oxygen, when both are adsorbed on the TiO_2 surface. Ultimately, oxygen spilled over to the surface is strongly bound due to "surface mediated ionic bonds", and the origin of this unique bonding mechanism is rooted in: (1) the tendency for oxygen to accumulate charge, (2) the availability of charge donation by Pd, and (3) the ionic nature of the underlying TiO_2 surface and the resiliency of Ti and O to change in oxidation state. Further, a molecular depiction of the relationship between oxygen spillover and strong metal support interactions is proposed. The relationship between these two experimentally-observed phenomenon is proposed to be related to the way an adsorbing oxygen atom (in a spillover mode) weakens the interactions between the lattice Ti site to which it binds to and the lattice O sites neighboring that Ti. The studies also indicate that the energetic cost of interchanging "TiO motifs with spillover O" and Pd is minimum. Such exchanges could highlight the microscopic

mechanisms underlying SMSI processes. As both TiO and Pd have similar valence pools of 10 valence electrons and 3d states, such a finding may open the pathway to identify "exchange mimics" that govern SMSI in a wider class of systems.

In regards to Pd_n clusters used as catalysts in oxidation reactions, these studies often refer to the Pd-O bond strength as a critical parameter in controlling the oxidation efficiency. The results presented within this PhD provide theoretical insight to this critical parameter by highlighting the inverse relationship between the oxygen bond strength and the cluster's surface stability. However, when adsorbing oxygen is not exclusively bound to the Pd_n cluster (i.e., spillover oxygen) the cluster's surface stability becomes less critical, and emphasizes the importance of understanding the long range binding that is shown to occur between distant Pd and O sites.

To summarize the implications of these theoretical studies, while also providing ideas for prospective studies, two points will be made. First, the results presented in this PhD, along with the experimental evidence that most oxygen ends up adsorbing in a spillover mode, emphasize the role of oxygen spillover in affecting oxidation reactions. This suggests that research efforts focused on weakening the oxygen binding energy, in an attempt to increase the efficiency in oxidation reactions, should be directed specifically towards weakening the binding energy of spillover oxygen. As the enhanced spillover O is partly due to ionic interaction with Pd_n species, one way to reduce the binding energy may be to weaken this ionic interaction. To this end, model studies can be performed where either (1) alkali metals or (2) halogen elements are co-adsorbed on rutile TiO_2 with Pd and O, as a means to screen the ionic interactions between a supported Pd and O species. Second, the studies presented here highlight, for a given cluster, a comparison of oxygen adsorption sites by simply comparing total energies. Considering that in experiments, molecular oxygen dissociatively adsorbs at the Pd_n cluster, not all adsorption configurations may be feasible. To this end, the

adsorbed oxygen atom mobility on the Pd_n cluster should be considered to provide a more coherent picture of the way these clusters oxidize.

Bibliography

[1] J. P. Borel, *Surface Science* **106**, 1 (1981).

[2] N. D. Spencer, R. C. Schoonmaker, G. A. Somorjai, *Journal of Catalysis* **74**, 129 (1982).

[3] A. J. Cox, J. G. Louderback, S. E. Apsel, L. A. Bloomfield, *Physical Review B* **49**, 12295 (1994).

[4] M. Chen, D. Goodman, *Catalysis Today* **111**, 22 (2006).

[5] P. Roach, W. Woodward, A. Castleman, A. Reber, S. Khanna, *Science* **323**, 492 (2009).

[6] B. K. Rao, S. N. Khanna, P. Jena, *Journal of Cluster Science* **10**, 477 (1999).

[7] R. E. Leuchtner, A. C. Harms, A. W. Castleman, *The Journal of Chemical Physics* **91**, 2753 (1989).

[8] J. Cox, D. Wagman, V. Medvedev, *CODATA Key Values for Thermodynamics* (Hemisphere Publishing Corp., New York, NY, 1984).

[9] B. V. Reddy, S. N. Khanna, B. I. Dunlap, *Physical Review Letters* **70**, 3323 (1993).

[10] D. M. Cox, R. Brickman, K. Creegan, A. Kaldor, *Zeitschrift fr Physik. D* **19**, 353 (1991).

[11] G. A. Somorjai, *Introduction to Surface Chemistry and Catalysis* (John Wiley and Sons, New York, NY, 1994).

[12] E. Fialko, A. Kikhtenko, V. Goncharov, K. Zamaraev, *Journal of Physical Chemistry B* **101**, 5772 (1997).

[13] M. Boudart, *Topics in Catalysis* **13**, 147 (2000).

[14] W. A. de Heer, *Reviews of Modern Physics* **65**, 611 (1993).

[15] S. N. Khanna, P. Jena, *Physical Review Letters* **69**, 1664 (1992).

[16] S. N. Khanna, P. Jena, *Physical Review B* **51**, 13705 (1995).

[17] D. E. Bergeron, A. W. Castleman, T. Morisato, S. N. Khanna, *Science* **304**, 84 (2004).

[18] R. L. Whetten, *et al.*, *Advanced Materials* **8**, 428 (1996).

[19] H. Hakkinen, M. Walter, H. Gronbeck, *Journal of Physical Chemistry B* **110**, 9927 (2006).

[20] H. Hakkinen, *Chemical Society Reviews* **37**, 1847 (2008).

[21] P. Andre Clayborne, O. Lopez-Acevedo, R. L. Whetten, H. Gronbeck, H. Hakkinen, *The Journal of Chemical Physics* **135**, 094701 (2011).

[22] S. A. Claridge, *et al.*, *ACS Nano* **3**, 244 (2009).

[23] A. W. Castleman, S. N. Khanna, *Journal of Physical Chemistry C* **113**, 2664 (2009).

[24] C. Binns, *Surface Science Reports* **44**, 1 (2001).

[25] F. Cinquini, C. Valentin, E. Finazzi, L. Giordano, G. Pacchioni, *Theoretical Chemistry Accounts: Theory, Computation, & Modeling* **117**, 827 (2007).

[26] U. Diebold, *Surface Science Reports* **48**, 53 (2003).

[27] B. L. Mojet, *et al.*, *11th International Congress On Catalysis - 40th Anniversary, Proceedings of the 11th ICC* (Elsevier, 1996), vol. Volume 101, pp. 1165–1174.

[28] K. Okazaki, Y. Morikawa, S. Tanaka, K. Tanaka, M. Kohyama, *Physical Review B* **69**, 235404 (2004).

[29] V. E. Matulis, A. S. Mozheiko, O. A. Ivashkevich, *Russian Journal of General Chemistry* **80**, 1068 (2010).

[30] A. Mazheika, V. Matulis, O. Ivashkevich, *Journal of Molecular Structure-Theochem* **909**, 75 (2009).

[31] A. Asaduzzaman, P. Kruger, *Journal of Physical Chemistry C* **112**, 19616 (2008).

[32] T. Bredow, G. Pacchioni, *Surface Science* **426**, 106 (1999).

[33] M. A. San-Miguel, J. Oviedo, J. F. Sanz, *Physical Review Letters* **99**, 066102 (2007).

[34] J. Sanz, A. Marquez, *Journal of Physical Chemistry C* **111**, 3949 (2007).

[35] P. Murugan, V. Kumar, Y. Kawazoe, *International Journal of Modern Physics B* **19**, 2544 (2005).

[36] A. K. Santra, D. W. Goodman, *Electrochimica Acta* **47**, 3595 (2002).

[37] C. Lun Pang, R. Lindsay, G. Thornton, *Chemical Society Reviews* **37**, 2328 (2008).

[38] Y. Du, Z. Dohnalek, I. Lyubinetsky, *The Journal of Physical Chemistry C* **112**, 2649 (2008).

[39] S. Wendt, *et al.*, *Surface Science* **598**, 226 (2005).

[40] M. Bowker, E. Fourre, *Applied Surface Science* **254**, 4225 (2008).

[41] S. J. Tauster, S. C. Fung, R. L. Garten, *Journal of the American Chemical Society* **100**, 170 (1978).

[42] S. J. Tauster, *Accounts of Chemical Research* **20**, 389 (1987).

[43] M. Bowker, P. Stone, R. Bennett, N. Perkins, *Surface Science* **497**, 155 (2002).

[44] M. Bowker, *et al.*, *Journal of Catalysis* **234**, 172 (2005).

[45] L. Spenadel, M. Boudart, *Journal of Physical Chemistry* **64**, 204 (1959).

[46] R. A. Bennett, *et al.*, *The Journal of Physical Chemistry B* **106**, 4688 (2002).

[47] Q. Fu, T. Wagner, S. Olliges, H. Carstanjen, *The Journal of Physical Chemistry B* **109**, 944 (2005).

[48] M. Bowker, *Physical Chemistry Chemical Physics* **9**, 3514 (2007).

[49] U. Heiz, W. Schneider, *Journal of Physics D: Applied Physics* **33**, R85 (2000).

[50] S. Abbet, K. Judai, L. Klinger, U. Heiz, *Pure and Applied Chemistry* **74**, 1527 (2002).

[51] J. Norskov, *Journal of Catalysis* **209**, 275 (2002).

[52] B. Yoon, *et al.*, *Science* **307**, 403 (2005).

[53] D. Matthey, *et al.*, *Science* **315**, 1692 (2007).

[54] W. S. Epling, C. H. F. Peden, M. A. Henderson, U. Diebold, *Surface Science* **412-413**, 333 (1998).

[55] T. Shimizu, *et al.*, *Combustion and Flame* **157**, 421 (2010).

[56] W. Kaden, T. Wu, W. Kunkel, S. Anderson, *Science* **326**, 826 (2009).

[57] W. E. Kaden, W. A. Kunkel, M. D. Kane, F. S. Roberts, S. L. Anderson, *Journal of the American Chemical Society* **132**, 13097 (2010).

[58] T. Wu, W. E. Kaden, W. A. Kunkel, S. L. Anderson, *Surface Science* **603**, 2764 (2009).

[59] R. Robles, S. Khanna, *Physical Review B* **82** (2010).

[60] M. Born, J. R. Oppenheimer, *Annalen der Physik* **84**, 457 (1927).

[61] L. H. Thomas, *Mathematical Proceedings of the Cambridge Philosophical Society* **23**, 542 (1927).

[62] P. A. M. Dirac, *Mathematical Proceedings of the Cambridge Philosophical Society* **26**, 376 (1930).

[63] R. M. Martin, *Electronic Structure: Basic Theory and Practical Methods* (Cambridge University Press, New York, NY, 2004).

[64] P. Hohenberg, W. Kohn, *Physical Review* **136**, B864 (1964).

[65] W. Kohn, L. J. Sham, *Physical Review* **140**, A1133 (1965).

[66] S. H. Vosko, L. Wilk, M. Nusair, *Canadian Journal of Physics* **58**, 1200 (1980).

[67] J. Perdew, K. Burke, M. Ernzerhof, *Physical Review Letters* **77**, 3865 (1996).

[68] N. Umezawa, *The Journal of Chemical Physics* **128**, 044105 (2008).

[69] G. Kresse, J. Furthmller, *Computational Materials Science* **6**, 15 (1996).

[70] P. Blochl, *Physical Review B* **50**, 17953 (1994).

[71] G. Kresse, D. Joubert, *Physical Review B* **59**, 1758 (1999).

[72] W. H. Press, B. P. Flannery, S. A. Teukolsky, W. T. Vetterling, *Numerical Recipes* (Cambridge University Press, New York, NY, 1986).

[73] P. Pulay, *Chemical Physics Letters* **73**, 393 (1980).

[74] Vasp user's guide website, http://cms.mpi.univie.ac.at/vasp/vasp/vasp.html (2011).

[75] J. Hafner, *Journal of Computational Chemistry* **29**, 2044 (2008).

[76] G. Henkelman, A. Arnaldsson, H. Jnsson, *Computational Materials Science* **36**, 354 (2006).

[77] F. A. Grant, *Reviews of Modern Physics* **31**, 646 (1959).

[78] H. Remy, *Treatise on Inorganic Chemistry, Vol. II, p. 59* (Elsevier Publishing Company, Amsterdam, 1956).

[79] T. Bredow, L. Giordano, F. Cinquini, G. Pacchioni, *Physical Review B* **70**, 035419 (2004).

[80] G. Pacchioni, *The Journal of Chemical Physics* **128**, 182505 (2008).

[81] L. Kavan, M. Grtzel, S. E. Gilbert, C. Klemenz, H. J. Scheel, *Journal of the American Chemical Society* **118**, 6716 (1996).

[82] C. Adamo, V. Barone, *The Journal of Chemical Physics* **110**, 6158 (1999).

[83] J. Heyd, G. E. Scuseria, M. Ernzerhof, *The Journal of Chemical Physics* **118**, 8207 (2003).

[84] I. D. Prodan, G. E. Scuseria, R. L. Martin, *Physical Review B* **76**, 033101 (2007).

[85] V. I. Anisimov, J. Zaanen, O. K. Andersen, *Physical Review B* **44**, 943 (1991).

[86] A. I. Liechtenstein, V. I. Anisimov, J. Zaanen, *Physical Review B* **52**, R5467 (1995).

[87] S. L. Dudarev, G. A. Botton, S. Y. Savrasov, C. J. Humphreys, A. P. Sutton, *Physical Review B* **57**, 1505 (1998).

[88] C. Di Valentin, G. Pacchioni, A. Selloni, *Physical Review Letters* **97**, 166803 (2006).

[89] B. Amadon, F. Jollet, M. Torrent, *Physical Review B* **77**, 155104 (2008).

[90] G. Jomard, B. Amadon, F. Bottin, M. Torrent, *Physical Review B* **78**, 075125 (2008).

[91] F. Jollet, G. Jomard, B. Amadon, J. P. Crocombette, D. Torumba, *Physical Review B* **80**, 235109 (2009).

[92] B. Dorado, B. Amadon, M. Freyss, M. Bertolus, *Physical Review B* **79**, 235125 (2009).

[93] B. Dorado, G. Jomard, M. Freyss, M. Bertolus, *Physical Review B* **82**, 035114 (2010).

[94] Y. Wang, G. S. Hwang, *Surface Science* **542**, 72 (2003).

[95] H. Iddir, S. Ogut, N. D. Browning, M. M. Disko, *Physical Review B* **72**, 081407 (2005).

[96] S. J. Thompson, S. P. Lewis, *Physical Review B* **73**, 073403 (2006).

[97] S. Chretien, H. Metiu, *The Journal of Chemical Physics* **127**, 244708 (2007).

[98] V. Celik, H. Unal, E. Mete, S. Ellialtioglu, *Physical Review B* **82** (2010).

[99] J. Sanz, N. Hernandez, A. Marquez, *Theoretical Chemistry Accounts* **104**, 317 (2000).

[100] R. Lindsay, *et al.*, *Physical Review Letters* **94** (2005).

[101] I. M. L. Billas, A. Chtelain, W. A. d. Heer, *Science* **265**, 1682 (1994).

[102] G. Valeria, H. Toulhoat, *Journal of Physical Chemistry* **26**, 10827 (1996).

[103] M. Moseler, H. Hkkinen, R. N. Barnett, U. Landman, *Physical Review Letters* **86**, 2545 (2001).

[104] V. Kumar, Y. Kawazoe, *Physical Review B* **66**, 144413 (2002).

[105] C. E. Moore, *Table of Atomic Energy Levels* (U.S. National Bureau of Standards, Washington, D.C., 1971).

[106] F. M. Mueller, A. J. Freeman, J. O. Dimmock, A. M. Furdyna, *Physical Review B* **1**, 4617 (1970).

[107] N. W. Ashcroft, N. D. Mermin, *Solid State Physics p. 307* (Thomson Learning, Inc., U.S., 1976).

[108] V. N. Popok, I. Barke, E. E. Campbell, K. Meiwes-Broer, *Surface Science Reports* **66**, 347 (2011).

[109] M. Todorova, K. Reuter, M. Scheffler, *The Journal of Physical Chemistry B* **108**, 14477 (2004).

[110] R. Bennett, P. Stone, M. Bowker, *Catalysis Letters* **59**, 99 (1999).

[111] O. Dulub, W. Hebenstreit, U. Diebold, *Physical Review Letters* **84**, 3646 (2000).

[112] D. R. Jennison, O. Dulub, W. Hebenstreit, U. Diebold, *Surface Science* **492**, L677 (2001).

[113] M. D. Negra, N. M. Nicolaisen, Z. Li, P. J. Mller, *Surface Science* **540**, 117 (2003).

[114] G. te Velde, *et al.*, *Journal of Computational Chemistry* **22**, 931 (2001).

[115] X. Wu, A. Selloni, M. Lazzeri, S. K. Nayak, *Physical Review B* **68**, 241402 (2003).

[116] M. D. Rasmussen, L. M. Molina, B. Hammer, *The Journal of Chemical Physics* **120**, 988 (2004).

[117] M. A. Henderson, W. S. Epling, C. L. Perkins, C. H. F. Peden, U. Diebold, *The Journal of Physical Chemistry B* **103**, 5328 (1999).

[118] B. J. Berne, *Classical and Quantum Dynamics in Condensed Phase Simulations* (World Scientific, Singapore, 1998).

[119] Q. Fu, T. Wagner, *The Journal of Physical Chemistry B* **109**, 11697 (2005).

[120] E. C. Tyo, A. W. Castleman, A. C. Reber, S. N. Khanna, *The Journal of Physical Chemistry C* **115**, 16797 (2011).

[121] C. Xu, X. Lai, G. W. Zajac, D. W. Goodman, *Physical Review B* **56**, 13464 (1997).

[122] X. Lai, T. P. S. Clair, M. Valden, D. W. Goodman, *Progress in Surface Science* **59**, 25 (1998).

[123] P. Murugan, V. Kumar, Y. Kawazoe, *Physical Review B* **73** (2006).

[124] G. Mills, H. Jnsson, G. K. Schenter, *Surface Science* **324**, 305 (1995).

[125] Volmer, Weber, *Z. Physik. Chem.* **119** (1926).

[126] I. N. Stranski, L. Krastanow, *Akad. Wiss. Wien Math.-Naturwiss. Kl. IIb* **146** (1939).

[127] A. M. Koster, *et al.*, *Journal of the American Chemical Society* **133**, 12192 (2011).

[128] A. C. Reber, S. N. Khanna, P. J. Roach, W. H. Woodward, A. W. Castleman, *Journal of the American Chemical Society* **129**, 16098 (2007).

[129] V. E. Henrich, G. Dresselhaus, H. J. Zeiger, *Physical Review Letters* **36**, 1335 (1976).

[130] R. Schaub, *et al.*, *Physical Review Letters* **87**, 266104 (2001).

[131] G. Pacchioni, *ChemPhysChem* **4**, 1041 (2003).

[132] A. S. Woerz, U. Heiz, F. Cinquini, G. Pacchioni, *Journal of Physical Chemistry B* **109**, 18418 (2011).

[133] A. Sanchez, *et al.*, *The Journal of Physical Chemistry A* **103**, 9573 (1999).

[134] S. Abbet, *et al.*, *Journal of the American Chemical Society* **122**, 3453 (2000).

[135] J. Antonietti, *et al.*, *Physical Review Letters* **94**, 213402 (2005).

[136] I. N. Remediakis, N. Lopez, J. K. Nrskov, *Angewandte Chemie International Edition* **44**, 1824 (2005).

[137] T. Bredow, G. Pacchioni, *Chemical Physics Letters* **355**, 417 (2002).

[138] C. Calzado, N. Hernandez, J. Sanz, *Physical Review B* **77** (2008).

[139] H. Unal, E. Mete, S. Ellialtiohlu, *Physical Review B* **84**, 115407 (2011).

[140] Z. Hu, H. Metiu, *The Journal of Physical Chemistry C* **115**, 5841 (2011).

[141] B. J. Morgan, G. W. Watson, *Surface Science* **601**, 5034 (2007).

A. Enhanced Oxygen Bonds (DFT+U Results)

As stated in Section 3.2, conventional DFT exchange correlation functionals, such as those based on GGA, notoriously underestimate the TiO_2 band gap; and this underestimation is directly a result of DFT artificially delocalizing the Ti 3d electrons. Recall that this can be corrected by the inclusion of a Hubbard U term in the Hamiltonian, which energetically penalizes the delocalized solution (refer to Chapter 2). Because one of the major conclusions of Chapter 5 was based on the calculated result of charge distribution across the surface layer atoms, DFT+U calculations were carried out. If the physical picture is one where the charge *is* distributed, then the DFT+U calculations should make no difference, and DFT calculations are appropriate. If the physical picture is one where charge *is not* distributed, then the DFT+U calculation should correct this result, providing a more realistic solution. To this end, supplemental calculations corresponding to those reported in Chapter 5 were performed using the DFT+U approximation. Note that these supplemental calculations are still based on the generalized gradient approximation (GGA), and hence the method can also be referred to as the GGA+U approximation. The implementation as proposed by Dudarev was used, which requires a parameter U_{eff} to be supplied (U_{eff} = U-J).[87] The value of U_{eff}=4.5 eV was chosen based on previous work on TiO_2, which suggested this value provides the most reasonable description of the electronic structure

without introducing too large a geometrical distortion.[98]

It is important to note that since the U parameter is added as a term of the Hamiltonian, the GGA+U approach requires the Kohn-Sham equations to be resolved self-consistently. The calculated total energies are entirely different than compared to the GGA approach, because the prescription to compute the total energy has now changed. Likewise, the geometries must be re-optimized within GGA+U. Fortunately, for the sake of computational expense, the optimized GGA geometries can be used as initial atomic coordinates.

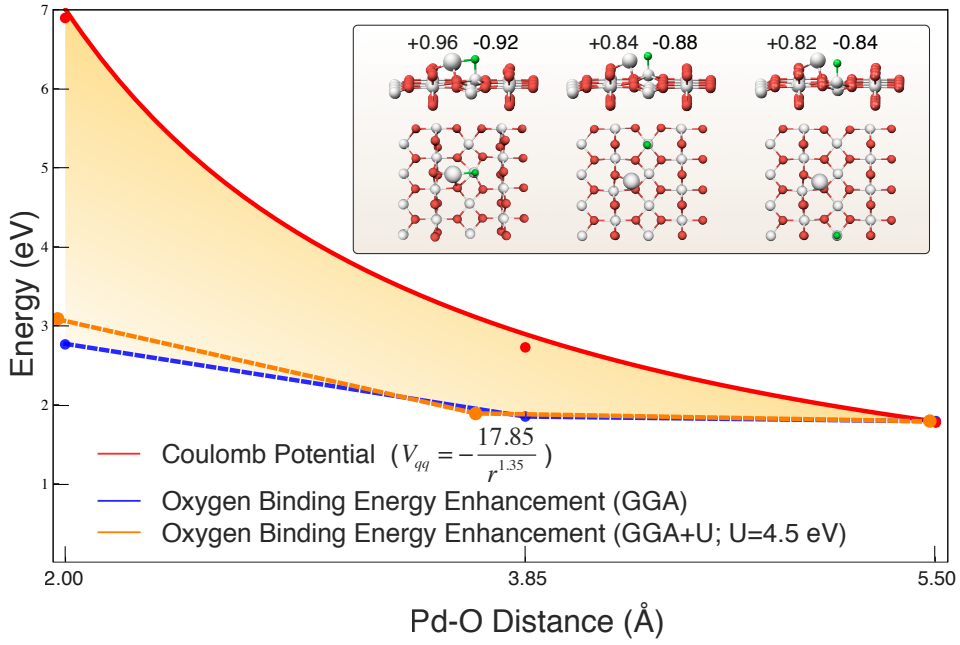

Figure A.1: Supplemental figure showing the results of GGA+U on enhanced oxygen binding calculations. The orange dots indicate the GGA+U results.

The results of geometry re-optimizations and total energy calculations are shown in Figure A.1 and are plotted along with the GGA results from Chapter 5. Like Figure 5.3, the oxygen binding *enhancement* is plotted. Recall, the binding enhancement is defined as the difference between O_{ad} binding energy to the bare surface and O_{ad} binding to the surface when Pd is present. Both of these binding energies were

calculated to be lower in the GGA+U scheme, but they were lower by the same amount meaning the overall binding energy enhancement remained the same. Any differences in the points shown in Figure A.1 are due to the slight changes in the optimized Pd-O distances. The atomic charges were calculated by a Bader charge analysis, as in the GGA approach, and were found to be slightly different (compare with Figure 5.3), but by no more than 0.07 e^-.

B. Pd_n Clusters on Reduced TiO_2 (DFT+U Results)

Previous theoretical studies have drawn attention to the inadequacies of conventional GGA functionals (e.g., PBE) in accurately predicting the band gap of reduced TiO_2 and the position of the defect state that is introduced when an oxygen vacancy is present.[138–140] Consequently, these references suggest that supplemental GGA+U calculations should be performed, as the method is proposed to offer a better theoretical description of the reduced surface. To this end, supplemental calculations were performed to determine the geometries and corresponding binding energies of Pd_n clusters supported on the TiO_2(110) surface marked with oxygen vacancies. Like the results shown in Appendix A, a Hubbard U parameter of U_{eff}=4.5 eV was used. First, the bare, reduced surface was re-optimized as the total energy was needed to calculate the cluster binding energies. The optimized GGA geometry was used as a starting point for the optimization. Subsequently, all the Pd_n clusters geometries shown in Figure 7.2 were re-optimized using the GGA+U method.

The primary effect of the U parameter on the bare, reduced surface is an increase in the energy difference between the magnetic spin states. The energy difference between the ground state triplet and higher energy singlet state increases from 0.05 eV (the value determined by the GGA calculations) to 0.52 eV with the inclusion of the U parameter. The removal of a bridging O_{2c} atom from the TiO_2 surface, formally,

leaves two unpaired electrons that are delocalized at Ti 3d sites near the oxygen vacancy.[141] The stabilization of the spin triplet state in the GGA+U scheme is a direct result of the increased localization of these Ti 3d electrons. The inclusion of U also causes the reduced TiO_2 slab to undergo slight changes in geometry. The characteristic bond lengths corresponding to those previously shown in Figure 3.5(a) are reported in Table B.1. Compared to the GGA results (U=0 eV column), the inclusion of U leads minor changes. The largest changes occur for the bonds labeled G and H.

Bond Lengths (Å)		
Bond Label	U=0	U=4.5
A	n/a	n/a
B	2.03	2.03
C	1.96	1.98
D	1.96	1.98
E	1.81	1.85
F	2.18	2.16
G	1.97	2.06
H	2.03	2.11
J	2.05	2.05
K	2.01	1.95
L	1.90	1.94

Table B.1: Characteristic bond lengths calculated for the reduced titania surface without Hubbard U and with Hubbard U, where U=4.5 eV. The labels refer to the bonds drawn in Figure 3.5(a), and refer to the bond lengths directly at/beneath the vacancy site.

Referring back to the Figure 3.5(a), it can be seen that the increase in bonds G and H both indicate a change in the local bonding of the Ti site directly one trilayer beneath the oxygen vacancy site, which is again a direct result of the increased Ti 3d orbital localization.

Unlike several previous studies,[138–141] identifying the differences between GGA and GGA+U in predicting the structure of reduced TiO_2 is not the primary goal of this

work. In this study, the primary question is to determine the effect of Hubbard U on the Pd_n cluster adsorption properties on reduced TiO_2. The results of the geometry optimizations are shown in Figure B.2. There is a slight energetic preference towards binding at the vacancy site that is observed in several ways. First, consider the energy difference of the Pd_2 cluster binding at and away from the vacancy. Like the GGA results, the cluster still prefers binding at the vacancy, however the difference between the two binding sites increases from 0.12 eV (GGA results) to 0.85 eV (GGA+U results). On the other hand, the Pd_4 and Pd_7 clusters preferred binding away from the vacancy within GGA, but recall that binding at the vacancy was not much higher in energy (0.30 and 0.01 eV, respectively). Within the GGA+U results, the binding site preference is reversed, and now binding away from the vacancy is slightly less stable. Lastly, the GGA+U results indicate that Pd_5 and Pd_6 still prefer binding away from the vacancy site, but the relative energy difference between binding at and away from the vacancy site is less than was calculated within GGA.

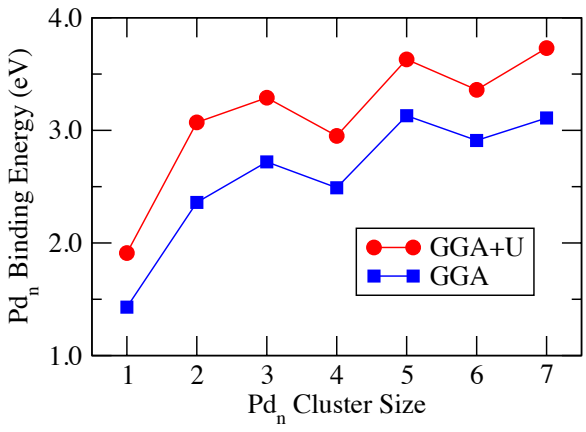

Figure B.1: A comparison of the GGA and GGA+U (U=4.5 eV) results for Pd_n cluster binding energy to the reduced TiO_2 surface.

Lastly, the inclusion of U affects the calculated cluster binding energies as shown in Figure B.1. The overall trend clearly remains the same, but the binding energies

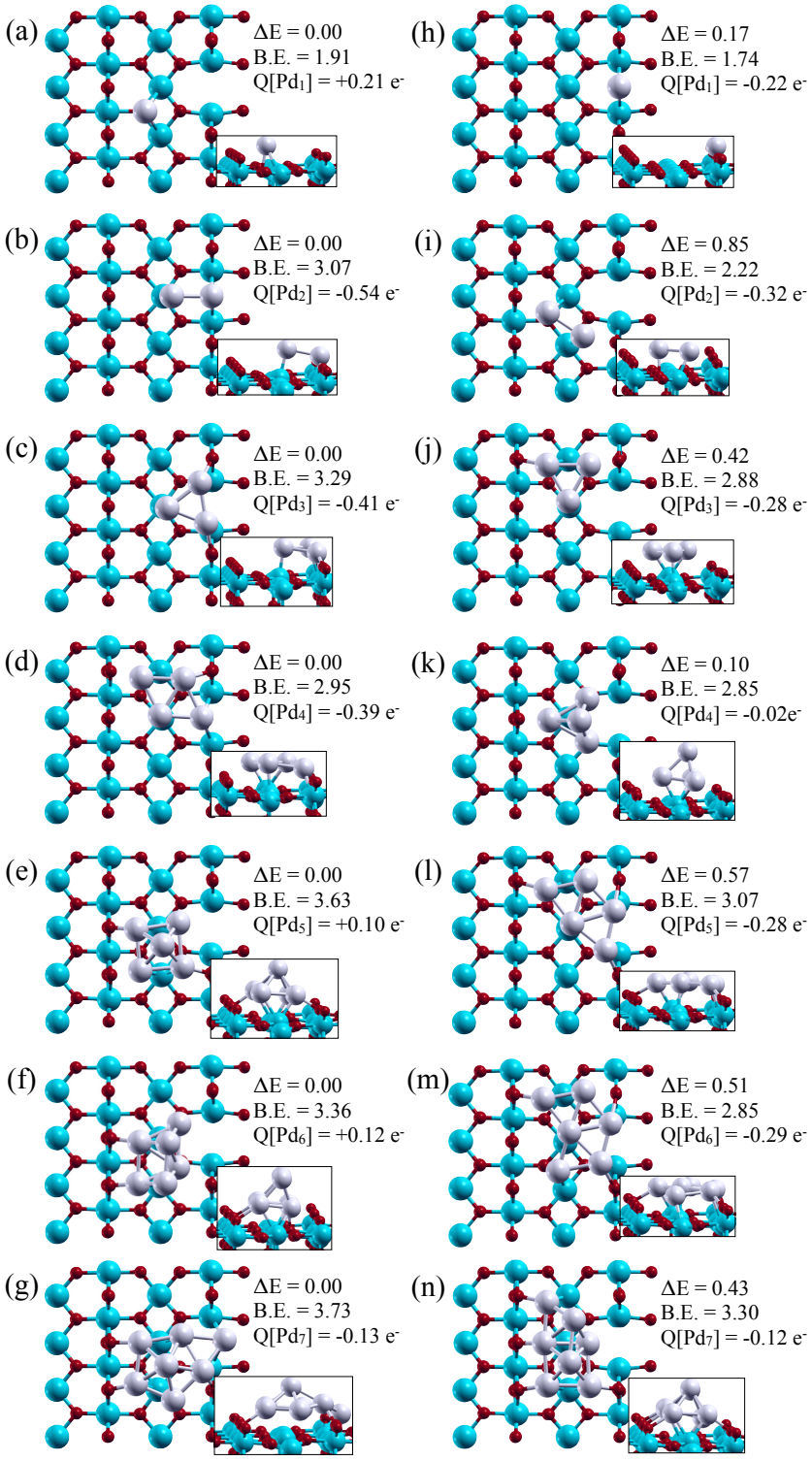

Figure B.2: Ball and stick drawings of Pd_nO clusters on reduced TiO_2: GGA+U results.

increase by an average value of 0.54 eV. This is a directly a result of the lowering in total energy of the spin triplet state of the surface. That is, the shift in binding energies is a reflection of the energy difference between spin states calculated by GGA compared to GGA+U.

In summary, the inclusion of Hubbard U has the most noticeable effect on electronic structure of reduced TiO_2 by resulting in an increased energy difference between magnetic spin states. However, upon adsorption of Pd_n clusters, the U approximation leads to no major qualitative differences in the adsorption characteristics. Although certain clusters do show an energetic preference toward vacancy site binding with the inclusion of U, the energy difference between cluster binding at compared to away from the vacancy was not very large without U.